Metasurfaces for Antennas, Energy Harvesting and Imaging

by

Mohamed El Badawe

A thesis
presented to the University of Waterloo
in fulfillment of the
thesis requirement for the degree of
Doctoral of Philosophy
in
Electrical and Computer Engineering

Waterloo, Ontario, Canada, 2018

Examining Committee Membership

The following served on the Examining Committee for this thesis. The decision of the Examining Committee is by majority vote.

External Examiner	Tayeb Denidni Professor
Supervisor(s)	Omar Ramahi Professor
Internal Member	Amir Khandani Professor
Internal Member	Karim Karim Professor
Internal-external Member	Kevin Musselman Professor

This thesis consists of material all of which I authored or co-authored: see Statement of Contributions included in this thesis. This is a true copy of the thesis, including any required final revisions, as accepted by my examiners.

I understand that my thesis may be made electronically available to the public.

Statement of Contributions

What follows is a list of publications, which I have co-authored and used their content in this dissertation. For each publication, I present a list of my contributions:

1. Mohamed El Badawe, Thamer S. Almoneef, and Omar M. Ramahi. "A true metasurface antenna." *Scientific reports 6 2016*, 19268.

    - Developed the concept
    - Conducted the experiments
    - Analyzed the data
    - Wrote the manuscript

2. Mohamed El Badawe, Thamer S. Almoneef, and Omar M. Ramahi. "A metasurface for conversion of electromagnetic radiation to DC." *AIP Advances 7.3 (2017)*, 035112.

    - Developed the concept
    - Performed the experiment work
    - Analyzed the data
    - Wrote the manuscript

3. Mohamed El Badawe, Omar M Ramahi, "Metasurface for near-unity electromagnetic energy harvesting and wireless power transfer," 2016 *IEEE International Symposium on Antennas and Propagation* (APSURSI), Fajardo, 2016, pp. 609-610.

    - Developed the concept
    - Performed the simulation
    - Analyzed the data
    - Wrote the manuscript

4. Mohamed El Badawe, Omar M Ramahi, "Polarization independent metasurface energy harvester," 2016 *IEEE Wireless and Microwave Technology Conference* (WAMICON), 2016, pp. 1-3.

    - Developed the concept
    - Performed the simulation

- Analyzed the data
- Wrote the manuscript

5. Mohamed El Badawe, Omar M Ramahi, "A cylindrical metasurface antenna," 2017 *IEEE International Symposium on Antennas and Propagation* (APSURSI), 2017, pp. 1945-1946.

    - Developed the concept
    - Performed the simulation
    - Analyzed the data
    - Wrote the manuscript

6. Mohamed El Badawe, Omar M Ramahi, "Towards a methodology for conformable antenna design," 2017 *IEEE The International Workshop on Antenna Technology* (iWAT), 2017, pp. 233-234.

    - Developed the concept
    - Performed the simulation
    - Analyzed the data
    - Wrote the manuscript

7. Mohamed El Badawe, Omar M Ramahi, "Design of Conformal Antennas using Electrically-Small Radiators," 2017 *IEEE TRANSACTIONS ON ANTENNAS AND PROPAGATION* Submitted.

    - Developed the concept
    - Performed the simulation
    - Analyzed the data
    - Wrote the manuscript

8. Mohamed El Badawe, Omar M Ramahi, "Efficient Metasurface Rectenna for Electromagnetic Wireless Power Transfer and Energy Harvesting," 2018 *Progress In Electromagnetics Research 161 (2018): 35-40.*

    - Developed the concept
    - Conducted the experiments
    - Analyzed the data
    - Wrote the manuscript

Abstract

Metamaterials are materials with artificial structures, engineered to produce electromagnetic properties not readily available in nature. Metamaterials have generated broad interest and utilization in various applications because of their engineer-able permittivity and permeability. Metasurfaces form the most-used class of metamaterials in all electromagnetic applications, from microwave to optical, because of their simplicity compared to bulky 3D structures. Metasurfaces are created using an ensemble of electrically small resonators. Previously, the metasurface concept was used to redirect or focus light, with the surface profile being tailored to control the phase and magnitude of the current at each cell.

In the first part of this dissertation, a metasurface is used to create a new antenna concept by tailoring the feed for each resonator to create optimal radiation behaviour. The resonators are placed on a flat surface and connected to one feed point using different feed mechanisms to achieve desired current phase at each resonator. Unlike conventional array antennas, in which the distance between adjacent antennas is maintained at approximately half the wavelength to reduce mutual coupling between adjacent antennas, here the distance between the radiating elements is electrically very small. This effects good impedance matching of each resonator to its feed. The metasurface antenna has strong potential for a variety of traditional and non-traditional applications. Its flexible design (high degree of optimization freedom) facilitates its use on a variety of non-Cartesian and platforms. A prototype was fabricated and tested, showing positive agreement between numerical simulations and experimental results of the metasurface antenna. In this part, a concept is presented to enable a systematic design of low-profile conformal antennas. The concept is based on using closely spaced electrically-small radiators. An ensemble of the radiators is placed in a periodic arrangement and the phase of the feed for each element is set to create a phase front orthogonal to the direction where maximum radiation is desired. The phase front is created based on the assumption that each electrically-small radiator is essentially a Huygens source radiating in the open space.

A novel method is proposed in the second part of the thesis that emerge metasurface for energy harvesting and wireless power transfer. Unlike earlier designs of metamaterial harvesters where each small resonator was connected to a load, in this design, the power received by the resonators is channeled collectively into one load, thus maximizing the power density per load. Another contribution of the metasurface harvester of this work, based on the concept of perfect absorbance and channeling to one load, is the design of a metasurface medium with near unity electromagnetic energy harvesting. Two different

feed networks with different impedances matching techniques are proposed to deliver the maximum power

collected by all cells to just one load. Prototypes were fabricated and tested; the numerical simulation and the experimental measurements showed that the proposed metasurface harvester was sufficient to collect microwave energy and deliver it to one load through vias using one feed network. The third part presents a new paradigm of imaging objects using metasurfaces. In this part, an extensive study has been done to examine the metasurface panels for imaging. In conventional imaging methods, a raster scan is used to sense any differences or changes in the object, whereas here, objects are imaged without any scan. The mothed leveraging the voltage from each cell and by using a simple Matlab code these voltages will build the image of the object. This method showed promising results through the numerical simulation of imaging for both metal and dielectric materials.

Acknowledgments

In the name of Allah the All-Merciful, The Ever-Merciful. First and foremost, I would like to thank Allah, the Almighty, for giving me the strength to successfully accomplish this thesis and for blessing me with great family and friends, who have been my greatest support in both my personal and professional life. I also want to express my sincere gratitude to my supervisor Prof. Omar M. Ramahi. I want express my thanks for his supervision, advice, and encouragement throughout the period of this work. He never hesitated to make time for me when I required guidance. I am thankful for his kindness, understanding and support during these years.

I am also very thankful to the committee members, Prof. Amir Khandani, Prof. Karim Karim, Prof. Kevin Musselman and Prof. Tayeb Denidni for spending their valuable time to review my thesis and give helpful comments. I owe a debt of gratitude to my mother, siblings, and friends for their support throughout this academic journey.

I would also like to thank all members of Prof. Ramahi's group for their valuable discussions. I would like to thank my current and former electromagnetic research group members at the University of Waterloo. I would like to thank all of them for their technical help, and friendship. Specifically, I would like to thank Prof.Vahid Nayyeri, Dr.Babak Alavikia, Dr.Zhao Ren, Dr.Khawla Alzoubi, Dr.Mohammed Al Shareef, Dr.Miguel Ruphuy, Dr.Abdulbaset Ali, Dr.Thamer Almoneef, Humayra Naosaba, Hu Sun, Faruk Erkmen, Ahmed Ashoor, Ali Albishi, Dawood Alsaedi, Maged Aldhaeebi, Seyed Mirjahanmardi, Mohammed Aldosari, Saeed Bamatraf, Melad Olaimat and Abdulrahman Aloraynan.

This work has been carried out at the Faculty of Engineering and Applied Science at the University of Waterloo, Canada. It has been funded by the Ministry of Education and Scientific Research of Libya.

In the name of Allah, the most Gracious, the most Merciful and praise be to Allah

Dedication

This is dedicated to my parents and siblings.

Table of Contents

List of Tables

List of Figures

Chapter 1

Introduction

1.1 Background

Metamaterials are artificial electromagnetic materials engineered to have unconventional response functions that satisfy prescribed requirements. These unconventional responses are often generated by subwavelength periodic metallic inclusions, which produce a new class of materials having exotic electromagnetic properties not readily observed in the constituent materials or observed in nature. The desire for artificial materials started long ago when Jadagis Chunder Bose experimented with constructed twisted elements (chiral characteristics) in 1898 [1,2]. Five years later in 1904, a research paper by Lamb addressed a wave that had phases and group velocities moving in opposite directions [3]. Four decades later, L. Mandelshtam studied the idea of backward waves as well [4].

Modern metamaterial was first hypothesized and then experimentally realized as a medium that simultaneously has negative permittivity and permeability at a given frequency [5, 6]. As is well known, the response of a system is determined by the properties of its materials, which are permittivity and permeability . Thus, metamaterials are defined as artificial electromagnetic materials that can control electromagnetic fields if the permittivity and permeability of the materials are suitably engineered [7].Metamaterials are often manufactured as a periodic ensemble of conducting elements such as metallic rings and roads or even spherical particles, which collectively act as an electromagnetic medium with effective permittivity and permeability [6, 8]. Metamaterials have different classes: double-negative (DNE) [9], left handed materials (LHMs) [10], backward-wave (BW) media [11], single index (media with a negative refractive index) [5–7, 12, 13], and

another material property that cannot be found in nature such as the near-zero refractive index [14].

The fundamental concept of metamaterials identifies them as an ensemble of electrically small resonators creating an electromagnetic media; such resonators have varied compositions from spheres to simple wires, which can construct different shapes and will be scalable in geometries. Examples of such resonators are split ring resonators (SRR) and complementary (C), which essentially consist of a broken loop with controllable dimensions to create a tailored response to an electromagnetic field [6]. Metamaterials have been established in technologies in all spectrum bands from radio [15], microwave [6], millimetre wave [16], terahertz wave [17], to near optical [18]. Artificial materials have generated great interest in the scientific and engineering communities, leading to the numerous applications for electromagnetic research, including advanced lenses [12, 19], cloaking [20], energy harvesting [21, 22], and metamaterial-based antennas [23]. However, in some applications, the metamaterial structures are bulky because they are three-dimensional (3D).

1.2 Metasurfaces

A metasurface is a two-dimensional (2D) surface version of a three-dimensional volume (3D) metamaterial, in which the surface is a distribution of electrically small scatters originally named metafilm [24]. The metasurface consists of two-dimensional periodic structures of sub-wavelength scattering particles engineered in a way which reconstructs the incident waves to the desired level of reflection and transmission. Two important aspects of the structure of metasurfaces are the thickness and the periodicity, which are much smaller than the surrounding media wavelength. Metasurfaces have the advantages of having less physical space than 3D-metamaterial structures and are less-lossy structures due to the reduction of volume metamaterials. Additional advantages are that they are light, easy to fabricate, flexible, and reliable [25, 26].

As was already mentioned, metasurfaces are two dimensional periodic structures and they are very thin sheets compared to bulky volume structures. Within this general definition, metasurfaces fall into two different categories. First is metafilm, where the structure is an array of isolated scatters elements following the $'cermet$ topology. The name metafilm was coined for such surfaces in [24]. The second category is metascreen where the arrangement of the scatters elements follow the $fishnet$ topology where the elements are periodically spaced apertures on the surface. The term metascreen is assigned to a homogenous sheet with isolated aperture. Besides these two categories, other kinds of

metasurfaces can be defined based on a mixture of these two extreme kinds [8,27]. Fig.1.1 depicts different classes of materials from ordinary materials to the artificial materials.

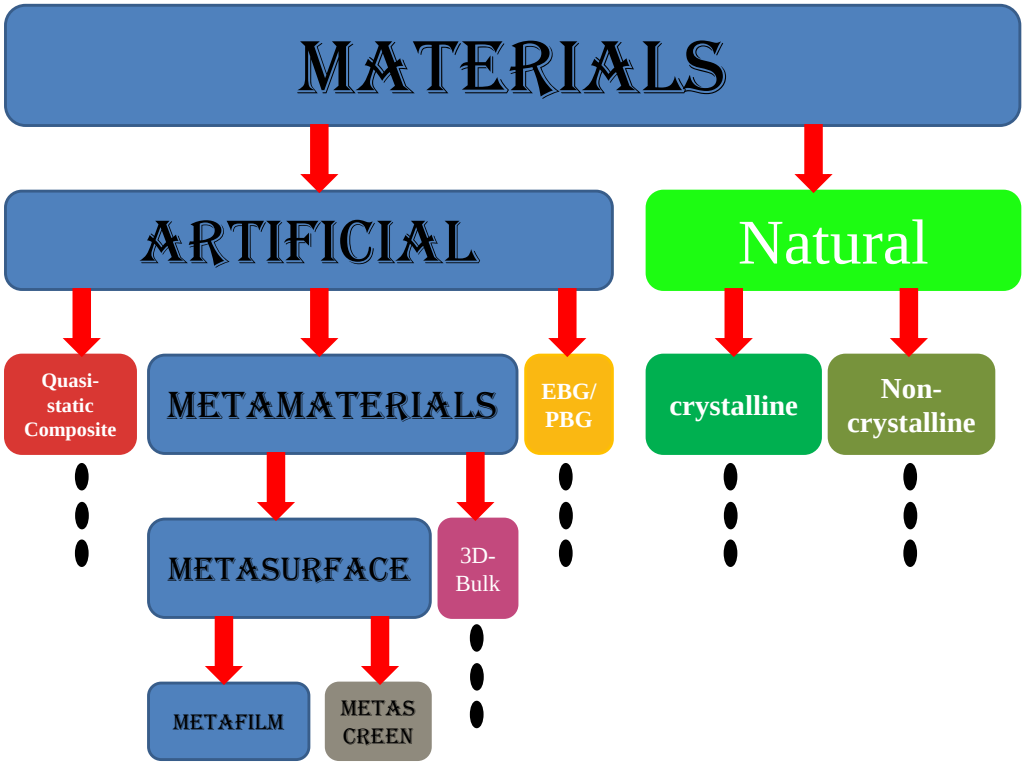

Figure 1.1: Different classes of materials and how the metafilm as a type of metamaterials.

Due to all these features of metasurfaces, there are wide ranges of applications for these surfaces. Along with the features mentioned earlier, the metasurface particles are scalable, which gives the freedom to use them in the desired frequency band. Over the past years, there has been growing interest in the scientific and engineering communities for developing metasurface applications due to their versatility. Metasurfaces have wide potential applications, such as but not limited to: absorbers [28,29], harvesters [30], detectors of microwave radiation [31], microwave-associated organic chemistry [32,33], fluid controllable surfaces [33], to name a few. The most critical application of metasurfaces is as antennas, where it can be used in transmitting mode or in receiving mode (it can be used for both absorbing and harvesting applications).

1.3 Antennas

Antennas with dimensions smaller than the wavelength of free space are typically referred to as electrically-small antennas. This type of antenna has generated much interest especially in wireless communication systems requiring small form factor, which can be applicable for personal communication systems (e.g. headphones, watches, and pagers), military applications, unmanned aerial vehicles, and more [23, 34]. In order to have lightweight, low profile, and inexpensive antennas that would be efficient, easy to build, and easy to integrate with other communication devices, while also having a desirable bandwidth and gain, important and complicated steps must be considered throughout the design procedure. One of these steps is impedance matching of the antenna to the feed circuitry [23,34,35]. Antenna arrays are topological arrangements of antennas that are distanced and phased in such a way to produce higher gain and/or beam scanning in various directions. The array, however, brings a higher-order complexity to the design procedure especially if it needs to be fed by one point [36, 37]. Moreover, electrically small antennas have fundamental theoretical limitations on gain, radiation efficiency, and bandwidth where the antenna size is inversely correlated to the quality factor and the radiation loss as explained in [38].

1.3.1 Conformal Antennas

With the modern drive to improve communication technologies and military applications, conformal antennas have attracted much attention in the past few years. A conformal antenna is one that conforms to a prescribed shape. The antenna can take any curvature shape; usually it is cylindrical [39,40], spherical [41,42], or conical. In conformal antennas, the radiating elements will be either mounted on or integrated into the arbitrary surface [43, 44]. Micro-strip antennas and slot antennas are the most-common radiating elements used in conformal antennas because of their low profile structure and design simplicity [45–47].

In the engineering and science communities, extensive research has been carried out for decades on planner antennas, which have a low profile, high durability and low manufacturing cost. However, the planner antenna arrays are not easy to integrate with certain platforms and have definite drawbacks. A conformal antenna is a non-planner antenna that can be fitted on parts of an airplane, a high speed train, a vehicle, a ship, a missile, and other types of physical entities. The focus now is to utilize conformal antennas on aircraft instead of planner antennas because of their potential to improve aerodynamics when

adjusted to the contour of the vehicles to gain a large field of view and low observability. In [48], a conformal controlled reception pattern antenna with active vibration is built onto an aircraft. Moreover, conformal antennas have high potential for application in mobile communication systems because of their new far field behaviour. Most conformal antenna design provides interesting radiation patterns with wider beams, high gain, and different pattern shapes (for instance, omnidirectional). Conformal antennas are often used for military application because of the advantages of integration with structures, which makes these structures less visible to the human eye. In [10], a conformable antenna is developed for a solider suit and has the ability to transmit and receive signals from up to 2.75 km. However, outside the military the use of conformal antennas in commercial application is rare. In one commercial application, in [46], a conformal antenna is used for remote health monitoring.

A conformal antenna has a different radiation pattern than planner and linear antennas. Therefore, most of the traditional pattern synthesis methods are not valid for conformal antennas [49]. Pattern synthesis is the process of choosing the antenna array parameters that produce the desired radiation characteristics. In other words, it is the optimization process used to achieve desired radiation characteristics. Many optimization techniques have been developed for traditional antenna arrays. The most-common optimization approach used in conformal antennas is the Genetic Algorithm technique. However, the analysis approaches used with antenna structure are typically based on method of moment, finite element method, or finite difference time domain, all of which have fueled a need for a more powerful and versatile computational domain [50–53].

Recently, many studies carried out on conformal antenna array have involved mutual coupling [52–54], broad band and multi band [43, 55], and beam steering [56–58]. Since the dawn of radar in 1940s, beam steering haswidely been used in radar and wireless communication systems. In addition, phased antenna arrays with different beam steering techniques have attracted much attention for planner arrays. Some of these techniques such as phase shifting have been used with non-planner antennas as well [57]. In some antenna array applications it is critical to have a phase shifter to produce phase shifts between the antenna radiators and so gain a directional beam. However, the phase shifter usually costs around half the price of the entire electronically scanned phase array. Also, the phase shifter has a complex design, and it needs sufficient space to integrate with the antenna array, even though the distance between the antenna elements is usually only $\lambda/2$. Also related to the distance between antenna elements, in some applications such as unmanned aerial vehicles (UAVs), high data rate communication is desired, which occur at wavelengths larger than the size of the unmanned aircraft itself. Therefore, conformal, light-weight, low cost, highly reliable and low profile antennas are highly desirable with

the growth of wireless communication system applications.

1.4 Wireless Electromagnetic Energy Transfer (Energy Harvesting)

Nikola Tesla started the concept of wireless power transfer early in 1891, and he performed the first experiment to transmit power without using a wire in 1899 [59]. Sixty four years later, the first microwave Wireless Power Transfer WPT system was demonstrated by Brown [60].The procedure of converting DC power to radio frequency (RF) power and transmitting it through space then collecting the power and converting to DC power again at the receiver is known as power transmission. The idea of collecting RF power and converting it to DC power (microwave energy harvesting) has received much attention lately. In 1968, Glaser introduced the concept of harvesting power from the sun known as Space-Based Solar Power (SBSP). SBSP collects the solar energy (power) by using arrays of solar cells and then converting the solar power to microwave power. By using high directive antennas, this power is transmitted to the earth where large rectenna arrays placed at the receiver site receive the microwave power and convert it back into DC [61].

The rectenna (rectifying antenna) was introduced by Brown of Raytheon Company in the early of 1960. The rectenna systems are fundamentally converting and rectifying the microwave energy into DC current, such systems consist of antenna, rectifying circuit, and RF filter between the antenna and the rectifier circuit [62, 63]. Utilizing rectennas to harness the energy from the space in WPT systems has attracted much interest especially in the aspect of improving the conversion efficiency [64, 65]. Since the conversion efficiency of the WPT mainly depends on the receiving system (collectors), extensive research has been carried out on the subject of rectenna efficiency improvement of the whole system rather than focusing on the main energy collector, which is the antenna.

Energy harvesting or energy scavenging is the process of harvesting readily available energy from the environment or from surrounding systems and converting it to usable electrical energy to, for instance supply electronic devices. The main advantage of using such harvesters is that they improve system efficiency by using waste energy to help power the system; are environmentally friendly, taking the place of batteries that need replacing or recharging; and, above all, they enable new technologies and applications [66–68]. Increasingly research is focussing on what are called smart cities, which are based on wireless sensor networks [69]. A huge number of sensors will be deployed in cities to collect surrounding information. The technology of sensor networks can also be used to monitor

remote areas or under-water locations, with no need for battery replacement if energy harvests are used [67, 68]. Along with the applications mentioned above, energy harvesters can also be used in many small applications and technologies such as health monitoring sensors [70], spinal cord injury evaluator [71]. and microaccelerometers [72], etc.

The energy harvesters in all the above applications are being introduced to replace the main energy source in those electronic devices, the battery, with its limited lifetime and need for regular replacement or recharging. Such sensors need to be self-sustaining, with the ability to gain energy from existing sources such as, but not limited to, solar, thermal, vibration, and electromagnetic (EM) [68, 73]. Electromagnetic energy harvesting is a very promising solution for future supplying power to autonomous electronic devices. EM harvesters are also the focus of much attention because urban areas are strongly backed with EM waves at different frequency bands, produced by the ubiquitous presence of television stations, FM radios, Bluetooth devices, cell phones and other communication devices, WiFi stations, and much more. Among all the applications mentioned, some need to absorb energy rather than harvest it [67, 68].

Based on all above-mentioned applications, an efficient collector of electromagnetic energy is desirable. Maximizing the conversion efficiency, minimizing the footprint, and channeling and collecting the power are the most important and critical objectives in electromagnetic energy harvesting. Recently, much attention has been paid to the use of metamaterial cells as collectors toward higher conversion efficiency in both microwave [21, 74] and infrared regimes [22].

1.5 Imaging

Imaging objects has gained much interest long time ago. X-ray and ultrasonic are the most effective imaging methods that have been used over the years for diagnostic anomalies, cracks, pores, etc. However, despite significant progress in improving these techniques, persisting limitations result in relatively high false negative and false positive rates. For instance, finding cracks in thick aluminum walls; X-rays can find surface cracks, but not ones deep inside thick bodies; moreover, X-ray techniques are usually unreliable because they need two-way access and stringent safety procedures. Ultrasonic methods, on the other hand, can detect discontinuities in heavy aluminum parts; however, most are single point (single transducer) methods. Ultrasonic methods have difficulty diagnosing anomalies in thin or rough materials and in irregular shaped materials [75–77].

Because of their ability of penetrating various materials, microwaves imaging techniques have gained increasing interest in large domains such as but not limited to non-destructive

testing, civil engineering and medical application. Microwaves have ability to detect the presence and shape of hidden or buried objects [78, 79]. Essentially, the main advantage of microwave imaging method over others is that microwave determine the differences in physical properties that affect electromagnetic propagation in inhomogeneous media. Most importantly, microwave methods are highly sensitive to humidity because of the high dielectric constant of water, and this sensitivity helps to find spots where water pervades composite structures.

Imaging based metamaterials have been studied and investigated in various methods and frequency spectrums [80–82]. In [82, 83], microwave imaging based on complementary split ring resonators (CSRR) is used to define any anomalies and defects in composite materials. CSRR is electrically very small and scanned over the objects to find any changes in the materials under test. The authors in [84] proposed metamaterial imaging based on waveguide probes and take advantage of these probes sensitivity to near field communication. Another interesting method proposed in [80], metamaterial aperture, fed by one source or a small number of sources, is used to produce a complexe.g., pseudorandombeam pattern that illuminates large portions of the target

1.6 Research Problem

The pursuit of light weight, low profile and inexpensive antennas is not new. Currently, electrically small antennas have a wide variety of applications. However, such antennas have fundamental theoretical limitations on gain, radiation efficiency, and bandwidth. Due to these limitations and the need for small antennas, and due to the availability of metasurfaces and their features, this work introduces a new antenna concept based on metasurfaces. This antenna has strong potential in a variety of traditional and non-traditional applications where its flexible design (high degree of optimization freedom) facilitates use on a variety of platforms. Therefore, the contribution in this section of the work is focused on the following:

1. **Analyze and Study** conventional antennas and their properties.
2. **Analyze and Study** the use of metamaterial to miniaturize conventional antennas as well as the use of enhancing antenna properties such as gain and directivity.
3. **Introduce** a new concept of antennas design based on metasurfaces to achieve distinctive characteristics.

4. **Analyze and Study** the comparison between the new metasurface antennas and conventional antennas.

5. **Analyze and Study** the circular polarization and gain enhancement for the new antenna.

6. **Utilizing** the new antennas for beam steering.

7. **Extend** the concept of the new antenna to operate in higher frequency regime.

8. **Introduce** new conformal antenna arrays that can be fitted to non-planar surfaces and will resemble the shape of the body to which they are attached.

9. **Study** Huygens' Principle.

10. **Analyze and Study** different conformal antenna curvature examples.

The proposed concept is further applied to metasurface energy harvesters. The idea here is to use harvesters as collectors instead of conventional antennas such as the one mentioned in conjunction with a rectenna for wireless power transfer systems. Moreover, harvesters have a variety of applications in different fields such as wireless network sensors; they could replace batteries, leading to environmentally friendly (smart) cities. To supply these sensors, a very small amount of power is needed. Metasurface harvesters are excellent candidates for utilizing such sensors and replacing the batteries. The metamaterial collectors proposed in previous works are very efficient on harvesting electromagnetic energy by using finite structures, but challenges and complexity arise at the measurements stage, because each metamaterial collectors work individually. To address these problems, metasurface harvester arrays are introduced that harvest microwave receiving energy and then channel it to one load, thereby increasing the energy density per rectification circuit. Therefore, the contribution in this section of the work is focused on the following:

1. **Analyze and Study** the conversion efficiency of the collectors in the rectenna systems, which are classical antennas.

2. **Analyze and Study** the conversion efficiency of the electromagnetic energy collectors based on metamaterials.

3. **Introduce** metasurface harvester arrays that harvest the microwave energy and then utilize a new mechanism by which the energy is received by the metasurface array channels to one load only through transmission lines.

4. **Analyze and Study** rectification circuitry for measuring DC output of the proposed harvesters.

5. **Propose** near unity conversion efficiency metasurface harvesters based on the concept of perfect absorbers, and the microwave received power channelled to one resistive load as well.

6. **Propose** different feed networks topologies to deliver the maximum collected power to one resistive load.

7. **Analyze and Study** the difference between simulation, AC and DC results of the two proposed harvesters.

Another critical application for metasurfaces is imaging. Therefore, we extended the concept of measurface antenna to have these antennas as receivers and each small resonators acts as a pixel. The work in literature have used metamaterials for microwave imagining based on scanning techniques. To address some of literature issues, we proposed metasurface imager that image objects without any need of using scanning techniques.

1. **Study** other imaging techniques.

2. **Analyze and Study** microwave imaging techniques.

3. **Introduce** metasurface imager that images objects without any scanning.

4. **Analyze and Study** various examples with different composite materials.

1.7 Dissertation Outline

The remaining of this dissertation is outlined as follows:

Chapter 1 reviews the relevant literature and discusses metamaterials and their applications. This chapter also sheds light on the motivation and contribution of this work.

Chapter 2 proposes a new and novel generation of antennas. Using metamaterial particles as electromagnetic radiating elements. The antenna proposed to work in the microwave regime. Both numerical and experimental results showing a validation of the proposed antenna.

Chapter 3 In most works, new paradigm ideas need to be compared with existing ideas if there are some. Therefore, this chapter presents a comprehensive study comparing the

new novel antenna with classical antennas. Furthermore, the new antenna was redesign it to operate in V-band and to see how valuable in other regimes.

Chapter 4 presents new conformal antennas based metasurfaces and a comprehensive study with different antenna shapes is been presented in this chapter.

Chapter 5 introduces a new breakthrough electromagnetic energy harvesting based on metasurfaces. This method is utilizing a corporate feed network to connect all electromagnetic collectors to one load. In this chapter, both radiation to AC and radiation to DC were calculated through the simulations and experiments. Rectifier circuitry introduced as well to have radiation to DC measurements.

Chapter 6 presents a combination of the method in 5 and a method in the literature to control and increase the power conversion efficiency of these harvesters. Numerical and experimental results show higher conversion efficiency can be achieved.

Chapter 7 studies the feasibility of metasurfaces in a very critical application which is imaging. This chapter parents a novel idea of imaging objects without need for scanning while the object in the footprint area of the sensor.

Chapter 8 concludes the work and outlines remaining challenges and possible topics for future work.

Chapter 2

Metasurfaces Antenna

2.1 Introduction

In this chapter, a true metasurface antenna based on electrically-small resonators is proposed. The resonators are placed on a flat surface and connected to one feed point using corporate feed. Unlike conventional array antennas where the distance between adjacent antennas is half wavelength to reduce mutual coupling between adjacent antennas, here the distance between the radiating elements is electrically very small to affect good impedance matching of each resonator to its feed. A metasurface antenna measuring $1.2\lambda \times 1.2\lambda$ and designed to operate at 3GHz achieved a gain of 12dBi. A prototype was fabricated and tested showing good agreement between numerical simulations and experimental results. Through numerical simulation, we show that the metasurface antenna has the ability to provide beam steering by phasing all the resonators appropriately.

2.2 Metamaterial and its Potential for Antennas

Over the past few years, metamaterials have been used in many different ways to miniaturize antennas, such as complementary split ring resonator (CSRR) loaded antenna [85], slotted complementary split-ring resonator (SCSRR) [86], and artificial magnetic materials with fractal Hilbert inclusions [87]. Moreover, metamaterials have been used as an effective medium to enhance the conventional antennas gain [88] and directivity [89] rather than consider it as the main radiators. Metamaterial based antennas were proposed earlier to develop small antennas by miniaturizing the antenna size while maintaining good antenna

performance [23,35]. However, pure metamaterial antennas have not been presented up to now.

In this chapter, the first generation of metasurface antennas operating in the microwave regime is presented. Unlike classical and traditional antennas where radiation is initiated by enhanced concentration of current density by exploiting wavelength-based resonance, the metasurface antenna concept presented in this work is based on an ensemble of electrically-small resonators whose resonance strongly resembles classical circuit resonance, however with the difference that the impedance elements have spacial dimension thus allowing coupling to external fields. The ensemble of the electrically-small resonators gives high degree of freedom for controlling the magnitude and phase of the current over a large portion of the metasurface. While each of the resonators does not constitute a good radiator if it were considered individually, the ensemble of elements acting together provide excellent radiation characteristics facilitated by good impedance matching due to tailored inter-element coupling.

2.3 Design Methodology

The particular electrically-small resonators chosen for demonstrating the metasurface antenna concept are the electrical ring resonator (ERR) reported earlier in the literature [90]. Arranging a periodic array of these symmetric metallic elements will create a class of sub-wavelength particles which exhibit a strong resonance response to the electrical field and negligible response to the magnetic field. We propose a feed network to connect all radiators to one feed point. The feed network was designed in a way to match the radiators impedances to the feed impedance to ensure optimal antenna gain and bandwidth.

The commercial program CST Microwave Studio 2013 Maxwell equations solver was used to model the proposed antenna [91]. In order to examine the ERR behavior, to simulate the S-parameters response to achieve minimum return loss (S_{11}), and to find the surface impedance of the cell at $3GHz$, the ERR was placed in the center of a waveguide with perfect electric wall in the $x-z$ plane and perfect magnetic wall in the $x-y$ plane to realize TEM mode excitation in the z-direction (using two open ports in the z-direction). These boundary conditions were chosen to force the incident electric and magnetic fields to be parallel to the structure surface (see Fig.2.1). From the impedance results obtained, it is evident that the media provided a surface having an impedance of 377Ω at the operating frequency, as shown in Fig.2.3. This indeed gives validation that the antenna surface acts as a metasurface since it can be successfully be represented by an equivalent surface with a homogenous permittivity and permeability

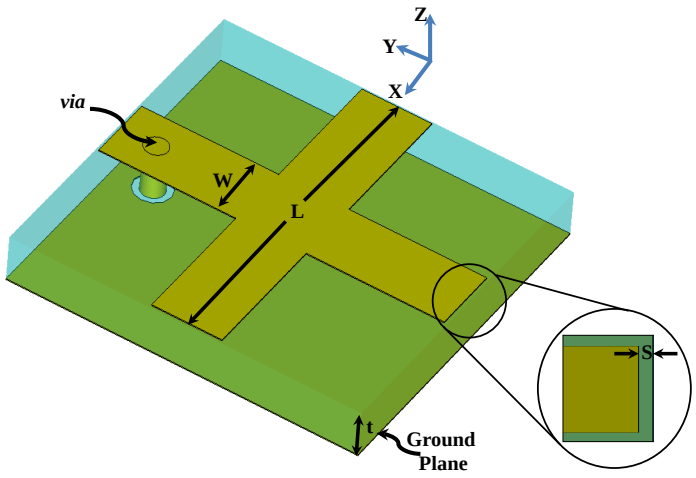

Figure 2.1: A schematic showing the proposed unit cell of a metasurface antenna and its optimized dimensions as well as the placement of the via.

A via with diameter of $d = 0.5mm$ was chosen due to the fabrication constraints which required a via size of $0.5mm$ to channel the current to the load. The optimal via position is heuristically optimized and it is shown in Fig.2.3. From the results, a via position of around $5mm$ away from the center of the cross resonator and a via size of $0.5mm$ provided a reflection coefficient of less than $10dB$ at the operating frequency. The load resistance was chosen to be 200Ω to simplify the feeding network design. By doing so, one can design the feeding network with minimum number of stages to arrive at the impedance of the feed port of 50Ω. Of course, other feed networks could be chosen, but it is advantageous to choose impedance levels that avoid the need for very thin transmission line widths which are challenging to fabricate and thus can lead to measurements uncertainties.

2.4 Metasurfaces Antenna Design

The metasurfaces antenna presented here is an array of 8×8 ERR elements periodically arranged on a square substrate with total dimensions 12cm×12cm as shown in Fig.2.4(a). Each resonator has a 200Ω input impedance which was adjusted by careful tuning of the inter-element spacing and geometrical dimensions of the resonator. All radiators were connected to one feed port having a 50Ω input impedance. A matching circuit based on

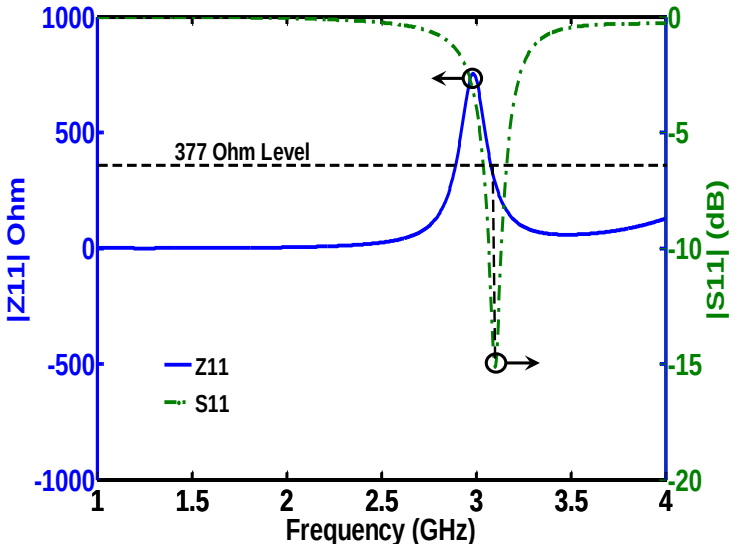

Figure 2.2: Surface impedance of the metasurface at the resonance frequency. The surface impedance was calculated over a range of frequency depends on the permittivity and permeability of the cell. The blue curve shows the surface impedance magnitude of the cell and the green curve shows the return loss magnitude of the cell.

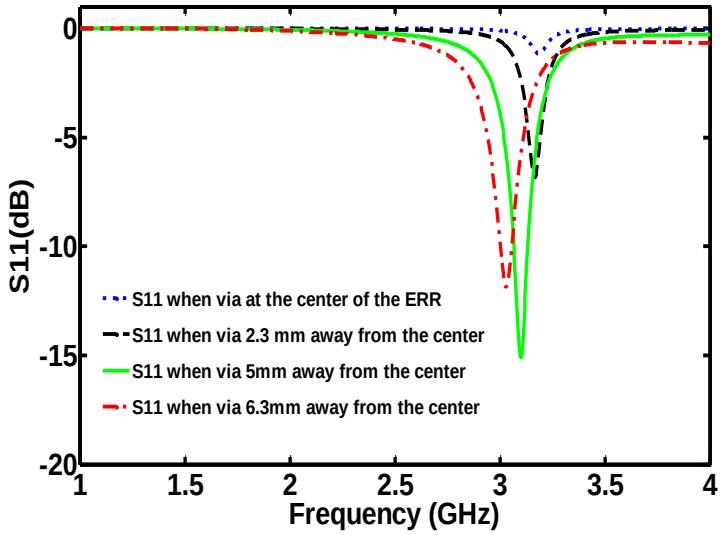

Figure 2.3: Dependence of $|(S_{11})|$ on the via position.

microstrip transmission lines is used to connect all the elements to one 50Ω feed port. Unlike conventional antennas where the antennas are typically separated by a distance of half wavelength which allow for sufficient space within the antenna structure to build the feeding network for the metasurface antenna, the distance between the radiating elements is very small which cannot fit the feeding network. Therefore, a 1mm thick Rogers RT5880LZ substrate with a dielectric constant of 1.96 and a loss tangent of 0.002 (at the chosen operating frequency) was added to the structure. Fig.2.4(b) shows the corporate feed network that was used to connect all radiators to a 50Ω feed port. In this arrangement, all radiating elements were fed in phase in order to achieve highest gain in the z-direction (broadside). The width and length of the traces were calculated using the following equations [92].

$$W = d\frac{8e^A}{e^2A - 2} \qquad for\frac{W}{d} < 2$$

$$W = d\frac{2}{\pi}[B - 1 - \ln(2B - 1) + \frac{\epsilon_r - 1}{2\epsilon_r}(\ln(B - 1) + 0.39 - \frac{0.61}{\epsilon_r})], \qquad for\frac{W}{d} > 2$$

$Where$

$$A = \frac{Z_0}{60}\sqrt{\frac{\epsilon_r + 1}{2}} + \frac{\epsilon_r - 1}{\epsilon_r + 1}(0.23 + \frac{0.11}{\epsilon_r})$$

and

$$B = \frac{377\pi}{2Z_0\sqrt{\epsilon_r}}$$

ϵ_r is dielectric constant, d is the substrate thickness, Z_0 is the characteristic impedance, and W is the microstrip line width. Guided wavelength is

$$\lambda_g = \frac{\lambda_0}{\sqrt{\epsilon_{re}}} \qquad or \qquad \lambda_g = \frac{300}{f(GHz)\sqrt{\epsilon_{re}}}$$

Where λ_0 is free space wavelength and ϵ_{re} is the effective dielectric constant which is given by

$$\epsilon_{re} = \frac{\epsilon_r + 1}{2} + \frac{\epsilon_r - 1}{2}\frac{1}{\sqrt{1 + 12\frac{d}{W}}}$$

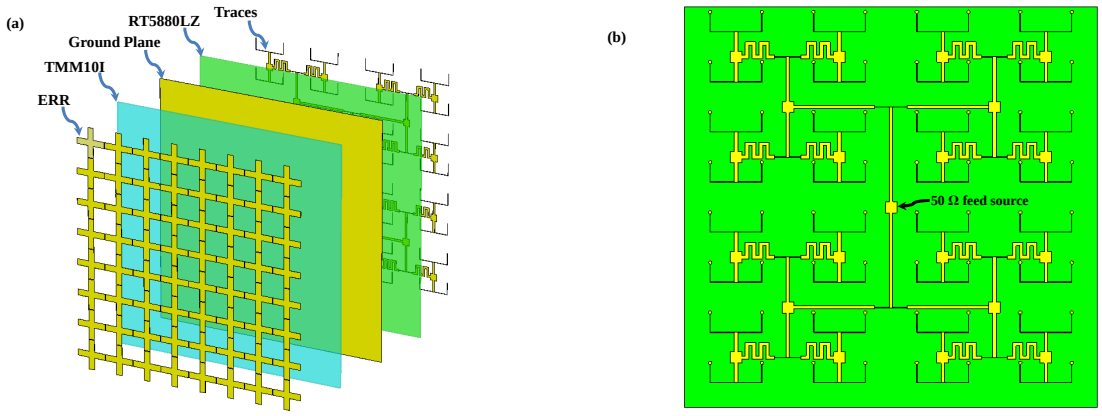

(a) (b)

Figure 2.4: Architecture of the proposed metasurface antenna. (a) Diagram of the antenna elements is shown as exploded view, including the electrical ring resonators, Rogers TMM10I substrate as first substrate, ground plane (copper), Rogers RT5880LZ as second substrate, and the transmission line traces. (b) Symmetrical configuration of the corporate fed array (64-element).

2.5 Simulation Results

Fig.2.5 shows the simulated current, which is observed to be distributed uniformly over the metasurface. As shown, the current is high in one direction of the ERR and low in the other direction because each element was excited by a via placed at one side of the y-directed arm of the resonator (see Fig.2.1). The asymmetry in current distribution on the ERRs at the top and bottom edges of the metasurface is because the input impedance of those ERRs are slightly different from 200Ω. The simulated 3D gain radiation pattern of the metasurface antenna is shown in Fig.2.6. The gain, directivity, and the radiation efficiency at $2.97GHz$ were found to be $11.7dBi$, $12dBi$, and 91.5%, respectively. The uniformity of the current distribution and its highly directional intensity is responsible for the achieved high antenna directivity.

2.6 Experimental Verification

An 8×8 elements metasurface antenna was fabricated based on the simulated design, as in Fig.2.7. All 64 radiators were connected together to a 50Ω feed point as shown in

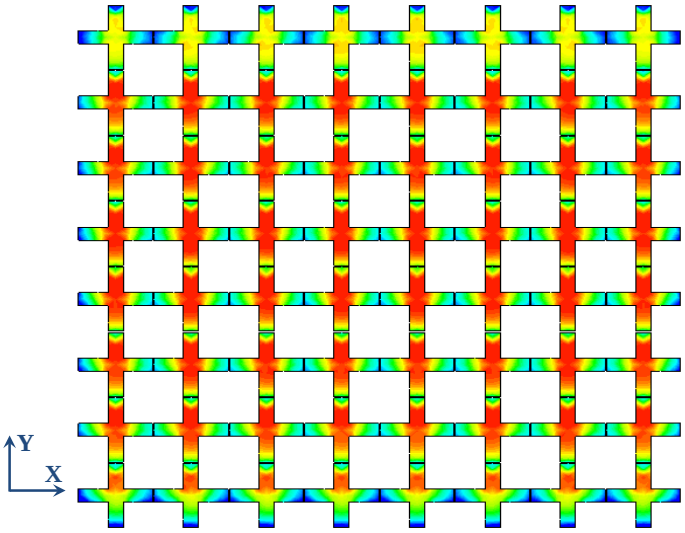

Figure 2.5: Current distribution on the ERRs at the resonance frequency of 2.97GHz. The highest intensity (red) corresponds to 138 A/m and the lowest intensity (blue) corresponds to 0 A/m.

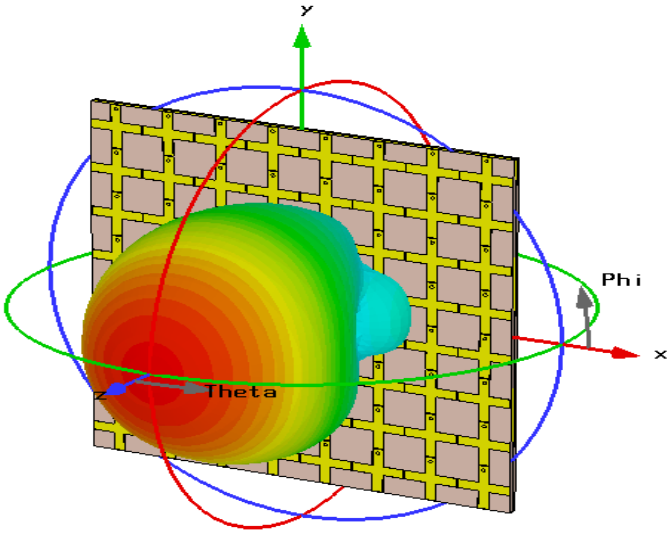

Figure 2.6: The simulated 3D gain radiation pattern of the metasurface antenna. The highest intensity (red) corresponds to 11.7 dBi and the lowest intensity (blue) corresponds to -28.3 dBi.

Fig.2.7(b). A vector network analyzer was used to measure the return loss (S_{11}) at the structure feed point. The measurement results were compared to the simulation results which are presented in Fig.2.8. Good agreement is observed between simulation and measurement with approximately $15MHz$ shift in the resonance frequency. We observe that the measurement gives wider bandwidth than the simulation.

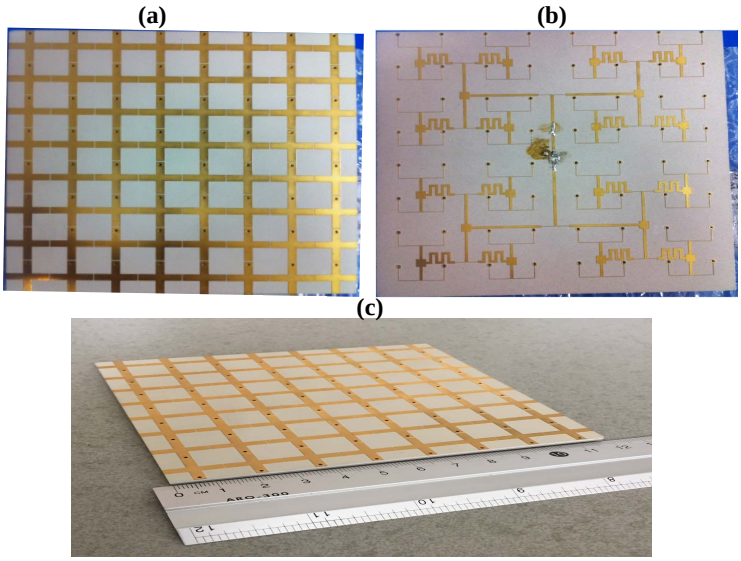

Figure 2.7: Photograph of the fabricated metasurface (a) top view (b) bottom view and (c) perspective view.

Measurements of gain were performed in an anechoic chamber, see Fig.2.9. The metasurfaces antenna was placed approximately four meters away from a standards horn antenna to ensure the incident field at the metasurface antenna is a far-field. Considering the linear polarization of the antenna under the present feed design, the metasurface antenna was positioned such that the radiated electric field was parallel to the section (strip) of the ERR resonators in which the vias were located as shown in the Fig.2.1. The gain was measured over a frequency range from $2GHz$ to $4GHz$ in $50MHz$ increments with highest gain of 9.4 dBi obtained at $2.95GHz$. Fig.2.10 shows the measurement and simulation gain plots.

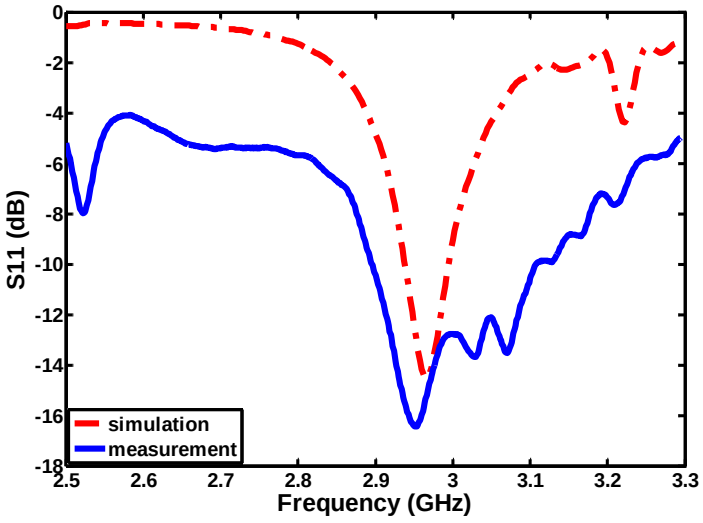

Figure 2.8: Simulated and measured results of the return loss of the metasurface antenna.

2.7 Discussion

Several factors contributed to the slight variation between the experimental and simulation results. The second layer of the structure was chosen to have very low dielectric constant (RT5880LZ) because the transmission line width needed to achieve specific impedance is highly sensitive to the dielectric constant of the material. The transmission line widths were calculated using standard microstip transmission line equations which were based on approximations. Furthermore, the RT5880LZ substrate was difficult to etch resulting in small miss-alignments and line-width discrepancies in the final design. The second reason is that the calibration was set it up for the antenna without any extra connecters, while our antenna has extra coaxial connecters and SMA's. Moreover, of the calibration reason is that frequency was set it up to change every $50MHz$ from $2GHz$ to$4GHz$to obtain the gain over wide frequency range, as the simulation results illustrate that the highest gain will be at $2.965GHz$. We also believe if we change the frequency every $10MHZ$ the results will be much better, but the measurements for more points will require more time to be finished. Finally, the ailment between the antennas was completed manually (visually), leaving room for human error.

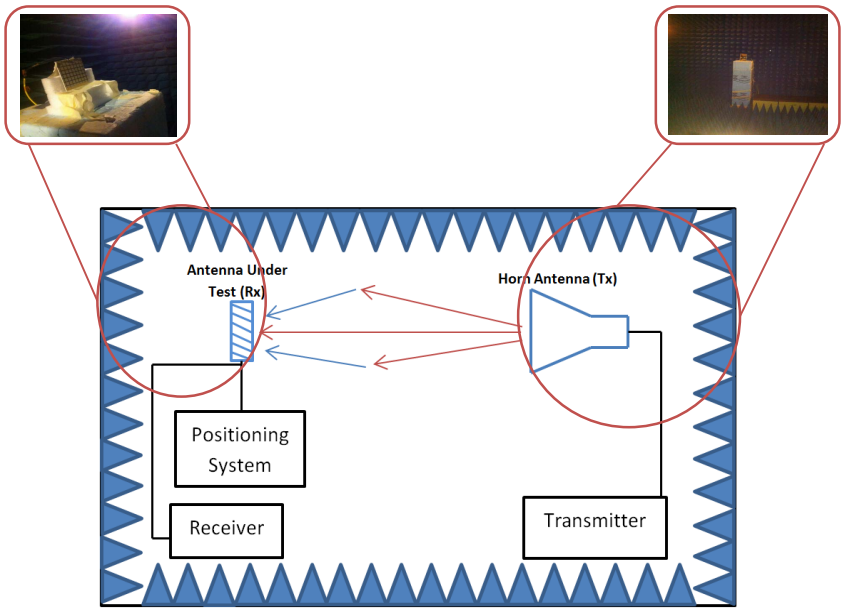

Figure 2.9: The gain measurement setup used in the experiment.

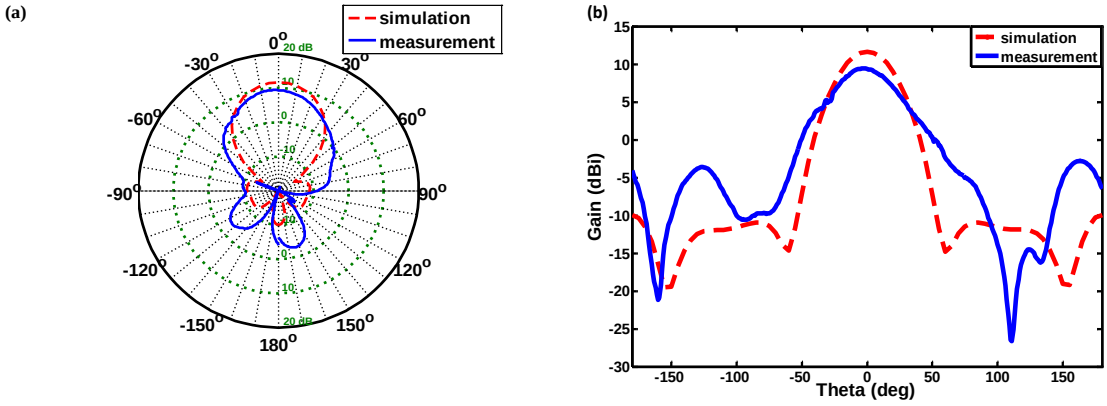

(a) (b)

Figure 2.10: Simulated and measured radiation pattern (a) Polar radiation pattern (b) Cartesian radiation pattern.

2.8 Conclusion

A new concept for antenna design based on metasurface is introduced. While each electrically-small resonator/element of the metasurface is a poor radiator if acting alone, the ensemble of elements work in synergy, including balance of the impedance of each element, to create highly directional antenna. We demonstrated the metasurface concept using simulation and laboratory measurements. The metasurface antenna has strong potential in variety of traditional and non-traditional applications where its flexible design (with a high degree of optimization freedom) facilitates its use on a variety of platforms.

Chapter 3

Metasurface Antenna Features

3.1 Introduction

This chapter investigates the features of our metasurface antenna and compares them to those of classical antennas. First, the metasurface antenna is compared with microstrip patch antennas in terms of gain and physical size. Simulation results show that the new antenna has the advantage in both categories. Next, a technique by which the gain can be enhanced is studied, as well as the feature of increasing the gain incrementally by adding additional elements. The beam steering scanning is investigated and shows the strong capability of the metasurface antenna to steer in both theta and phi planes with wide scanning range. This allows the antennas ability to be circularly polarized investigated. The last feature studied in this chapter is to design a metasurface antenna in higher frequency bands; V-band metasurface antenna designed and simulated.

3.2 Comparison of the Metasurface and Classical Antennas

Different classical patch antennas have been designed for comparison with the new antenna. The same footprint is used for all the antennas the distance between the patches is $\lambda/2$ and the distance between the patches and the edges is $\lambda/4$; thus, only one patch antenna operating at $3GHz$ can fit in this footprint. Therefore, the physical dimensions of the substrate had to be increased, and without considering the $\lambda/4$ distance to the edge,

Table 3.1: Comparison of simulated gain for two different material patch antennas with diferent distributions.

Patches	RT5880 Size(mm^2)	RT4003 Size(mm^2)	RT5880 Gain(dBi)	RT4003 Gain(dBi)
1×1	120×120	120×120	6.92	5.825
1×2	120×120	120×120	7.942	7.12
2×2	120×132.2	124.2×132.6	11.76	11.10

so as to fit 2×2 elements. Two different substrates were designed with three different distributions of elements. Table 3.1 shows the simulation results for the classical patch antennas. Fig.3.1(a) depicts the microstrip patch antenna on a Rogers RT5880 substrate; the patch dimensions were obtained by the microstrip patch antenna calculator [93] to operate at $3GHZ$. The dimensions were found to be width $W = 39.5mm$ and the length $L = 32.9mm$. Fig.3.1(b) depicts the somewhat larger substrate needed to fit four patches with their feeding network.

A comparison between the proposed antenna and the classical antenna showed that both produced similar gain when four patches are considered without taking distance to the edge into account. The metasurface antenna has a smaller dimensional size than the classical antenna.

3.3 Gain Enhancement

The gain is the key parameter of any antenna,and combines the antenna's directivity and the efficiency. In the metasurface antenna, the best way to enhance gain is to control the current distribution on the elements. The current is distributed uniformly on the elements, except the ones at the edges. The asymmetry in current distribution on the ERRs at the top and bottom edges of the metasurface occurs because the input impedance of those ERRs is slightly different from 200Ω. To overcome this issue, small strips are added at the top and bottom edges to affect ERR impedances, resulting in uniform current distribution on all ERRs. A slightly higher gain is achieved with approximately $0.5dBi$ enhancement, as shown in Fig.3.2.

The second feature of using this metasurface antenna is that the gain of the metasurface antenna can be increased incrementally by adding additional elements. For instance, through numerical simulation, a 10×10 element metasurface antenna achieved a gain of $13.5dBi$. This feature gives flexibility over how much gain one needs instead of the waste

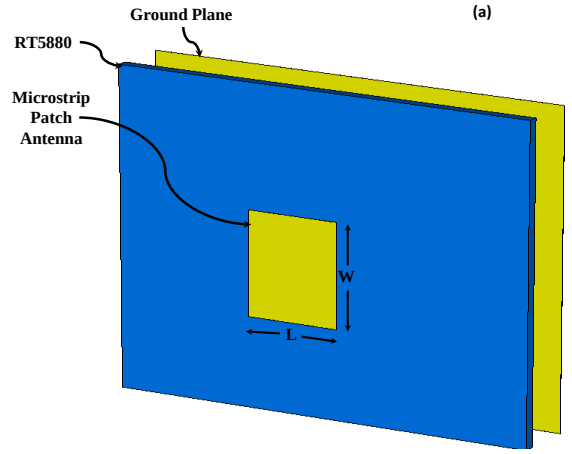

(a)

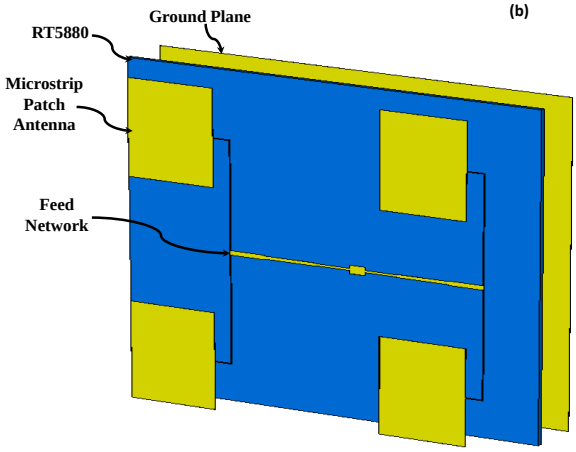

(b)

Figure 3.1: Architecture of the classical antenna (a) microstrip patch antenna operates at 3 GHz , (b) Four microstrip patch antennas operate at $3GHz$ and connecting to one source by a feeding network.

the extra gain that occur when a classical antenna is used, since in classical antennas, the gain increases by a certain value (not incrementally).

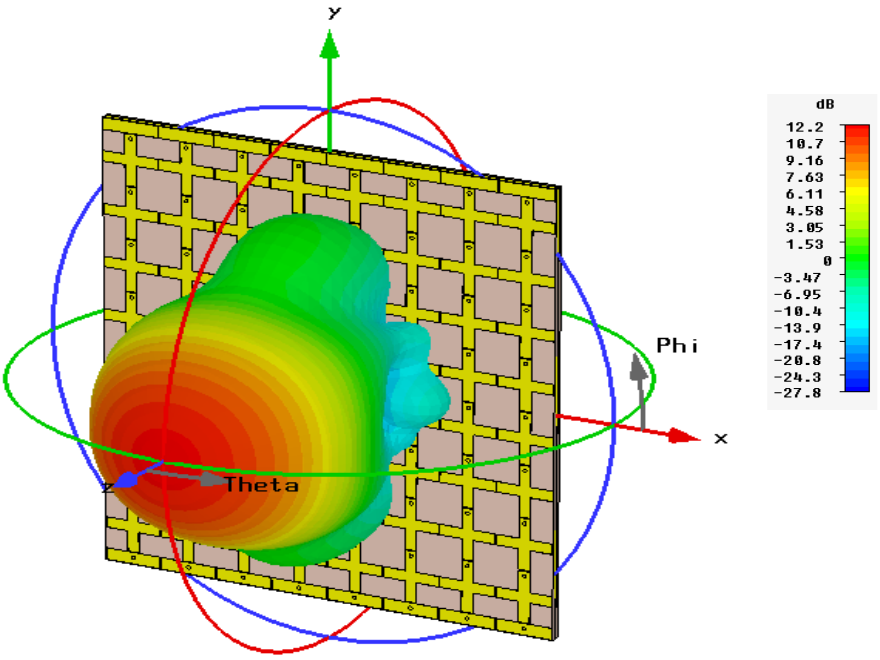

Figure 3.2: The simulated 3D gain radiation pattern of the 8×8 ERRs metasurface antenna. The highest intensity (red) corresponds to $12.22dBi$ and the lowest intensity (blue) corresponds to $-27.8dBi$.

3.4 Beam Steering

Beam steering is one of the most important features of antennas as it has a wide range of applications such as radar, satellite communication, radio astronomy, high-speed 5G cellular communication, automotive radar, imaging, sensing, to name few. The antenna can be used for scanning by varying the phase across the electrically-small resonators comprising the metasurface. In this work since the resonating elements were positioned very tightly next to each other, strong coupling between them precludes the use of antenna array theory to predict the scan angle. To scan in θ (see Fig.3.2), the elements along the x-axis were phased progressively while the elements along the y-axis had a constant phase. Fig.3.3 shows the scanning potential of the 8×8 element metasurface used in this work. While the gain is observed to slightly decrease with increasing scan angle, scanning is achieved despite the relatively small footprint of the antenna. The metasurface antenna is also capable of scanning in θ and ϕ by simultaneously phasing the elements along the x- and y-directions.

Finally, we note that the metasurface antenna can be used on irregular (non-Cartesian) platforms such as curved surfaces of air vehicles or the human body. Fundamentally, the radiation pattern can be tailored to achieve optimum performance by optimization of the phase of the N $\times$ N elements. Such a high degree of design freedom is not present in classical single element antennas. In fact, the tailoring of the phase to achieve desired gain in a specific direction has resemblance to the concept of metamaterial Huygens' surfaces [94] and designer metasurface for flat optics [95]. In those works, the metasurfaces provided control of electromagnetic wavefronts across electrically-thin layers. Here, the metasurface antenna generates the desired wavefront by direct manipulation of the phase of each element comprising the metasurface.Fig. 3.4 shows the 3D scanning in the $\phi = 0°$ plane and Fig. 3.5 shows the 3D scanning in the $\phi = 45°$ plane.

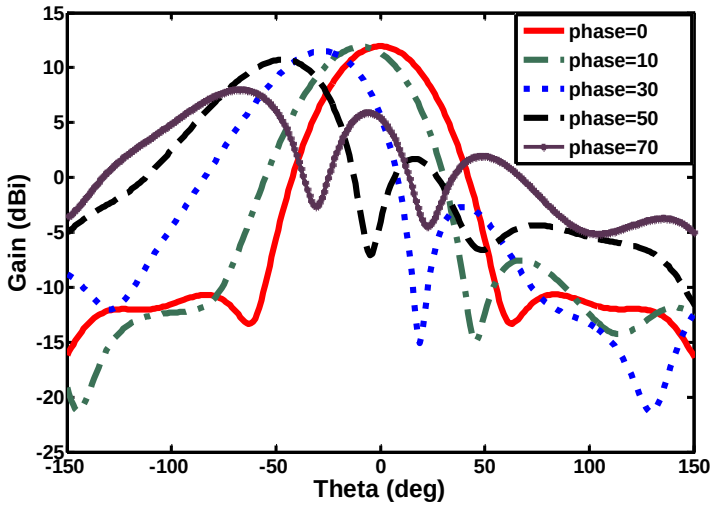

Figure 3.3: Scanning potential of the metasurface antenna obtained using numerical simulation. Correspondence between the progressive inter-element phase and the scan angle with maximum gain is as follow: Phase = 10° corresponds to θ= 9°, Phase = 30° corresponds to θ= 28°, Phase = 50° corresponds to θ= 47°, and Phase = 70° corresponds to θ= 66°.

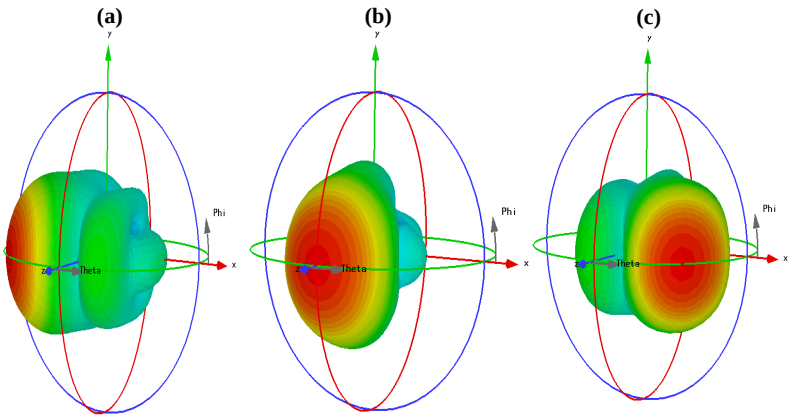

Figure 3.4: 3D scanning in $\phi = 0°$ plane, (a) Phase = 30°, (b) Phase = 0°, (c) Phase = -30°.

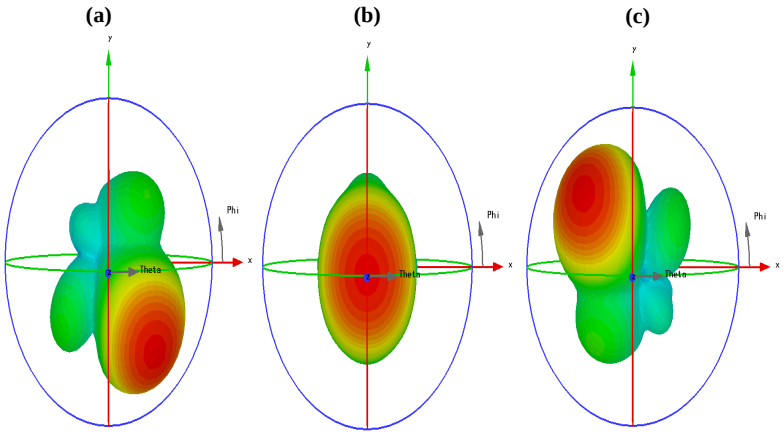

Figure 3.5: 3D scanning in $\phi = 45°$ plane, (a) Phase = 30°, (b) Phase = 0°, (c) Phase = -30°.

3.5 Circular Polarization

There are three different types of polarization: linear, circular, and elliptic polarization. The metasurface antenna mentioned above is linearly polarized, but it has the feature of being circularly polarized. We call an antenna circularly polarized if it consists of two perpendicular plane waves equal in magnitude and 90° different in phase. The polarization properties here were investigated by the axial ratio, which is the ratio of the orthogonal E-fields. Because the fields are equal in magnitude and 90° out of phase, the axial ratio is $0dB$. Fig.3.6(a) shows the axial ratio of the metasurface antenna linearly polarized (the axial ratio in the Z-direction is approximately $40dB$), while Fig.3.6(b) shows the axial ratio of the metasurface antenna circularly polarized (the axial radio in the Z-direction is approximately $0dB$).

3.6 A V-Band Metasurface Antenna

An array of 20×20 electrically small resonators arranged on Rogers substrate was designed to operate at 51 GHz. The antenna occupies an area footprint of $20 \times 20mm$ and the numerical simulation shows as high gain as $21Bi$ achieved by this small antenna. The new antenna has the ability of tuning the gain through incrementally adding additional elements and also able to have maximum gain in any practically any direction in the half plane.

3.6.1 Antenna Design

Figure.3.7 shows the unit cell considered in this work. The cell consists of two split-ring resonators sharing a common side, a dielectric substrate and a ground plane. The unit cell is hosted on top of a $t = 0.127mm$ thick Rogers RT5880 substrate with a dielectric constant of $\epsilon_r = 2.2$ and a loss tangent of $tan\delta = 0.0009$. For resonance at 51 GHz, the geometric dimensions of the unit cell optimized. The strip length $L = 0.9mm$, strip width $W1 = 0.2mm$, width of the parallel wire $W2 = 0.2mm$, split gap $g = 0.1mm$, separation distance $S = 0.05mm$, and copper thickness 35μm. The optimized input impedance of each resonator excitation was 125Ω.

While each electrically-small resonator is a poor radiator if acting alone, the ensemble of elements acting together provides excellent radiation characteristics. The proposed

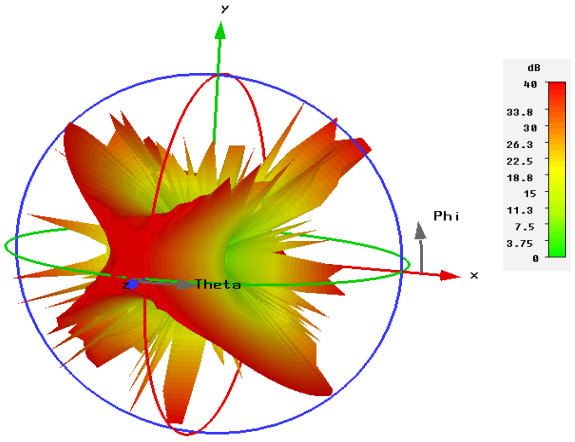

(a)

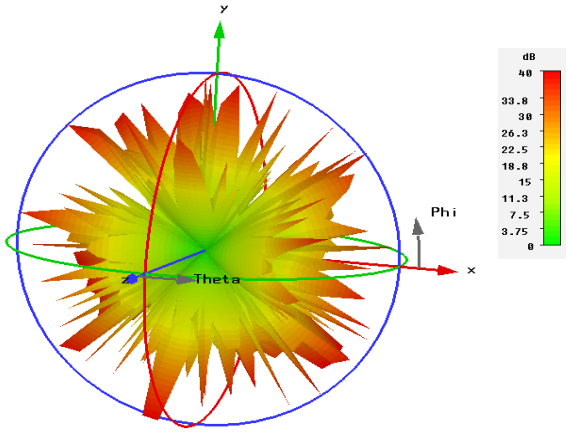

(b)

Figure 3.6: the axial ratio of the metasurface antenna (a) linearly polarized (b) circularly polarized.

metasurface antenna presented in this work is an array of 20×20 electrically small resonators periodically arranged on a square substrate with total dimensions of $20\text{mm} \times 20\text{mm}$ as shown in Fig.3.8. Each resonator has a 125Ω input impedance which was adjusted by careful tuning of the inter-element spacing and geometrical dimensions of the resonator.

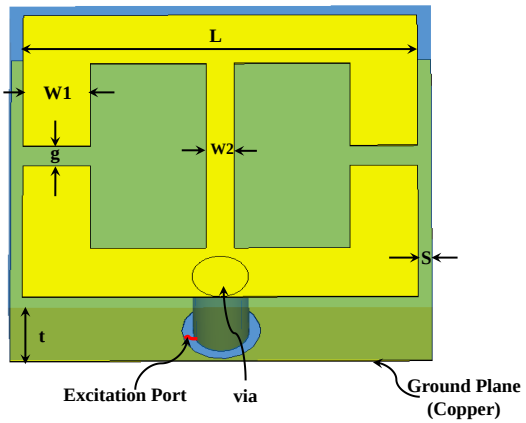

Figure 3.7: A schematic showing perspective view of the proposed unit cell of a metasurface antenna

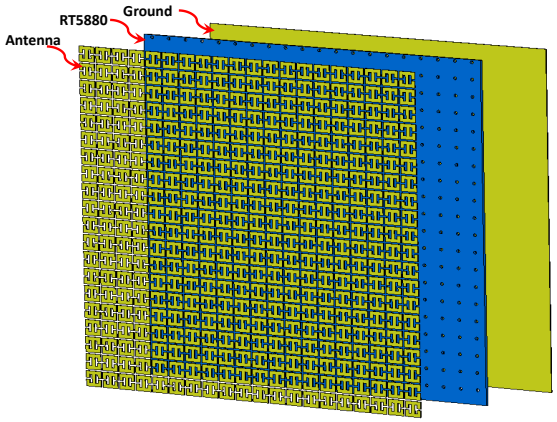

Figure 3.8: Diagram of the 20×20 antenna elements is shown as exploded view, including the electrically small resonators, Rogers RT5880 substrate as a hosting substrate, and a ground plane (copper)

3.6.2 Numerical Results

In order to examine the antenna behavior, the S-parameters response simulated. Figure.3.9 shows the achieved minimum return loss (S11) which is matched at 51 GHz.

The gain always is the key parameter of any antenna and combines the antenna's directivity and the efficiency. Figure.3.10 shows the he simulated 3D gain radiation pattern of the proposed metasurface antenna.

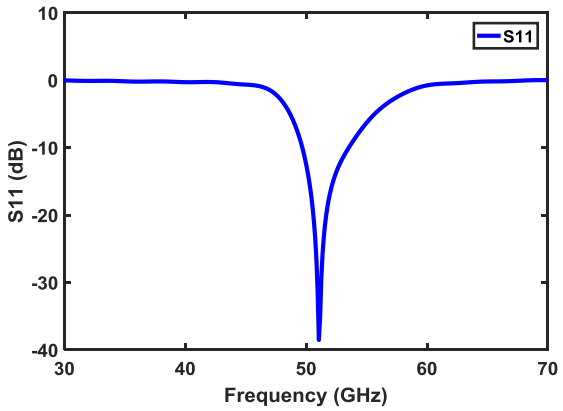

Figure 3.9: The simulated reflection coefficient of the proposed antenna.

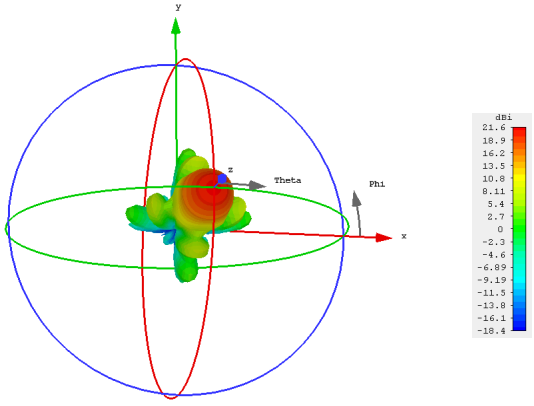

Figure 3.10: 20×20 ESRs metasurface antenna operats at 51 GHz, the highest intensity (red) corresponds to $21.6dBi$ and the lowest intensity (blue) corresponds to $-18.4dBi$.

3.7 Conclusion

A comparison between the new proposed antenna and classical antennas has shown that both have similar gain, but the metasurface antennas footprint is smaller than that of the classical antenna. Further, the proposed antenna was compared to a conventional microstrip patch antenna; the numerical investigation revealed the proposed antennas performance to be robust. Numerical simulations show that the metasurface antenna can incrementally change gain by changing the number of the resonator elements. As an example, 8×8 and 10×10 metasurface antennas were simulated, and the results showed sufficient increase in the gain from $11.7dBi$ to $13.5dBi$ respectively. Additionally, the antenna can be used for scanning by varying the phase across the electrically-small resonators comprising the metasurface. Moreover, the metasurface antenna has another advantage; it can be polarized linearly or circularly. A 400 element metasurface antennas were designed and simulated yielding antennas' gain of 21.6dBi.

Chapter 4

Design of Conformal Antennas using Electrically-Small Radiators

4.1 Introduction

A concept is presented to enable a systematic design of low-profile conformal antennas. The concept is based on using closely spaced electrically-small radiators. An ensemble of the radiators is placed in a periodic arrangement and the phase of the feed for each element is set to create a phase front orthogonal to the direction where maximum radiation is desired. The phase front is created based on the assumption that each electrically-small radiator is essentially a Huygens source radiating in the open space. The design concept presented here bypasses complex techniques used for conformal mapping and provides not only very simple design procedure but an improvement in radiation characteristics in comparison to other designs. Numerical simulation results are presented for conformal antennas operating at 7.2 GHz. While good radiation characteristics are reported for all antenna examples considered here, the design concept provides a systematic design approach, not only for electrically-large antennas, but also for antennas that are neither electrically small nor electrically large.

4.2 Background

Practically everything that can hold accelerating charges can radiate. To design effective radiators for communication purposes, however, one needs to excite accelerating charges

with information content but also to ensure efficient radiation in a specific direction and specific polarization. Throughout the past 100 years, antennas have evolved from the most simple dipoles and loops to highly complex structures with intricate feeding circuitry [96]. Some well-known antennas such as the Yagi-Uda antenna were designed with the help of empirical findings, while others, such as the microstrip and cavity-backed antennas, were designed based on circuit resonance principles. In fact, why certain antennas radiate was not clear when they were first used but this became known later. Overall, antennas can be grouped into three different categories based on their electrical size: small, comparable to the wavelength (CWL), which have the largest dimension (typically between 0.5 and 1.5 wavelengths), and large. The performance of electrically-small antennas is inherently limited in many respects as they are used whenever size is the most pressing constraint. Electrically-large antennas are made of arrays of CWL-type antennas (or elements) that collectively and predictably can achieve very high gain in specific directions. CWL antennas do not have the severe constraints of electrically-small antennas but are limited to specific designs such as dipoles, patches, inverted F, etc., which places constraints on their radiation pattern and gain.

In many applications, antennas need to be placed on platforms that are not planar, such as the surface of aircrafts or poles, while at the same time not being intrusive or high profile. Excluding electrically-small antennas, which have many limitations, array antennas are good candidates for conformal antennas [97, 98]. However, if the size of the platform is limited, then array antennas cannot be used. For instance, if a CWL antenna were to be placed on a conformal surface of, say a missile, then affecting the radiation pattern to maintain optimal performance in a specific direction becomes challenging if not impossible , unless the antenna is positioned at a specific location on the platform, which can potentially present a significant design constraint. Conformal antenna arrays have different radiation patterns than planar arrays. Therefore, most of the traditional pattern synthesis methods used for planar array antennas are not valid for conformal arrays, and their design relies heavily on optimization techniques coupled with full-wave three-dimensional Maxwell equation solvers [34, 99–101].

Several methods were introduced to synthesize the pattern of conformal antenna arrays and some methods to optimize the antenna in a desired direction [50, 102, 103]. These methods used the distance between the elements as a critical parameter. For instance, the conformal antenna introduced in [50] consists of a 9 patches array placed on a finite length conducting cylinder with center-to-center patch separation distances of 0.6 λ. This conformal antenna can be steered in specific directions using classical phased array scanning techniques along with additional optimization parameters. The equations used in conformal array synthesis [50, 102, 104] are significantly more complicated and restricted than what

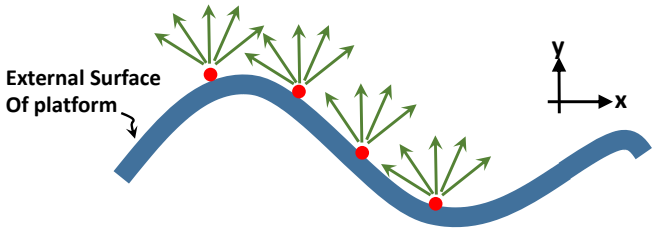

Figure 4.1: A schematic showing The elementary radiators placed on a non-planar surface. Since each element is electrically small, it radiates in all directions not hindered by the surface.

we present in this work.

In recent work, a specific design of a leaky-wave antennas was adopted as a conformal antenna [105]. While corrections for beam spreading due to the placement of the leaky-wave antenna on a conformal structure can be made by specific and highly specialized designs such as tapering of the antenna elements (as in the case presented in [105]), the design remains highly limited in its scanning potential and design flexibility and cannot be considered as a generic design for conformal antennas in general.

In this work, we introduce a concept for simple and systematic design of conformal low-profile antennas. The concept is based on using electrically-small radiators that have high resemblance to Huygens point sources. Each of the elements will radiate in all free-space directions. Building strongly on the concept of metasurfaces used for energy harvesting [106] and planar antennas [107], each element by itself is a poor radiator, however, the coupling between adjacent elements influences the input impedance of each element to affect efficient radiation [108].

4.3 Design Methodology

Huygens Principle, which dates back to the 17th century, states that every point on a wave-front becomes a source of wavelets or isotropic radiators. While Huygens visionary perspective preceded the full-fledged development of Faradays ground breaking work and the compilation of Maxwell Equations, its simplicity stood the test of time and proved highly effective in predicting, at least in a qualitative sense, scattering and radiation from slits and even radiation from electrically-thin flat lenses in a way that Snells Law could not [109, 110]. In fact, the finite-difference time-domain method (FDTD) is the numerical

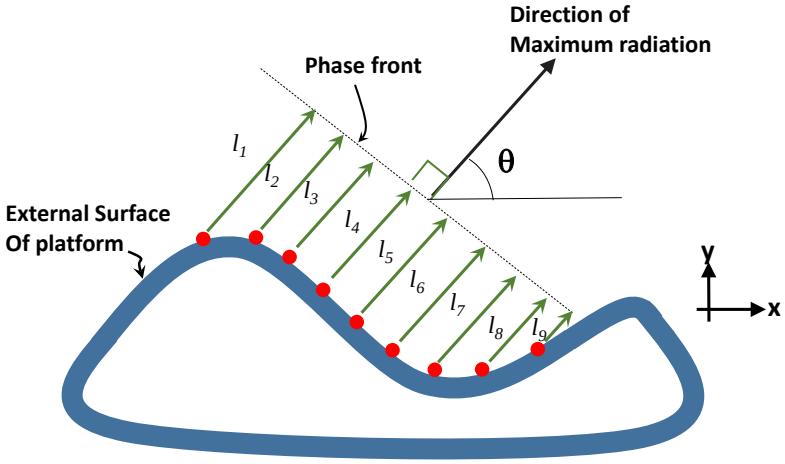

(a)

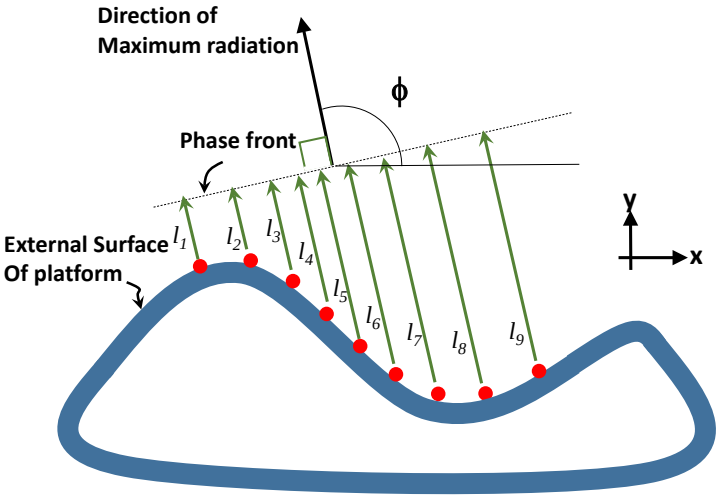

(b)

Figure 4.2: Schematic showing the design principle used to design a conformal metasurface antenna where maximum radiation is desired in two different direction using the same antenna and same structure. (a) maximum radiation in the θ direction. (b) maximum radiation in the ϕ direction.

simulation tool that can very closely demonstrate Huygens principle as the algorithm indeed qualitatively predicts how each grid point becomes a source for the surrounding grids. including those in the opposite direction to the direction of propagation. While Huygens principle postulates an infinite collection of secondary sources -essentially creating a continuum of sources- it is important to realize that each isolated source cannot provide perfect isotropy for the simple reason that electromagnetic radiation is a vector phenomenon.

The simple radiation model that Huygens genius provided was the inspirational foundation we used to design conformal antennas in this work. In principle, the idea is an extension of the concept of the true metasurface antenna presented earlier where each element of a metasurface was considered as an isolated radiator [108]. The design principle used in [108] is essentially the same design principle employed here for conformal antennas in that a reference plane is constructed such that it is normal to the direction where maximum radiation is desired. Unlike classical phased array design where the radiation pattern strongly depends on the relative distance between the elements, the pattern of each element, and the magnitude and phase of the input voltage at each element, here the design is based entirely on two considerations. The first is choosing the direction where maximum radiation is desired, and the second is adjusting the phase of the feed for each element to realize constructive interference in the said direction. Since the elements are positioned very close to each other, the coupling between adjacent elements is very strong. In fact, the tight proximity between the electrically-small radiators can be viewed as a continuum of elementary radiators.

Figure 4.1 shows a schematic of electrically-small radiators placed on a non-canonical surface. Under the assumption that each radiator emits radiation in all directions not hindered by the surface of the structure, we postulate that the rays emanating from all radiators can add either constructively or destructively to create the radiation pattern of the entire ensemble of radiators. Of course, each radiator will give rise to near- and far-field radiating components, but the far-field components are based on traveling waves that are simultaneously near to and far from the radiator. Under this model, which highly resembles the Huygens perspective of secondary radiators, considering that each radiator produces rays in all directions where radiation can take place (i.e., open space), the design principle will be based on tailoring the phase of each radiator to provide a uniform phase front that is orthogonal to the direction where maximum radiation is desired (see Fig.4.2). Maximum radiation can be achieved in a specific direction, say the direction indicated in Fig.4.2(a) by the angle θ, by having all elements fed by a source with uniform magnitude but varying in phase according to

$$\theta_i = k_0 l_i \tag{4.1}$$

where k_0 is the wavenumber in free space and l_i is the physical distance between each element and the reference plane (having a uniform phase front). The angel θ_i represents the phase of the excitation for the ith radiating element. To change the direction of maximum radiation to a different angle, say the angel ϕ shown in Fig.4.2(b), the phase for each element is adjusted in accordance with the new reference plane.

This design principle or requirement for achieving maximum radiation in a specific direction can alternatively be understood by positioning all radiators, while fed with uniform magnitude and phase, along the reference plane and tracing the phase from each element towards the structure surface along the trajectories that parallel the required direction of maximum propagation. The resulting phase at each point will then be equivalent to $\theta_i = k_0 l_i$. This design procedure gives flexibility, and in essence provides a systematic procedure for designing low-profile antennas in general in contrast to ad hoc optimization of weekly coupled radiating elements. The design principle here is similar to the design procedure used to design flat lenses reported in recent works, where the lens material is chosen such that converging rays have equal electrical (or optical) length [109, 110].

Unlike conventional array antennas where the distance between adjacent antennas is at least a half-wavelength to reduce mutual coupling between adjacent radiators, in the antenna proposed the distances between the radiating elements need to be electrically very small. Therefore, in principle, any electrically-small radiator can be chosen as the Huygens element. While Huygens principle is essentially a *model* that has the capability to predict desired radiation directions, radiators, however, have to include conductors to serve as charge carriers. Of course, infinite possibilities exist as to the type of elements that can be used, but a critical practical consideration is the impedance of each radiator which is important for maximizing power transfer to the antenna and the polarization of the radiated field. The radiating element (or unit cell) considered here is a type of Electric Ring Resonator (ERR) reported earlier, and was used to develop highly absorbent surfaces and to design planar metasurface antennas [29, 108].

4.4 Design Examples using Numerical Simulation

Figure 4.3 shows a schematic of the unit cell used here as the electrically-small radiating element, or the Huygens element. The unit cell comprises two orthogonal metallic strip lines, a dielectric substrate, a ground plane, and an excitation port connected between the strips and ground plane. The geometric dimensions and the periodicity of the cell were optimized to achieve minimum return loss, S_{11}, at 7.2 GHz (provided in the figure caption). The ERR resonators were chosen here because of their design simplicity and the ability

to control the polarization of the radiated field [108]. The ERR cell was designed and optimized using the commercially available solver CST Microwave Studio [91]. In order to numerically examine the behaviour of the ERR that operates in the C band, the unit cell was placed in the center of a waveguide with a perfect electric wall in the xz-plane, a perfect magnetic wall in the xy-plane, open space in the z-directions, and excitation by a discreet port. These boundary conditions were chosen to force the incident electric and magnetic fields to be parallel to the structure surface. Three different antenna examples operating at 7.2 GHz are provided below.

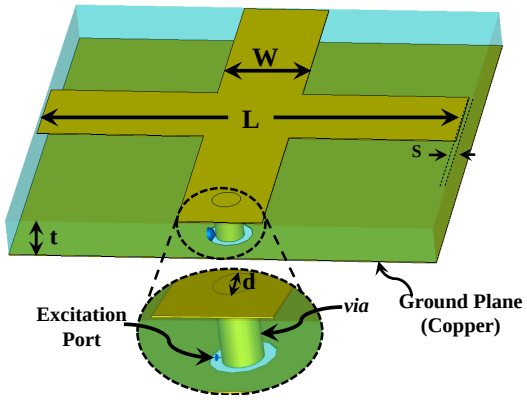

Figure 4.3: A schematic showing the proposed unit cell and its optimized dimensions and excitation port. (L = 14.75 mm, W = 3 mm, S = 0.25 mm, copper thickness of 35μm, via diameter of d = 0.5 mm. The Rogers RT5880 substrate has thickness of t = 2.2 mm, dielectric constant of 2.2 and loss tangent of 0.0009

4.4.1 An Antenna Conformal to a Semi-Cylindrical Surface

The first antenna is conformal to the surface of a half cylinder with total elements of 11 $\times$ 8 periodically arranged on a Rogers cylindrical substrate as shown in Fig. 4.4. The antenna surface has an outer diameter of D = 100 mm, and extends in the y direction by L_y =120 mm. A total of 88 ERR elements were dictated by the size of the surface. Each element is excited separately by a discrete port connected between the vias and ground plane. The entire antenna spans an area of 314 mm $\times$ 120 mm, corresponding to the angular direction along the circumference of the cylinder and the axial direction along the y direction, respectively. When all the elements were fed with uniform voltage magnitude and phase, the antenna achieved a gain of 11 dBi in the θ = 0 direction (z direction).

Next, the phase of the elements was set to have a maximum radiation in the $\theta = 0$ direction using Eq.(1). Figure 4.5 illustrates the reference plane and the radiating element trajectories needed to calculate the phase for each radiating element. The resulting half cylinder conformal antenna achieved an antenna gain of 16 dBi with a radiation pattern shown in Fig. 4.6.

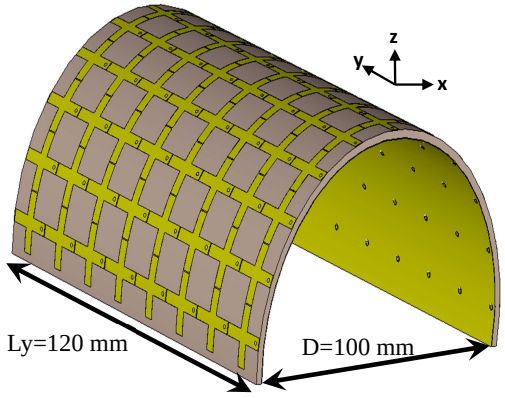

Figure 4.4: Architecture of an antenna conformal to a semi cylindrical surface. A total of 88 radiating elements were used on a Rogers RT5880 substrate backed by a copper ground plane.

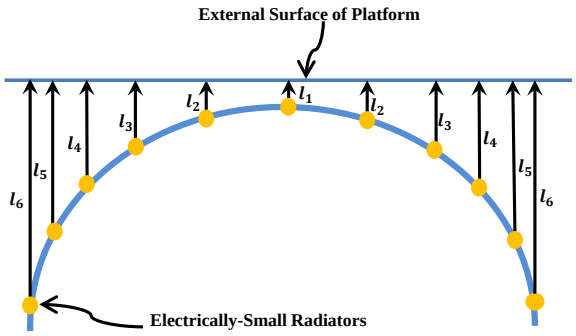

Figure 4.5: Schematic highlighting the procedure for calculating the phase of each radiating element.

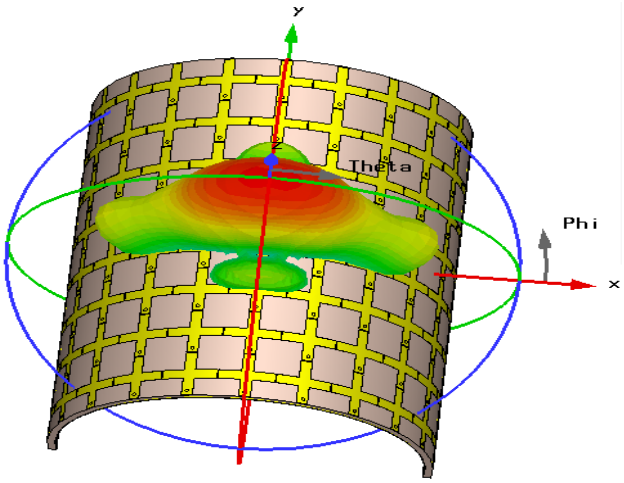

Figure 4.6: The simulated 3D radiation pattern of the antenna shown in Fig.4.4, maximum radiation in the $\theta = 0$ direction. The highest intensity (red) corresponds to 16 dBi and the lowest intensity (blue) corresponds to -24 dBi.

For comparison, we designed a conformal array antenna composed of conventional microstrip patches placed on a half cylinder, and also to gain a perspective of the relative performance of our proposed concept (see Fig. 4.7). The same footprint was used and was populated with a heuristically optimized number of patches totalling 27. (The trial-and-error based optimization was carried out without adhering to the convention of keeping a distance of $\lambda/2$ between the adjacent patches). The 27 microstrip patches hosted on the same footprint as our conformal antenna achieved a gain of 11 dBi. Furthermore, by progressively phasing the feed for each patch in accordance with Eq. (1), an antenna gain of 13.2 dBi was achieved.

The proposed antenna has the ability to steer the beam in the θ direction and also in the ϕ direction. To steer in the ϕ direction (see Fig. 4.6 for angle definitions), we follow the same procedure as above where the distance from the reference plane to each radiator is calculated first as shown in Fig. 4.8 and then the phase is calculated using Eq. (1). As an example, an antenna was designed to have a maximum radiation in the $\phi = 45^o$ direction. Figure 4.9 shows the simulated radiation pattern. The antenna achieved a gain of 15.8 dBi.

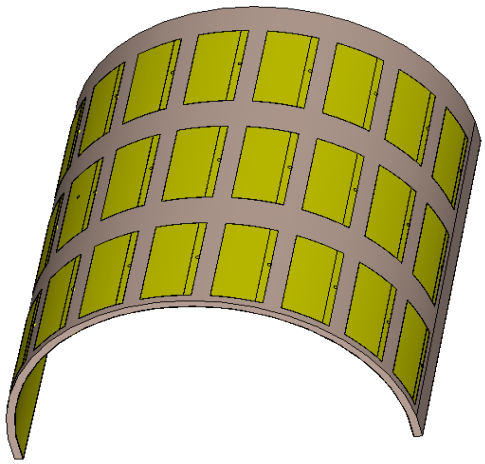

Figure 4.7: Patches antennas placed on semi-half cylinder substrate

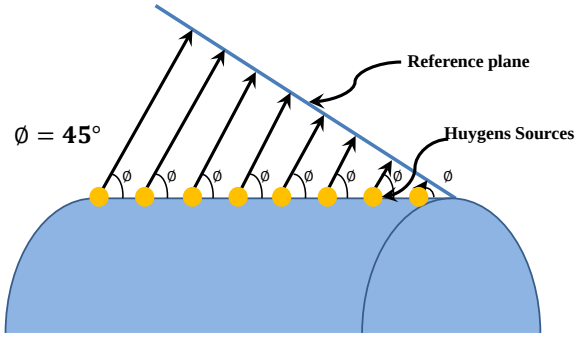

Figure 4.8: Schematic illustrating the geometry used for calculating the phase of each elementary radiator to achieve maximum radiation in the $\phi = 45^o$ direction.

4.4.2 An Antenna Conformal to a Quarter-Cylinder Surface

The second antenna example is an antenna conformal to the surface of a quarter cylinder. Unlike the previous example presented above, here, we desire the direction of maximum radiation to be in the z-direction, which is off the antenna's symmetry plane (see Fig. 4.10). The surface of this antenna dictated by 48 ERR elements arranged as 6×8, corresponding

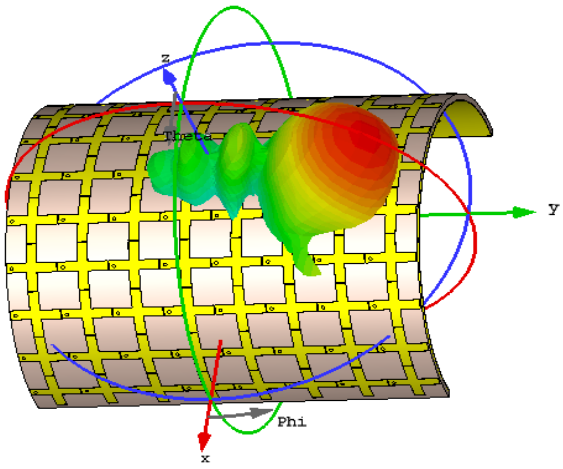

Figure 4.9: The simulated polar radiation pattern of the antenna shown in Fig.4.4 in ϕ =45^o direction. The highest gain is 15.8 dBi.

to 158 mm along the circumference of the cylinder in the angular direction and 120 mm along the y-direction, as shown in Fig. 4.11. Careful examination of the radiation pattern reveals maximum radiation in a direction approximately 10^o off the z-axis . This deviation of the main beam from the design requirement is attributed to the relatively small number of elements placed along the angular direction. However, the relative phase of the elements in the angular direction can be optimized to correct for this deviation (if the number of elements were to be kept unchanged). For this example, and without employing a complex optimization routine, it was found that progressive 30^o phase shifts added to the elements, starting with the second element closest to the z-axis, were sufficient to tilt the beam to the desired direction (the added phase shift per element needed to make the slight correction was found to be 30^o. The far-field radiation pattern with and without the optimization is shown in Fig. 4.12. An antenna gain of approximately 15 dBi was achieved with maximum radiation in the z-direction.

Similar to the first example, we designed a conformal antenna using microstrip patches for comparison. The optimized microstrip patch conformal array had a total of 15 patches hosted on the same footprint of the proposed antenna (see Fig. 4.13) achieving an antenna gain of 14.6 dBi gain with maximum radiation in the $\theta = 45$ direction. Interestingly, when the microstrip patches were progressively phased to achieve maximum radiation in the $\theta = 0$ direction, the gain dropped to 13.5 dBi.

The quarter cylinder conformal antenna is suitable for a variety of structures where

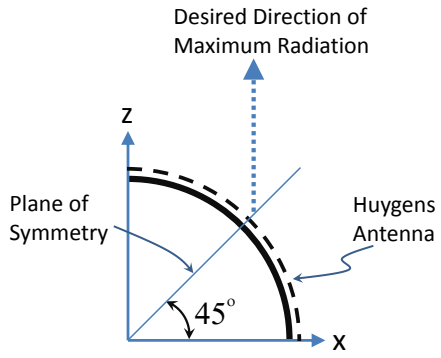

Figure 4.10: Cross-section of the metasurface quarter-cylinder conformal antenna showing the direction where maximum radiation is desired.

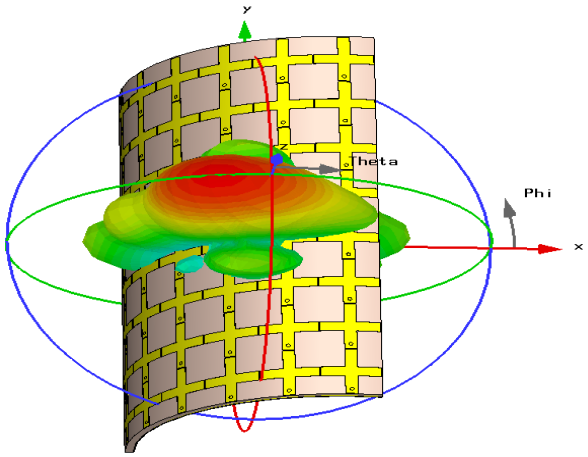

(a)

Figure 4.11: Architecture and the simulated 3D radiation pattern of the metasurface quarter-cylinder antenna. The highest intensity (red) corresponds to 16.2 dB and the lowest intensity (blue) corresponds to -23.8 dBi.

the antenna cannot be placed symmetrically with respect to the direction of maximum radiation but must conform to the surface of a specific platform. For example, if radiation is desired directly above a drone and the antenna cannot be placed on the top side, this antenna provides an effective solution (see Fig. 4.14). In fact, in such applications, the antenna can be used effectively for radiation in multiple directions.

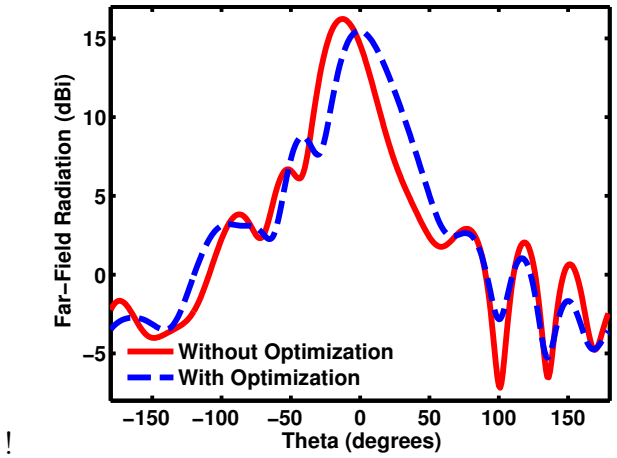

!

Figure 4.12: Far-field radiation for the metasurface quarter-cylinder antenna.

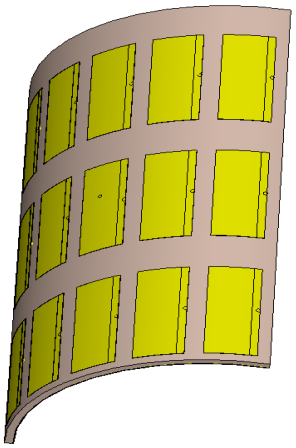

Figure 4.13: Microstrip patch antennas placed on quarter cylinder substrate.

4.4.3 An Antenna Conformal to a Double Curvature Surface

This design consists of a metasurface conformal to a surface having a uniform cross section describing a double curvature surface as shown in Fig. 4.16. The antenna is designed to consist of a periodic array of 20×8 elements in the y- and x-directions, respectively. The semi-circles of the cross section have a radius of 50 mm. The length of the antenna surface in the y-direction is 120 mm. Figure 4.15 illustrates the geometry needed to calculate

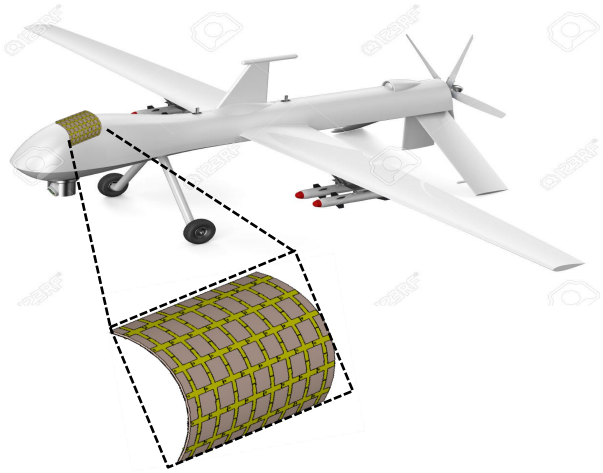

Figure 4.14: An example of the quarter-cylinder antenna placed on the side of a drone. (Drone illustration is courtesy of $http : //www.123rf.com/photo_39650119_unmanned - aerial - vehicle - uav - isolated - on - white - background.html.$)

the phase for each elementary radiator. If all elements were fed with a uniform phase, maximum radiation would occur in the $\theta = 0$ direction with a gain of 15.1 dBi. When the elements were phased according to the design criterion presented in Eq. (1), namely to construct a uniform plane wave in the $\theta = 0$ direction, the gain increased by 4 dB to 19.1 dBi (see Fig. 4.15).

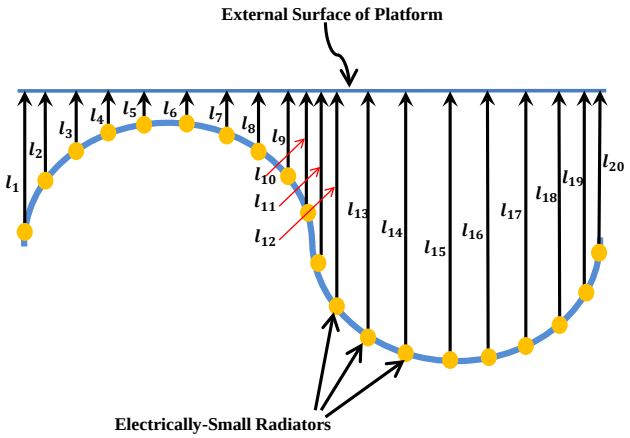

Figure 4.15: Schematic illustrating the geometry needed to calculate the phase of each elementary radiator for the double curvature surface antenna.

4.4.4 Cylindrical Metasurface Antenna

The proposed antenna is cylindrical with a total of 21×8 elements, periodically arranged on a Rogers cylindrical substrate as shown in Fig.4.17. The cylinder's outer diameter is $D = 100mm$, and the cylindrical length in the y-direction is $L_y = 120mm$. In total, 168 ERR elements cover the cylindrical substrate to create the antenna, and each element is excited separately by a discrete port connected between the vias and ground plane. A via with a diameter of $d = 0.5mm$ was chosen due to future fabrication constraints. Unlike conventional array antennas where the distance between the radiating elements is electrically large (half wavelength) to reduce mutual coupling, here we **want** to take advantage of the mutual coupling. Therefore, the distance between the radiating elements is electrically very small to affect a good impedance matching of each resonator, and that coupling gives flexibility in controlling the impedance value as well.

The entire antenna spans an area of $314mm$ (in the angular direction along the circumference of the cylinder) and $120mm$ in the axial direction (along the y-direction). The elements had been fed with a uniform phase and the antenna gain was omnidirectional and as high as $7.55dBi$ (see Fig.4.18).

To examine the antenna's gain displacement capability in the axial direction (along the y-direction), the elements are phased according to the desired gain position shift. The gain shifted in both positive and negative directions along the axial direction. To scan in the

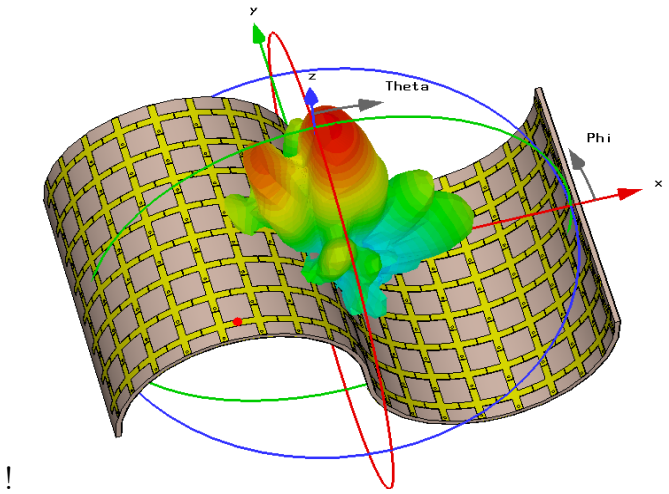

!

Figure 4.16: Architecture and the simulated 3D gain radiation pattern of the double curvature surface antenna. The highest intensity (red) corresponds to 19.1 dBi and the lowest intensity (blue) corresponds to -20.9 dBi.

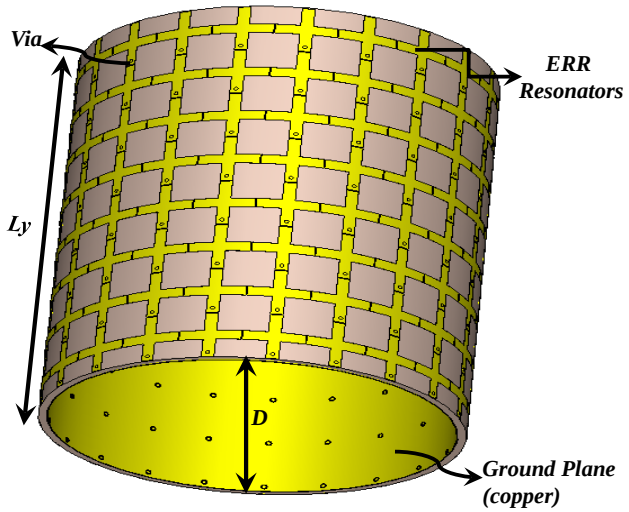

Figure 4.17: Architecture of a metasurface antenna conformal to a cylindrical surface. In total 168 radiating elements are used on a Rogers RT5880 substrate backed by a copper ground plane.

axial direction, the elements along the y-axis were phased progressively while the elements along the x-axis had a constant phase. Figure.4.19 shows the gain scan in the positive

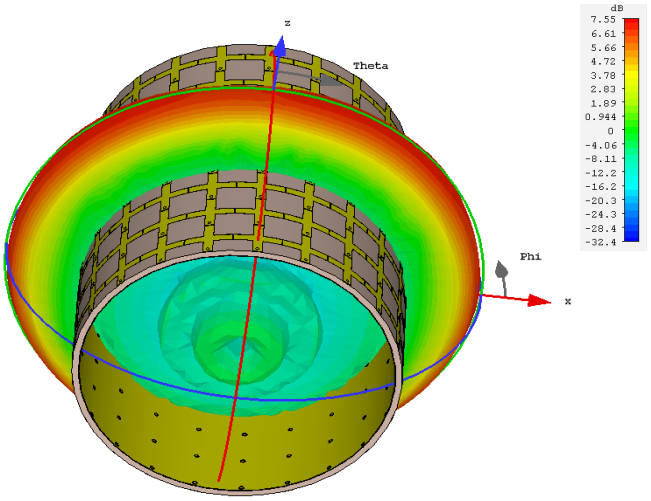

!

Figure 4.18: The simulated 3D omnidirectional radiation pattern of the metasurface conformal antenna. The highest intensity (red) corresponds to $7.55dBi$ and the lowest intensity (blue) corresponds to $-32.4dBi$.

direction with three different phasing values of 30^o, 60^o and 90^o, whereas, Fig.4.20 shows the gain scan in the negative direction with phasing -30^o, -60^o and -90^o.

!

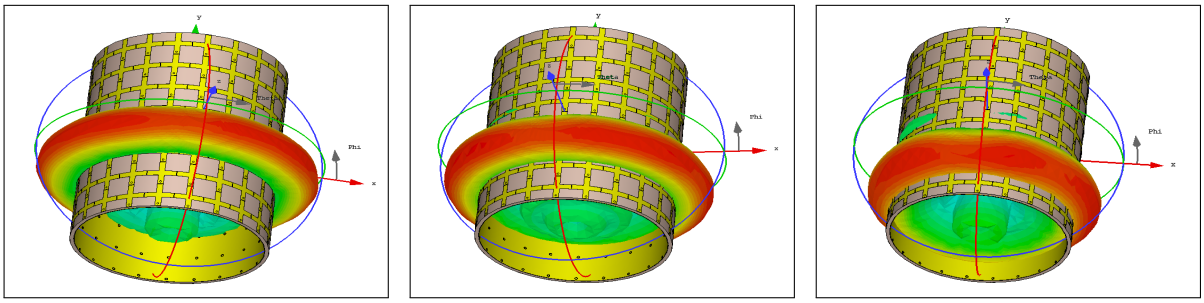

Figure 4.19: The simulated 3D omnidirectional radiation pattern of the metasurface conformal antenna. Correspondence between the progressive inter-element phase and the scan angle with maximum gain is as follow: (a) Phase= 30^o, (b) Phase= 60^o and (c) Phase= 90^o

!

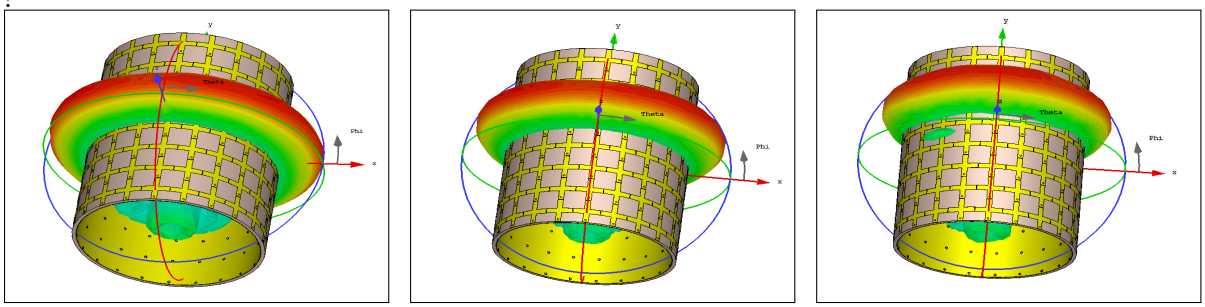

Figure 4.20: The simulated 3D omnidirectional radiation pattern of the metasurface conformal antenna. Correspondence between the progressive inter-element phase and the scan angle with maximum gain is as follow: (a) Phase= -30^o, (b) Phase= -60^o and (c) Phase= -90^o

4.5 Discussion

The antenna concept proposed here is based on using a metasurface that conforms to a non-planar structure. Metasurfaces have been used previously for absorption, energy harvesting, cloaking and lenses amongst other applications. The metasurface is composed of electrically-small radiators, typically referred to as metamaterial cells. Each radiator, by virtue of its electrically-small dimensions, behave like an small dipole when placed above a ground plane. However, unlike a single small dipole placed above a ground plane which would have very high reactive impedance, an ensemble of electrically-small dipoles, or radiators in general, placed in free space or above a ground plane can, individually, have

an input impedance that is purely real and having a magnitude that allows for matching to practical feed networks. Therefore, the ensemble of elements comprising the metasurface becomes an affective overall radiator or antenna. When the metasurface is placed on a non-planar structure with sufficiently reasonable curvature that exclude sharp corners, as the examples presented in this work, the input impedance of each radiator is expected to have very minor change, thus the new curved antenna remains an effective radiator. Since each radiator is electrically small, its radiation (in the open space not shielded by the ground plane) is similar to that of an electrically small dipole, thus radiating in all open directions. This understanding paves the way to interpret each elementary radiator as a source for the outgoing radiation in a manner similar to the Huygens model of propagation (through slits or otherwise). With the Huygens model in mind, radiation in a specific direction can be maximized by requiring constructive phase interference along a plane that is perpendicular to the said direction. The different examples provided above strongly validate this theory.

4.6 Conclusion

In this work, we have presented a fully-systematic procedure for designing conformal antennas using metasurfaces. Using an analogy comparison to Huygens theory of secondary radiators, the idea is based on phasing the elementary radiators that comprise the metasurface to ensure constructive phase interference in the desired direction of maximum radiation. Through several examples, we have showed through numerical simulation that conformal antennas can be designed systematically to achieve maximum radiation in a specific direction. The design procedure is very simple as it can be summarized by a single equation.

The examples of metasurface conformal antennas presented here used a specific elementary radiator, namely the ERR cell. In general, other elementary radiators can be used which would be expected to provide an additional polarization control parameter. It should be kept in mind, however, that the input impedance of each radiator within the ensemble depends on the type of radiator used and its proximity to adjacent radiators.

We emphasize that this thesis presented the concept of conformal metasurface antennas and the theory behind its operation. Numerical full-wave simulation was used to validate the concept by presenting several examples of antennas that conform to a wide range of non-planar surfaces. This work did not address the feed network needed for phase control for all radiators. We anticipate reporting on feed networks and antenna prototypes in a future publication.

Chapter 5

Metasurfaces for Wireless Electromagnetic Energy Transfer (Metasurface Energy Harvesting)

5.1 Introduction

In the second part of this work, a metasurface electromagnetic energy harvester based on electrically small resonators is presented. In this chapter, an array of 8×8 cross resonators arranged on Rogers substrate to operate in the microwave regime at $3GHz$ was designed. A new mechanism was proposed to channel the microwave energy collected by the array of electrically small resonators. Unlike the earlier designs of metamaterial harvesters where each small resonator was connected to a load, in this design, the received power by the resonators channeled to one 50Ω resistive load only. The critical advantage of the proposed structure is maximizing power density per diode which maximizes the diode turn-on time. The numerical simulation and the experimental measurements show that the proposed metasurface harvester is sufficient to collect microwave energy and deliver it to one load through vias and feed network. The numerical simulation and the experimental results showed AC conversion efficiency of 89% and 74%, respectively.For more practical applications, DC Conversion efficiency needs to be examined. Therefore, it is shown through simulation and measurements that the proposed metasurface harvester provides Radiation to DC conversion efficiency of more than 40%.

5.2 Energy Harvesting and Wireless Power Transfer

At the end of the 18th century, Nicola Tesla successfully demonstrated the practicality of Wireless Power Transfer (WPT). Sixty years later, the first WPT system operating at the microwave regime was demonstrated by Brown [60]. In a WPT system, DC power is fed to a transmitting circuitry which convert it to AC. The AC signal is then fed to an antenna, which transmits the energy through space to a distant receiving system (rectenna), which then collects the RF energy and converts it to usable DC power. A rectenna is the receiving constituent of a WPT system used to convert microwave energy into DC power. In general, a rectenna consists of an antenna, a diode, an RF filter and a DC filter to smooth the rectified energy [62, 63]. Rectennas are used in a number of applications such as remote sensing [29], RFID tags [111] and energy harvesting [112]. One critical and promising application of rectennas is Space Based Solar Power (SBSP) advocated by Glaser In 1968. In an SBSP system, a large array of solar cells in space is used to collect solar energy around the clock and then converts it to microwave power. Using high directive antennas, the power is transmitted to earth where large rectenna arrays receive the microwave power and convert it back into DC power [61, 113].

Utilizing rectenna to harness the energy from the space in WPT systems has attracted much interest especially in the aspect of improving the conversion efficiency [65, 114, 115]. Since the conversion efficiency of the WPT mainly depends on the receiving system (collectors), extensive research has been carried out on the subject of rectenna. Figures of merit that are used to evaluate rectenna systems are the Radiation to AC power and Radiation to DC power conversion efficiencies. To improve the efficiency of the rectenna system, a careful design procedure including matching networks is used to minimize the losses of each rectenna component. In most previous works, there was a heavy focus on improving the AC to DC power conversion efficiency, which was mainly attributed to the diode, RF filter, and DC filter. The antenna, which is the main energy collector component of the rectenna system, and its adiation to AC power conversion efficiency, however, were seldom discussed when calculating the overall power conversion efficiency.

Classical antennas have been used for more than a century as they play a crucial role in receiving RF energy. Therefore, different antenna types have been placed used in rectennas for harvesting electromagnetic energy. Examples include dipole antennas [116, 117], ring slot antennas [118, 119], microstrip patch antennas [120], cross dipole antennas [121], and coplanar strip line antennas [122]. Most of these antennas were used because of their ability to harness the energy either over a broad band [121, 123] or a duel band frequency [118, 119, 124]. To supply a practical system with feasible amount of power, an array composed of multiple antennas is needed [117, 123]. Recently, much attention has been paid

to metamaterial cells as collectors instead of classical antennas with the goal of increasing the Radiation to AC conversion efficiency in both microwaves [21,125] and infrared regimes [22].

5.3 Metamaterial and its Potential for Energy Harvesting

Despite the metamaterial collectors proposed in the previous works are very efficient to harvest the electromagnetic energy by using array of these collectors, more challenges and complexity raise at the measurements stage. In [31] an array of metamaterial absorbers operates as a microwave detection is presented where each unit cell works individually receiving radio signals and converted to electric current, then the electric current channeling through vias to a balun then to impedance matching circuit and then to the low nose amplifier , finally to the microwave power detector. In [30] an array of 13×13 unit cell metsurface operates as energy harvester, where each unit cell works individually also. Each cell channel the power through a via connected to a resistive load (82Ω). However, the efficiency was very high (near unity).

Maximizing the conversion efficiency, minimizing the footprint, and channeling and collecting the power are the most important and critical objectives in electromagnetic energy harvesting. This works introduces a metasurface harvester array that harvests the microwave receiving energy and then channel it to one load as AC energy. First, an array of electrically small resonators, particularly Electric Ring Resonator (ERR) cross resonator type reported earlier in [90], operates in the microwave regime is proposed here to collect the microwave energy. Second, a new mechanism of which the energy received by the metasurface array channels to one load point through transmission lines is proposed.

This work introduces a metasurface harvester array that harvests the microwave energy and then channels the AC energy collected from all metasurface elements into a single rectification circuit through a corporate feed network. The importance of the new design is not only the novelty of the load feed network, but rather the requirement of less power density per metasurface element to activate the rectification circuit since the contribution from each individual cell is added constructively. Therefore, the threshold for the power density at the metasurface antenna needed to activate the rectification circuitry (diode turn-on) will be minimized. Of course, reducing the number of rectification circuits has the added advantage of reducing the fabrication cost and fabrication complexity.

For example, Fig. 5.1(a) and (b) show two panels occupying the same footprint where

each panel contains 64 antenna elements. In Fig. 5.1(a) each antenna is connected to a diode while in Fig. 5.1(b) all antennas are connected together to feed one single diode. Voltage is the relevant parameter in this energy harvesters but the power is mentioned below for clarification. If a one mW of real power falls on both panels, each element will receive 1/64=0.015 mW. In the first scenario (5.1), the power available at the feed of each diode terminals is approximately 0.015 mW under the assumption that all elements have unity efficiency. In the case shown in Fig. 5.1(b), however, since all power is combined through a feed network to a single diode, the power available at the feed of the diode terminal is one mW. If the diode requires one mW of power to turn on, the diode in the case of Fig. 5.1(b) will turn on while the diodes in the case of Fig. 5.1(a) will remain turned off. Therefore, in general, a power channeling strategy that maximizes the power density per diode ensures higher probability of diodes turn-on time. To clarify, the voltages is the relevant parameter not the power,

5.4 Design Methodology

The same proposed metasurface antenna in **Chapter 2** is used as a harvester with some few changes as shown in Fig5.2. The unit cell used here is the one in Fig2.1. The commercial full wave simulator ANSYS® HFSS™ [126] was used to design and optimize the proposed harvester element. To measure the level of transmission and reflection of the incident wave at the unit cell surface, the proposed unit cell was placed in the center of a waveguide with perfect magnetic wall in the yz planes, perfect electric wall in the xz planes, and two excitation ports along the z-axis (see Fig.5.2) . These boundary conditions were applied to force the electrical and magnetic fields to be parallel to the element surface and to ensure that a transverse electromagnetic wave is incident on the unit cell surface. When the electric field of the incident wave is polarized such that it is parallel to the ERR arm containing the via (Fig.5.2), the ERR exhibits a strong resonance and thus maximum energy absorption potential.

An important considerations when maximizing the power delivery to the load is the via position (see Fig.5.2) and the resistive load value. These two parameters were optimized to yield maximum conversion efficiency. The optimal resistance value that resulted in maximum power transfer from the ERR cell to the resistive load is found to be 200 Ω (the spacing between the elements strongly affects the input impedance of each cell). Next, an array of 8×8 ERR elements arranged periodically on a square substrate was designed. The array was first numerically simulated to ensure that it provides good absorption of the incident power. The numerical simulation was performed by positioning the array at

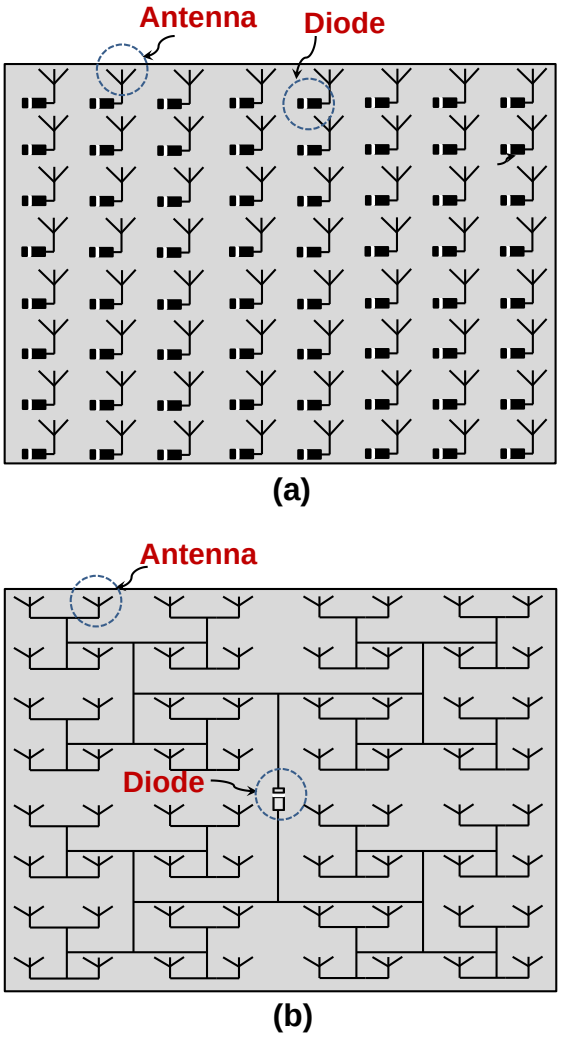

Figure 5.1: Energy harvester panel has 64 antenna elements (a) Each antenna is connected to a rectification circuitry (b) All antennas are connected together to one rectification circuitry.

the center of an open radiation box and excited by an incident plane wave such that the electric and magnetic fields were parallel to the element surface. Since the purpose of the simulation is to show the absorption efficiency of the metasurface panel, each individual ERR cell was terminated by the optimal resistive load of 200 Ω and the power received by

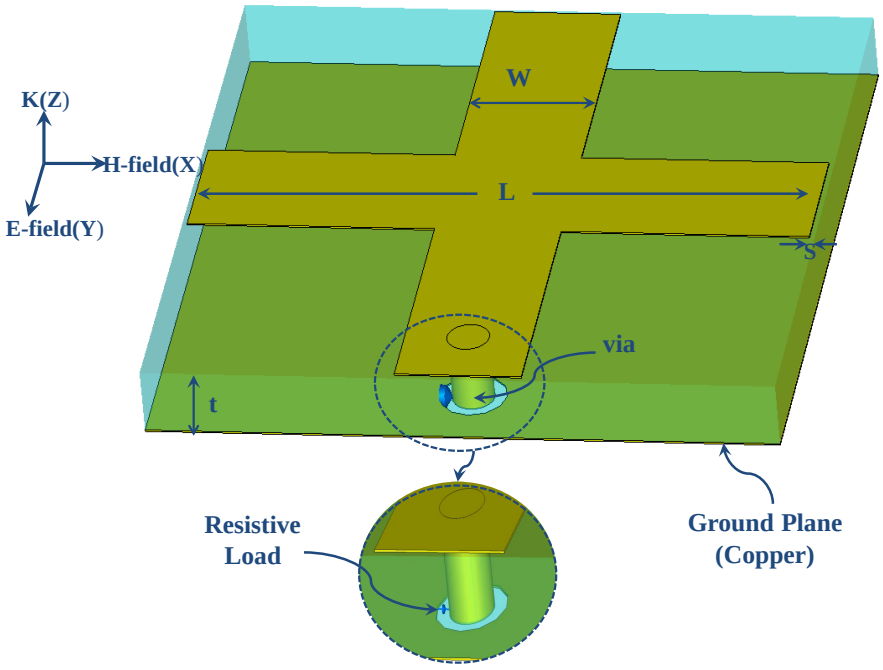

Figure 5.2: A schematic showing the proposed unit cell of a metasurface harvester and its optimized dimensions as well as the placement of the via.

all 64 cells was numerically computed. A maximum radiation to AC absorption efficiency of 92% was achieved. Scattering from the panel and dielectric absorption accounted for the remaining 8%. This simulation was a first step to ensure the potential of the design.

5.5 Metasurfaces Array for Power Channelling

Practically, in some scenarios, one unit cell is not enough to deliver an adequate power for a potential system; thus an array of these cells is needed to supply a practical system with a decent amount of power. Therefore, a set of 8×8 energy harvester elements periodically arranged on a square substrate was prepared. The array was centered in a open radiation box and exited by plane wave in a way that the electric and magnetic fields were parallel to the inclusion surfaces as referred to previously. After we observed that the ERRs array had high conversion efficiency, we proposed a new mechanism to channel the received power. The same metasurface antenna used in **Chapter 2** is used here with small difference in

the feed network. Fig.5.3 Symmetrical configuration of the corporate fed array with the resistive load position.

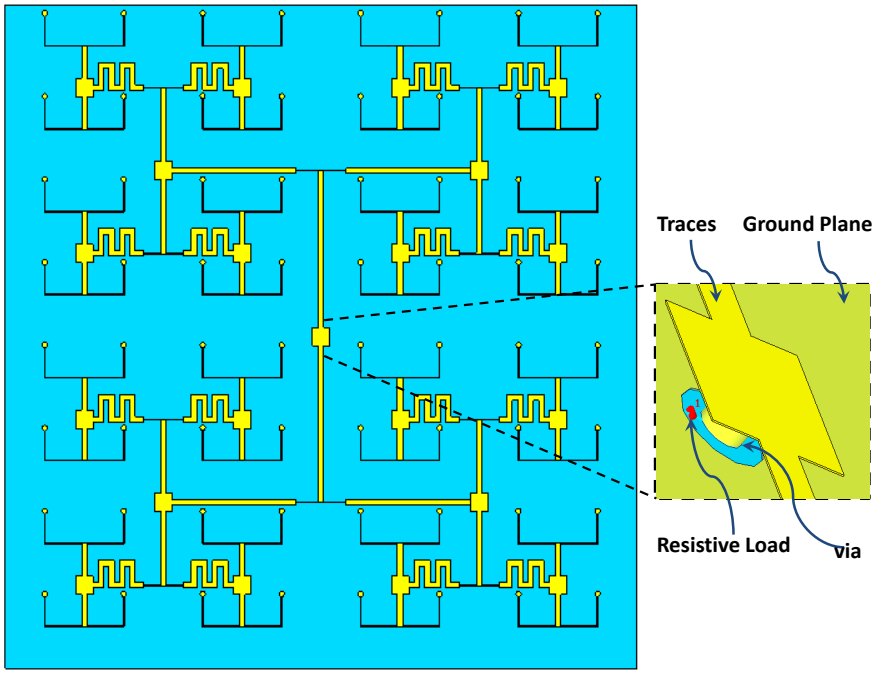

Figure 5.3: Symmetrical configuration of the corporate fed array with the resistive load position.

5.6 AC and DC Measurements,Results and Discussion

A 8×8 metasurface harvesting array was fabricated using the same designed as used in the simulation as shown in Fig.2.4. All collectors were connected to one resistive load (50Ω resistor) using microstrip transmission line corporate feed as depicted in Fig.5.3. Fig.5.4 shows the radiation to AC conversion efficiency with and without the corporate feed. Expectedly, the maximum efficiency was slightly decreased due to propagation losses in the feed network; nevertheless, the results of the numerical simulation validated the channeling network design.

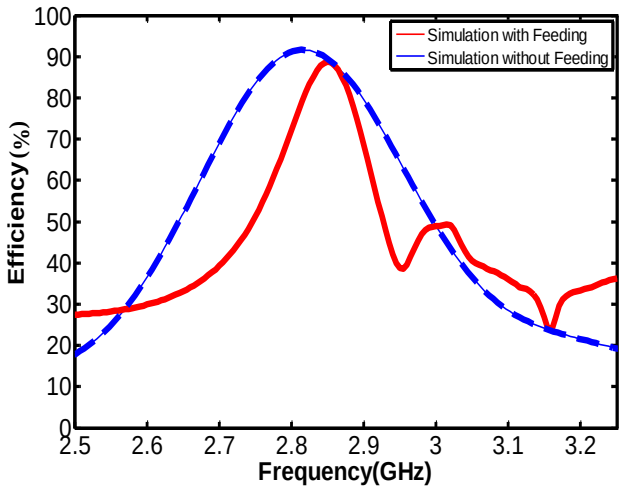

Figure 5.4: The Radiation to AC conversion efficiency of the proposed array. The case without feeding corresponds to collecting the AC power at 64 resistive loads while the case with feeding corresponds to collecting the AC power at a single load positioned at the end of the channeling network.

The incident field was generated using an $11.5dBi$ gain commercial wideband horn antenna excited by a frequency signal generator of power level $13dBm$. The metasurface array of the energy collectors was positioned a distance of 1m away from the transmitting antenna such that the electric field was parallel to the strip of the resonator that had the via (see Fig.5.2). One of the main advantages of the metasurface harvester proposed in this work is that all collectors were connected to one 50Ω load, the same load as most of the measurement devices are based on 50Ω systems. Therefore, no matching circuits are needed, and measurement connections will be simple and efficient. An Agilent power meter was connected directly to the load and measured the receiver power over a wide-band frequency, from $2GHz$ to$4GHz$. Fig.5.5 depicts the measurement setup used in the experiment.

Fig.5.6 shows the actual measurement setup. The AC power at the output of the corporate feed network was measured over the 2 GHz to 4GHz frequency range. The radiation to AC harvesting efficiency was obtained using the following formula [17]:

$$\eta_{rad-AC} = \frac{P_{received}}{P_{incident}},$$

where $P_{received}$ is the total time-average power received by the metasurface array (dissipated

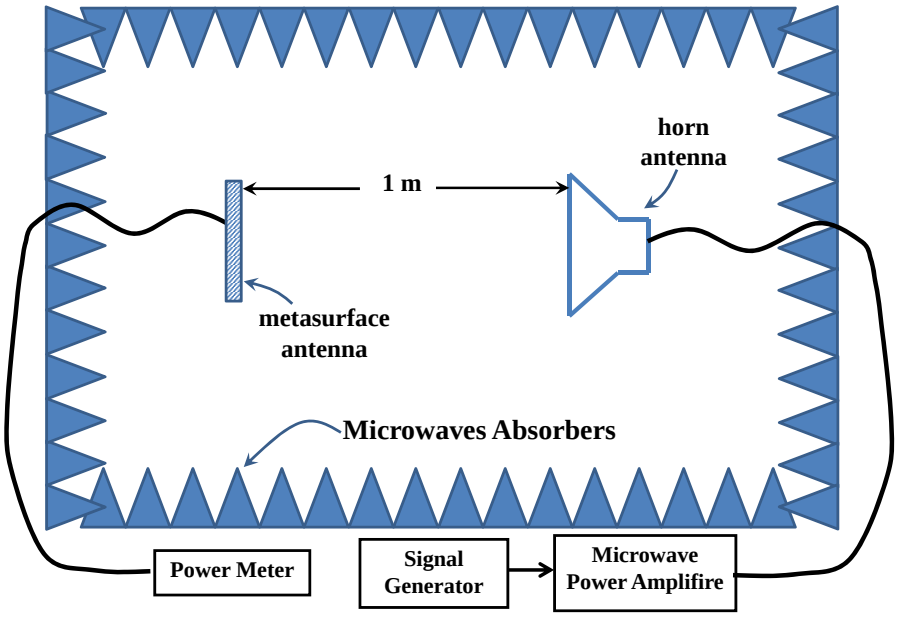

Figure 5.5: The measurment setup used in the experiment.

in the resistive load), and $P_{incident}$ is the total time average power incident on the entire metasurface. $P_{incident}$ was calculated using Friis equation [22]:

$$P_{incident} = \frac{P_t G_t}{4\pi R^2} A,$$

where P_t is the output power of the transmitting antenna, G_t is the gain of the transmitting antenna, R is the distance between the antennas, and A is the entire metasurface area. For the entire metasurface that contains N collectors, $P_{received}$ is given by:

$$P_{received} = \frac{{V_L}^2}{R_L},$$

where V_L is the voltage across the resistance of the single load resistor R_L.

Fig.**??** depicts the measured radiation to AC power conversion efficiency η_{rad-AC} of the proposed metasurface harvester before attaching the rectifier. The highest η_{rad-AC} achieved was 78% at 2.9 GHz.

For DC measurements, all collectors were connected to a single feed point where a 50Ω SMA connector was mounted. A rectifier was then designed using Agilent Advance Design

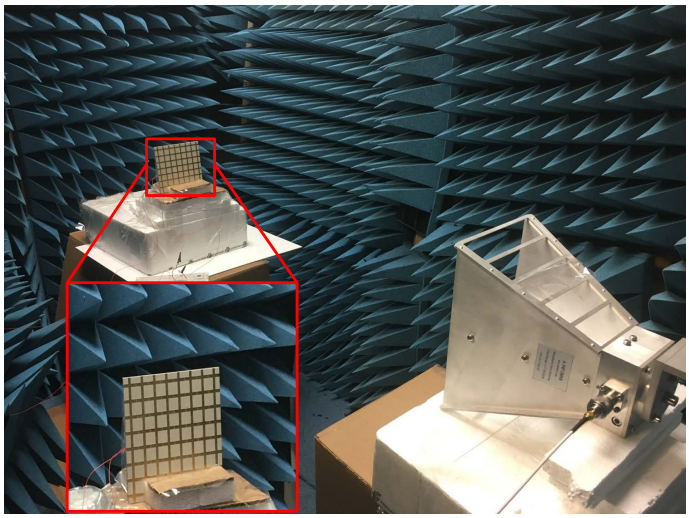

Figure 5.6: measurement setup showing the metasurface and the horn antenna in an anechoic chamber.

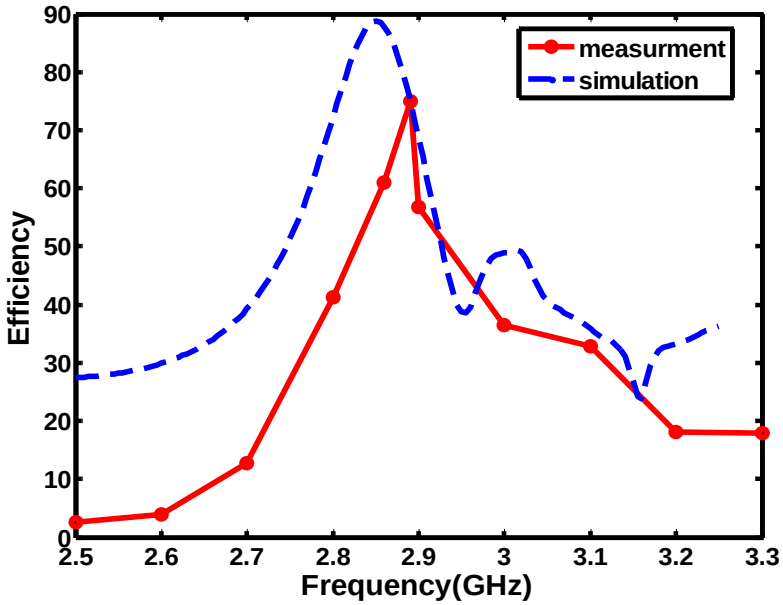

Figure 5.7: The simulated and measured conversion efficiency of the metasurface harvester.

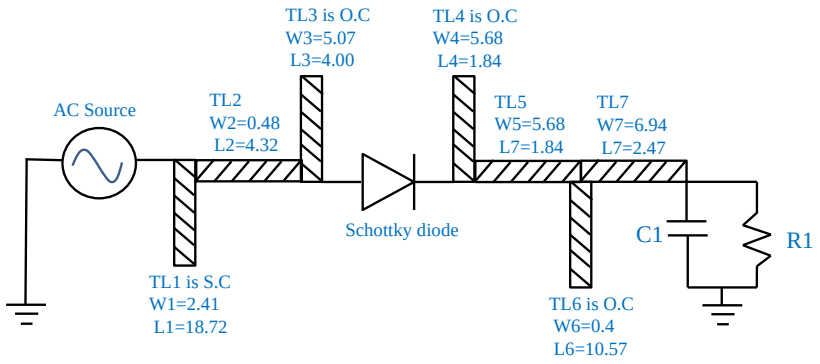

Figure 5.8: Design schematic of the rectifier circuit. The hatched thick lines represent transmission lines.

Systems (ADS) having an input impedance of 50Ω at the resonance frequency. Since the rectifier is non-linear, it was analyzed using the Harmonic Balance simulator. The diode was connected to the feed of the antenna through a matching network containing a short circuited stub, open circuited stub and a series transmission line. Then a DC filter containing two series transmission lines and two open circuited stubs along with a $150pF$ was connected to the cathode node of a HSMS 2860 Schottky diode. The rectifier circuitry was designed by Thamer Almoneef.The design schematic for the rectification circuit is shown in Fig.5.8 and the fabricated one in Fig.5.9.

The power across the DC load is then measured at the optimal frequency and incident power level. To obtain the optimal power level, the power output from the signal generator was connected to a 42 dB microwave power amplifier. It was found that the diode operates maximally at an incident power level of 12 dBm and a frequency of 2.82 GHz for a load resistance of 300Ω. The peak radiation to DC power conversion efficiency, η_{rad-DC}, of the array including the rectifier was 40% at 2.82 GHz (see Figure.5.10).

5.7 Conclusion

.

This work presented the design of metasurface harvester that efficiently collects electromagnetic wave radiation power and channels it to one resistive load. A corporate feed network was designed to match the input impedance of the ERR cells to one resistive load such that all cells were connected in phase to the resistive load. An ensemble of 8×8

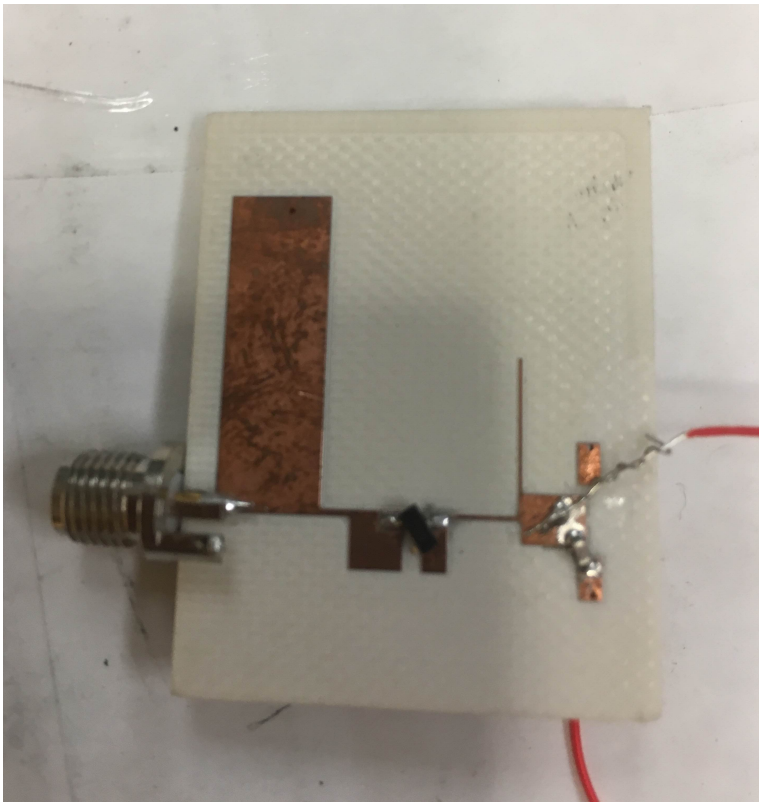

Figure 5.9: A photograph of the fabrication rectifier circuit.

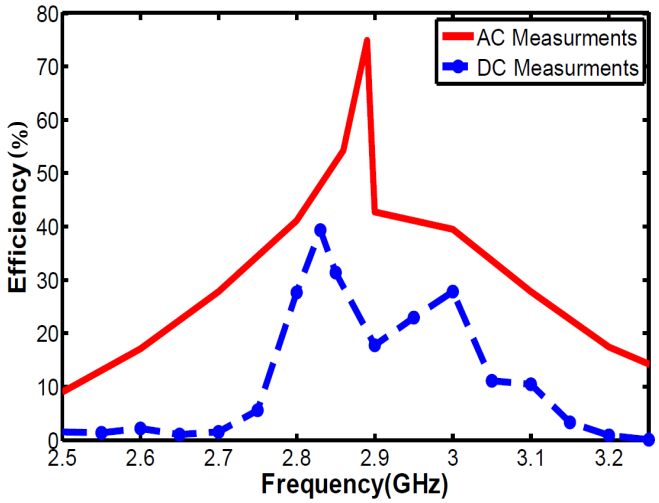

Figure 5.10: The measured radiation to AC efficiency, η_{rad-AC} (AC Measurements) and measured radiation to DC efficiency, η_{rad-DC} (DC Measurements) of the metasurface harvester.

ERR cells was designed, fabricated and tested. The experimental results show that the metasurface in conjunction with the corporate feed network provided a maximum total radiation to DC conversion efficiency of 40%.

In this particular work, the radiation illuminating the metasurface panel was incident normally to its surface. This resulted in all the metasurface elements (ERR cells) having uniform phase and thus the propagation of the AC signal on the corporate feed network resulted in constructive interference at the rectifier input. If the incident radiation was incident at other angles, the efficiency is expected to decrease due to non-uniformity of the phase at each element. Therefore, the presented design concept is most suitable when the radiation is arriving from a specific direction known to the receiver system.

Chapter 6

Efficient Metasurface Rectenna for Electromagnetic Wireless Power Transfer and Energy Harvesting

6.1 Introduction

In this chapter, a design for a metasurface that provides near-unity electromagnetic energy harvesting and RF channeling to a single load is presented. As a first step, a unit cell of metamaterial absorber is designed to operate in the S-band at $2.72GHz$. Next, we extend the concept of full absorbers to full harvesters by using the same unit cell while choosing the optimal resistive load value and the via position, where the harvester is required not only to receive the power and fully absorb it but also to channel the maximum power to a load. An 8×8 array of the harvester cells has been designed to harvest the maximum power (perfect harvester). Two different feed networks are proposed to deliver the maximum power collected by all cells to only one load. Numerical simulations show that the array of electrically small resonators can be highly efficient in delivering the maximum captured power to one load using different topologies of corporate feed networks. The two networks show 94% and 99.4% Radiation-to-RF conversion efficiency, respectively.

Then, a prototype was fabricated incorporating a rectification circuit. Measurements demonstrated that the proposed metasurface harvester provides Radiation-to-DC conversion efficiency of more than 55%, which is significantly higher than earlier designs reported in the literature.

6.2 Metamaterial Absorbing and Harvesting

Wireless power transfer is the process of transferring power between remote devices and converting it to usable electrical energy. The most important aspect of the energy transfer link is the Radiation-to-RF conversion and RF-to-DC conversion. The primary objective of this work is to provide a design that maximizes the conversion efficiency between the incident electromagnetic radiation and the DC power at the receiving load.

An absorber in general is a panel or a device that can absorb energy, and in electromagnetics particularly, is a medium that neither reflects nor transmits incident radiation. For example, a solar hot water system is an ensemble of collectors that absorbs the suns energy to heat water with an efficiency of up to 87% [127]; a bolometer is a device that converts electromagnetic energy to thermal energy, and the ideal bolometer detector can absorb most of the photons falling on the surface and then convert them to heat [128]. In both absorbers and energy harvesters, the main energy collectors are conventional antennas (rectennas). Previous works utilizing rectennas to harness the energy from space and the surrounding environment have attracted much interest, especially their improvement of conversion efficiency [64, 65]. Generally, any enhancements in recetnna systems have been focused on the rectifier circuit, matching circuit and other factors, rather than on the main component: the collectors. Recently, interest has been growing in using metamaterial cells as electromagnetic collectors.

Metamaterials are artificial electromagnetic materials engineered to allow manipulation of the electromagnetic field through control of the permittivity and permeability of the material [19]. The property of tuning the permittivity and permeability of the metamaterials have led to full absorption by matching the material surface impedance to the free-space impedance. Various metamaterial absorber designs have been proposed to operate in both microwave [28] and optical [129] regimes. Metamaterial harvester designs are also attracting attention, and high harvester conversion efficiency has been achieved in both microwave [21, 30, 74]. and infrared [22] regimes.

Each metamaterial absorber unit cell is a metallic inclusion hosted on a dielectric substrate and backed by a ground plane, whereas metamaterial harvester unit cells in only some designs are backed by a ground plane [30] and in some designs are not [21, 22]. However, higher conversion efficiency is reached when the harvesters are backed by a ground plane. In most designs, harvesters are the same as absorbers, with the only difference being that the harvesters required full absorption and maximum power delivered to the load.

In **Chapter 5**, a metasurface electromagnetic energy harvester based on electrically small resonators is presented. The footprint size of the structure was $120mm \times 120mm$

and 89% energy conversion efficiency achieved at resonance frequency of the design. 74% conversion efficiency was experimentally achieved at the resonance of the structure. The good agreement between the simulation and experimental results proved the concept of the design. However, the conversion efficiency is a critical parameter in developing electromagnetic energy harvesting. Moreover, the optimal goal of energy harvesting is to exploit the empty areas limited in the cities to harvest the maximum energy possible.

Minimizing the devices footprint and having full absorption are the main goals for energy absorbers. Energy harvesters require not only these two features but must also maximize conversion efficiency and channell the power to a load. In this work, we first proposed a design for a unit cell metamaterial absorber with near unity absorbance operating in the microwave regime. Full absorption of the incident field occurred when we matched the impedance to the free space. The unit cell designed is based on Electric Inductive Capacitive (ELC) resonators reported earlier in the literature [130]. Second, after experiencing full absorption, the same unit cell design was used as an energy harvester by channeling the received power to a load through a via. Third, an array of these cells, Electric Inductive Capacitive (ELC) resonators, operating in the microwave regime is proposed to collect microwave energy. Finally, different mechanisms are proposed by which the energy received from each individual cell is channeled to one shared load rather than each cell channeling the energy to its own individual load.

6.3 Design Methodology

Fig.6.1 show the unit cell used in this work to collect the EM energy is the ELC resonator element, similar to the one reported earlier to resonate in terahertz. The cell consists of two split ring resonators facing opposite each other, connected by a wire parallel to the split wire and hosted on a $t = 2.5mm$ thickness Rogers RT6006 substrate with a dielectric constant of $\epsilon_r = 6.15$ and a loss tangent of $tan\delta = 0.0027$. The cell is backed by a ground plane. The geometric dimensions of the cell were optimized to achieve full absorption and later maximum conversion efficiency at $2.72GHz$. The strip length $L = 7mm$, strip width $W1 = 1.2mm$, width of the parallel wire $W2 = 0.5mm$, split gap $g = 0.5mm$, separation distance $S = 0.25mm$, and copper thickness $t = 35mu$. The unit cell proposed for harnessing energy in this work is the same one we used for absorbing energy. However; a resistive load was connected to the ELC through a metallic via.

The individual unit cells for the absorber and harvester were designed using the commercial 3D electromagnetic simulation software CST MICROWAVE STUDIO 2015. To examine the S-parameter properties of the cell, the unit cell was placed in the center of

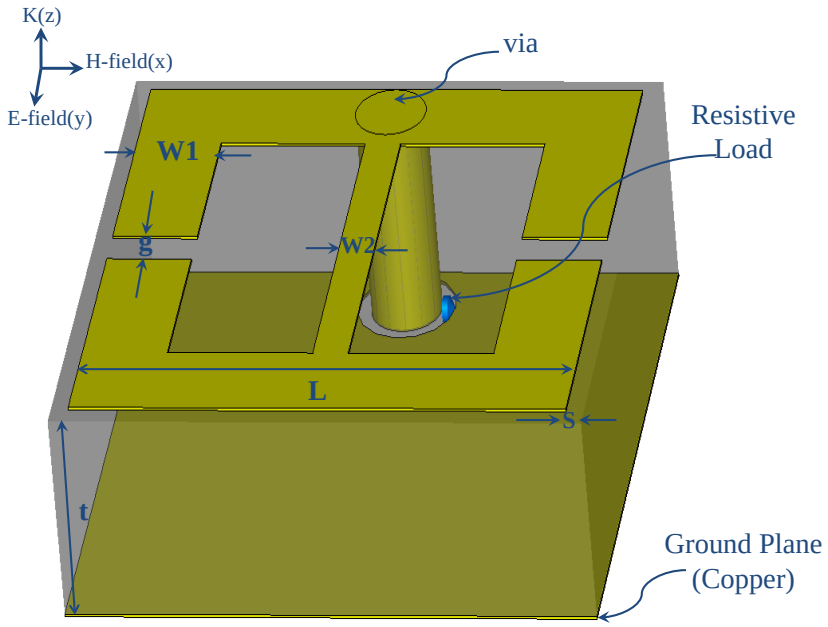

Figure 6.1: A schematic of ELC proposed unit cell.

a waveguide with proper boundary conditions; a perfect electric wall in the (xz-plane), a perfect magnetic wall in the (xy-plane), and two open ports in the z-directions. Such particular boundary conditions were chosen to ensure the electric and magnetic fields were parallel to the metallic surface inclusion, where these ELCs resonators were excited by a method explained in [90].

One can calculate the absorption of the unit cell using the S-parameters (S_{21} and S_{11} are the transmission and reflection coefficient respectively) produced by the simulation. The absorption of the unit cell is obtained by the formula $A = 1 - S_{11}^2 - S_{21}^2$. Full absorption can be achieved by tuning ϵ and μ of the unit cell to match the metamaterial impedance to the free space impedance 377Ω thus ensuring no reflectance occure. Full absorption also requires zero transmission, which can be done by using another layer serving as a ground plane. Fig.6.2 shows the reflectance and absorbance of the proposed cell at $2.72GHz$, where the peak absorption was 99.9% and the bandwidth was. Both the absorber and harvester are tremendously affected by the small distance between the cells, because the coupling plays the key role of changing the metamaterial unit cell input impedance.

The critical design parameters for the energy harvesting unit cell are the optimal resistive load and the via position. The optimized resistance value was found to be 180 Ω,

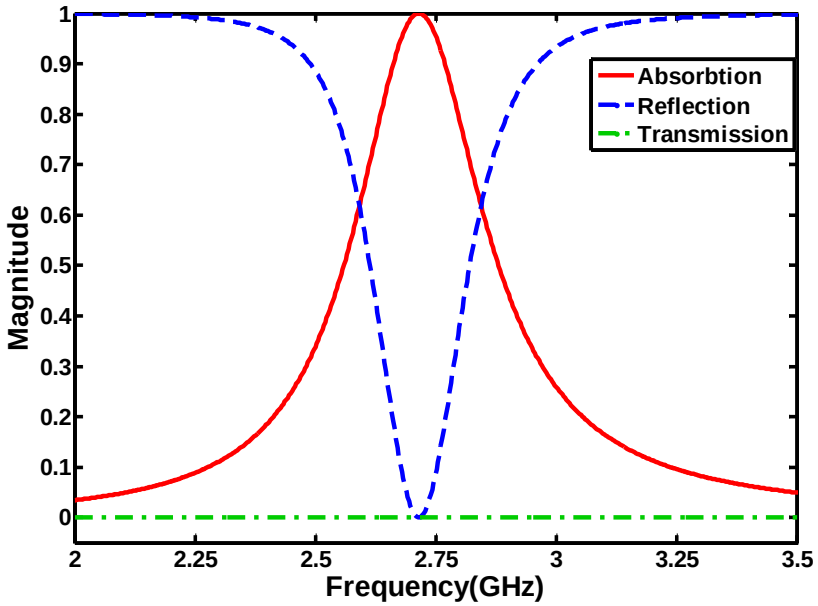

Figure 6.2: Simulation results of perfect metamaterial absorber: absorption, reflection and transmission.

which equal the impedance of the ELC resonator (as seen from the load). Having these matched impedance values ensured that maximum power was transferred from ELC to the load. The via was placed at the top of the ELC to create a path for the current to flow from the surface of the ELC to the resistive load (Fig.6.1).

6.4 Metasurfaces Array for Energy Harvesting

The proposed unit cell showed the promising ability of these harvesters to collect electromagnetic energy and channel it to a resistive load. On the other hand, the power received by the proposed element is too low to operate even small devices. For practical scenarios, an array of these elements is needed to supply a device or a system with a sufficient power. Therefore, an array with a $60mm \times 60mm$ footprint occupied by 8×8 ELCs (Fig.6.3) was designed and simulated to achieve near unity overall energy harvesting. The harvester array was designed using the commercial full wave simulator ANSYS® HFSS™. As in a unit cell, the array was centered in an open radiation box and excited by a plane wave to ensure that the electric field was parallel to the wire between split ring resonators that had

the via and the magnetic field was parallel to the split wire of the resonator (Fig.5.2).In this work, the harvesting energy efficiency was obtained by a formula reported in earlier work [21] as explained in **Chapter 5**:

$$\eta = \frac{P_{received}}{P_{incident}},$$

where $P_{received}$ is the total time-average power received by the metasurface array (dissipated in the resistive load), and $P_{incident}$ is the total time average power incident on the array.

For N collectors, $P_{received}$ is given by:

$$P_{received} = \frac{{V_L}^2}{R_L} \tag{6.1}$$

where V_L is the voltage across and the resistance R_L of all collectors at the load.

6.5 Power Channeling

In this section, we focus on developing two different feed networks to channel the array collected power to one resistive load by using the same mechanism that was used in **Chapter 4**. Significant power conversion efficiency (near unity) was achieved, which is a great improvement compared to the previous work. Moreover, this structure's footprint is three quarters smaller than the previous one.

As mentioned, the separation distance (periodicity) between the adjacent unit cells is a critical factor in energy harvesters; the metamaterial unit cell impedance can be controlled by changing this distance. Meanwhile, the periodicity is generally a very small distance, which results in high coupling between the array elements and leads to higher received power. On the other hand, the small periodicity distances have led us to introduce another substrate underneath the ground plane to build the feed network. The main idea behind the feed network is to channel overall energy collected by the array to one resistive load by matching the elements' impedance to the load impedance. Two different feed cases are considered in this work.

In both cases, a $0.5mm$ Rogers RT6002 substrate having a dielectric constant of $\epsilon_r = 2.94$ and a loss tangent of $tan\delta = 0.0012$ was attached underneath the ground plane to host the routing mechanism. As is pointed above, each element has an optimal 180Ω impedance value. The resistive load value was chosen as 50Ω to match the measurement devices, which

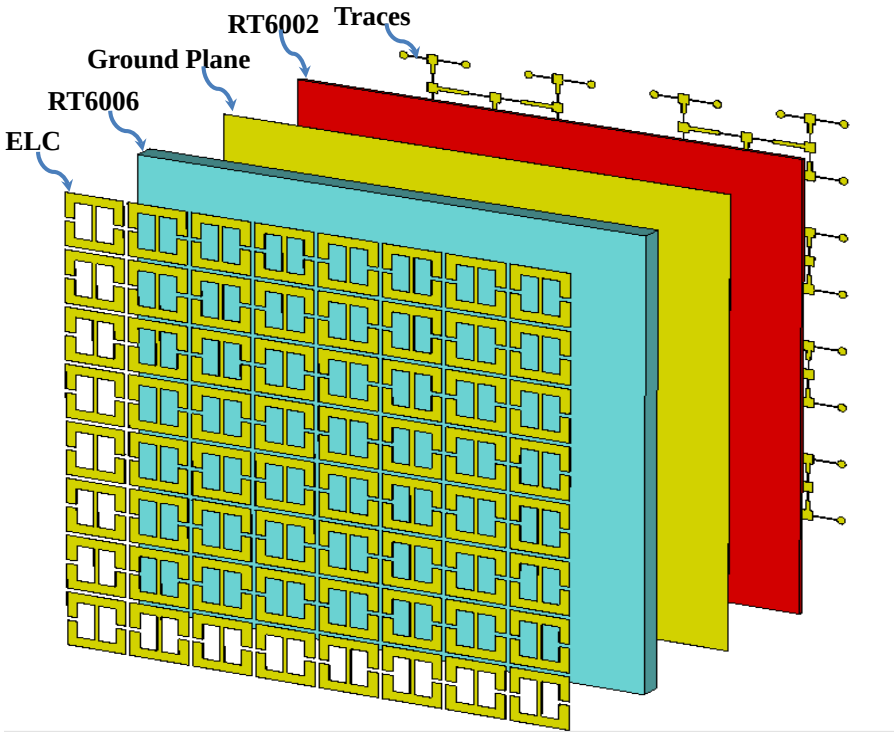

Figure 6.3: Diagram of the harvester elements is shown as exploded view, including the electrical inductive capacitive resonators, Rogers RT6006 substrate as first substrate, ground plane (copper), Rogers RT6002 as second substrate, and the transmission line traces.

are mostly based on 50Ω systems. This choice significant advantages in the measurements stage, as no matching circuits are needed.

In the first case, a corporate feed network was used without considering the traces' line impedances (i.e., all the transmission lines have the same impedance). Here, the routing traces have the same widths as depicted in Fig.6.4(a): 180Ω transmission line with width $0.02239mm$. In the second case, the routing traces were designed by using the same technique used in the antenna corporate feed. Six different transmission lines were used to design the routing to match all the elements to a 50Ω load. The transmission line widths for 50Ω, 90Ω, 94Ω, 100Ω, 127Ω, and 180Ω are $1.24426mm$, $0.4035mm$, $0.3626mm$, $0.3087mm$, $0.1462mm$, and $0.02239mm$, respectively. Fig.6.4(b) depicts the second proposed routing mechanism for channeling the array-collected power to one 50Ω resistive load.

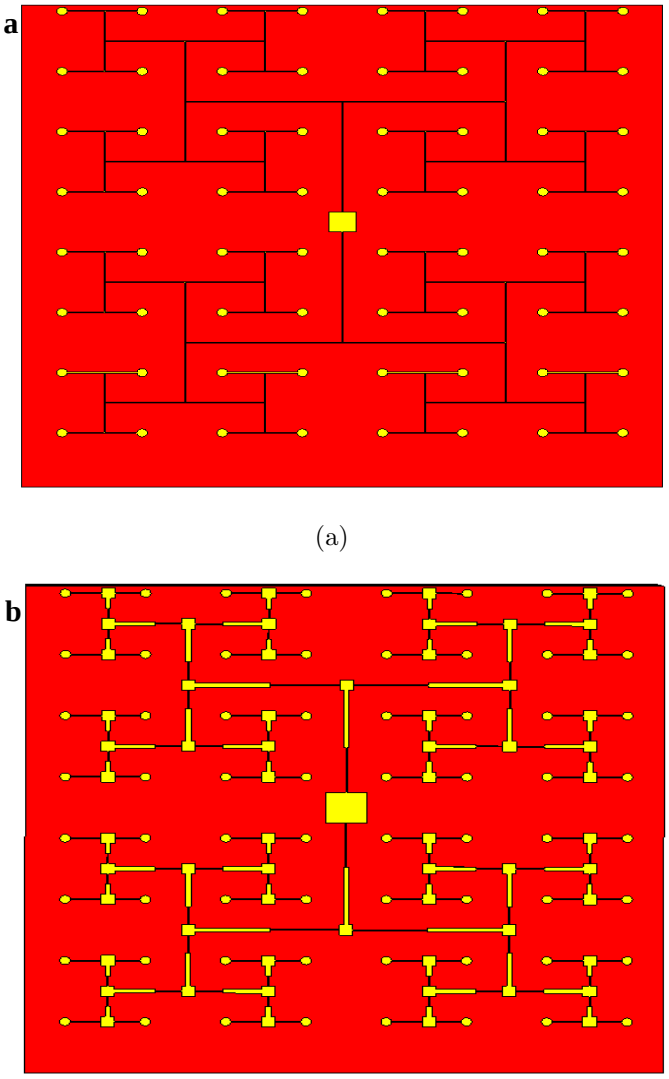

(a)

(b)

Figure 6.4: Symmetrical configuration of the corporate fed array (64-element) for (a) case1, (b) case2.

6.6 Simulation Results

In both cases, high conversion efficiency is maintained; however, in the second case, near unity conversion efficiency is achieved. Fig.6.5 depicts the conversion efficiency of both cases over a wide frequency range in the S-band. The highest conversion efficiency of the simulations, 94% and 99.4% for case 1 and case 2, respectively, occurred at the resonance frequency of the structure $2.72GHz$.

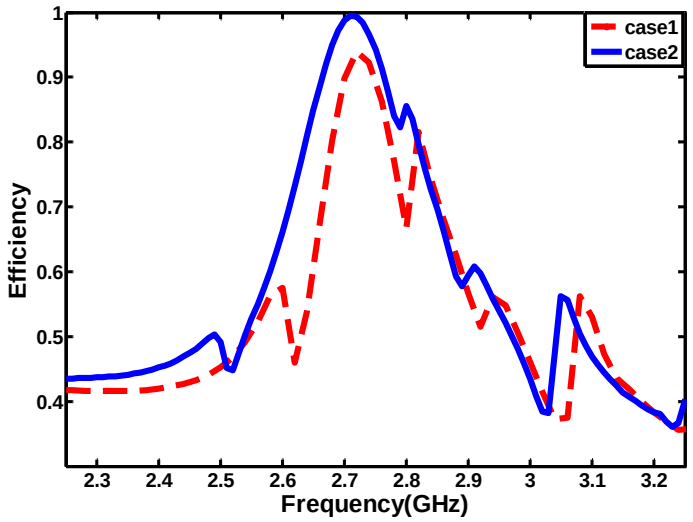

Figure 6.5: The simulated conversion efficiency of the metasurface harvester.

Figure 6.6 shows the simulated Radiation-to-RF conversion efficiency of the proposed harvester. Comparison is made to chapter 5. High conversion efficiency of approximately 99.4% is observed at the resonance frequency. Additional comparison is made to a conventional microstrip patch antenna designed to operate at the same frequency. For fair comparison using the most critical criteria of energy harvesters, namely their physical footprint, we could only position one patch antenna on the area of the harvester (viz., 60 mm×60 mm). As shown in Fig.6.6 , the metasurface harvester produced significantly more power than the patch antenna. We note that the placement of additional microstrip patches provided lower absorption than a single patch (the results are not shown here for brevity).

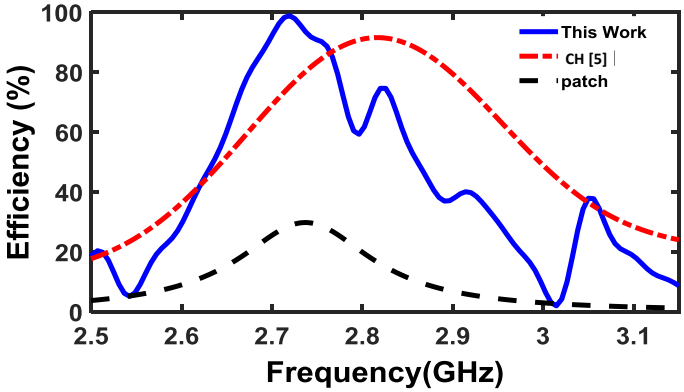

Figure 6.6: Comparison between the simulated Radiation-to-RF conversion efficiency of the metasurface design introduced here, the patch antenna and the metasurface design in chapter 5.

6.7 Experimental Verification and Discussion

An 8×8 elements metasurface antenna was fabricated based on the simulated design; for 180Ω transmission line with width of $0.1mm$ (instead of $0.02239mm$)was chosen due to the fabrication constraints which required minimum transmission line width $0.1mm$. Fig.6.7 shows the fabricated harvester. A rectifier was then designed using Agilent Advance Design Systems (ADS) having an input impedance of 50Ω at the resonance frequency. The diode was connected to the feed of the antenna through a matching network containing a short circuited stub, open circuited stub and a series transmission line. Then a DC filter containing two series transmission lines and two open circuited stubs along with a 150pF was connected to the cathode node of a HSMS 2860 Schottky diode along with a resistive load. The same rectifier circuitry used in (**Chapter 5**) is adopted here. The design schematic for the rectification circuit is shown in Fig.6.8a, and the fabricated rectifier is shown in Fig.6.8b.

Measurements of received power were performed in an anechoic chamber. The metasurface antenna was placed approximately positioned a distance of 1 m away from the transmitting antenna such that the electric field is parallel to the ERR arm containing the via (see Fig.6.1). The power across the DC load is then measured at the optimal frequency and incident power level. The peak radiation to DC power conversion efficiency, of the array including the rectifier was 55% at 2.85 GHz and 51% at 2.72 (see Fig.6.9).The proposed harvester has higher RF radiation to DC efficiency than the previous work [32] as shown in Fig.6.9.

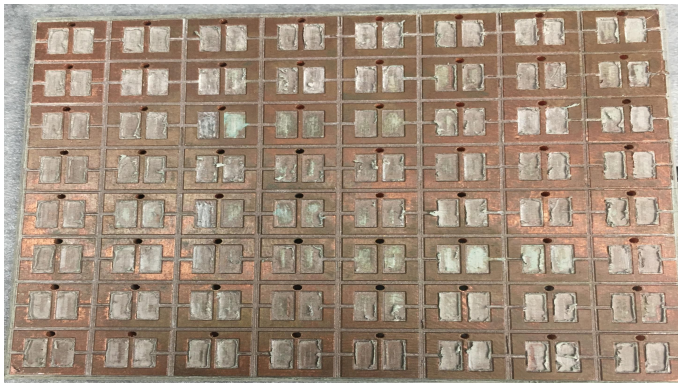

(a)

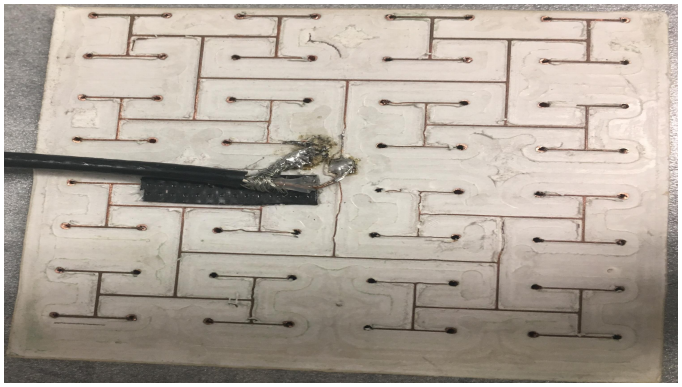

(b)

Figure 6.7: Photograph of the fabricated metasurface harvester (a) top view (b) bottom view.

The metamaterial harvester is compared with a conventional antenna to find of which can provide more power. Patch antenna designed to operate at the same frequency of the metamaterial harvester and only one patch antenna can fit the area of the harvester ($60mm \times 60mm$). As shown in Fig.6.10, the metamaterial harvester produces power more than the patch antenna. Without considering the distance between patches $\lambda/2$, four patches can fit the area but they will produce less power than one patch antenna because of the coupling between antennas; however, in metamaterial harvesters coupling is playing a key role of enhancing the efficiency.

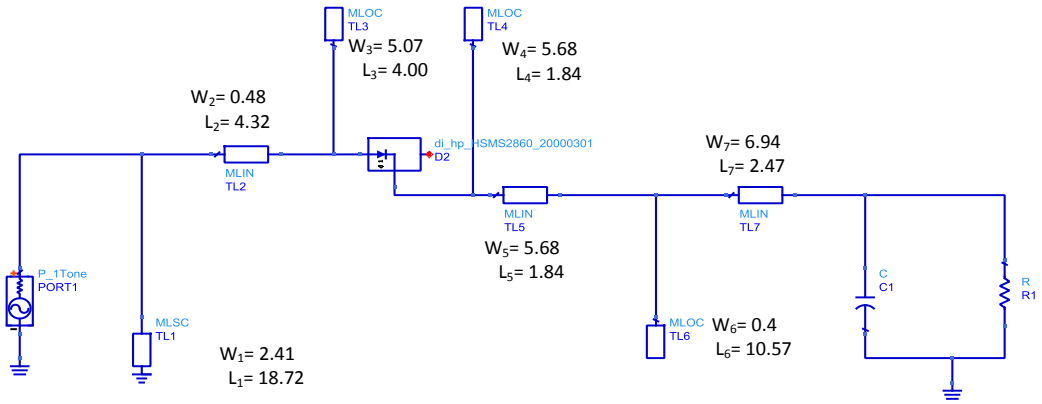

(a)

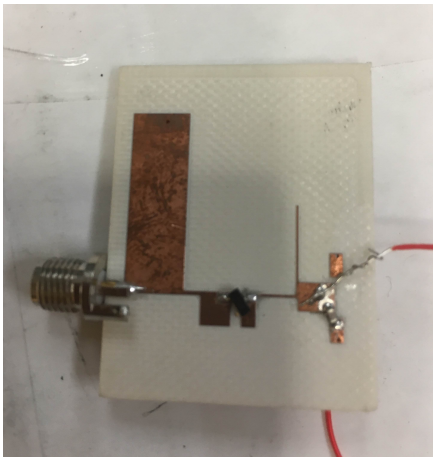

(b)

Figure 6.8: Rectifier circuit (a) schematic design (b) Photograph of the fabricated rectifier

6.8 Conclusion

In this work, a unit cell perfect absorber has been presented first.Then, we extended the concept of perfect absorbance to metasurface perfect harvesters, where most of the absorbed power is channeled to a resistive load. For practical scenarios, where more power is needed, an ensemble of 8×8 ELC cells was designed and simulated. After achieving high efficiency, the focus changed to channeling the network by a mechanism designed

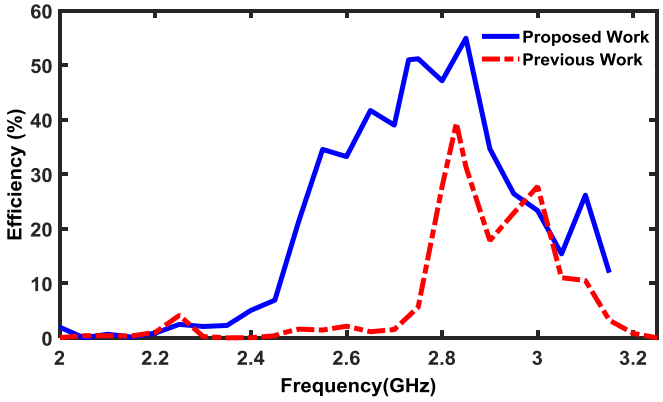

Figure 6.9: The measured RF radiation to DC efficiency of the previous and proposed metasurface harvesters.

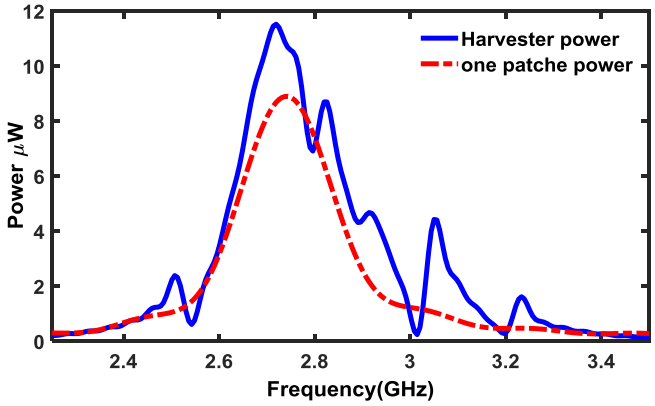

Figure 6.10: Power values of the proposed harvester and conventional antenna.

to deliver all the power collected by the cells to one resistive load only. Two different corporate feed networks have been proposed here to emphasize the impedance effect of the channeling circuit. One can observe that, for maximum power transfer, the impedance of the metasurface cell must be equal to the load impedance (viewed from the load) by using a proper matching circuit. Previous metamaterial energy harvesting focused on collecting energy from the sun and using wireless power transfer. Our metasurface harvester has the additional capability of collecting ambient energy and using it to power in other small applications such as sensor networks and health monitor sensor, with near unity efficiency.

Chapter 7

Metasurface Imaging

7.1 Introduction

We expand the concept further to use it for imaging. A novel metasurface sensor is presented to image objects without any scanning. An 20×20 array of Electric Inductive capacitor (ELC) resonators, operates at 2.5 GHz, occupied $150 \times 150mm$ footprint area has been designed and used to image different objects for both materials dielectric and metallic.

7.2 Metamaterials and its Potential for Imaging

Historically, there has been much interest in electromagnetic imaging because of it is important application including but not limited to health, military, security, aeronautics, and civil operations. Electromagnetic imaging technologies have been established in different spectrum bands microwave, millimeter wave, and submillimeter wave [131–133]. Electromagnetic waves have the ability of penetrating different materials and resulting in high resolution images for hidden people and hiding cracks where eyes and visual technologies can not define these hidden objects. The authors in [134] were able to image people in the farfield: they use the existing Wi-Fi signals to through walls. The previous work of the authors, sensors based on complementary split ring resonators (CSRR) have been developed to image anomalies and defects in different materials in the near-field microwave [82]. The sensor was very small comparing to the material under test, therefore; a raster scanning

technique is used to map the anomalies position and size [80]. Because of their small sizes, metamaterials have been widely used.

When Smith, Pendry and others started tinkering with Split-ring Resonators (SRR) for realizing double negative media, little did know then that these earlier ground-breaking works ushered the beginning of a completely different perspective on designing electromagnetic-based systems. The SRR, or any other resonator that has dimensions much smaller than the wavelength were used as the building blocks for single and double negative media and even near-zero media. While these exotic media enabled cloaking and design of dispersion-controlled media, the applications were largely limited. After 18 years of first realization of the modern metamaterials, technologies based on metamaterials have been established in all spectrum bands and various applications. One of the most critical applications of metamaterials is imaging. Advanced microwave imaging systems that uses metamaterial have been presented by different research groups and high-resolution images obtained, however; these systems have complex computational imaging techniques [80].

In this work, we introduce metasurface sensor to image objects without scanning in nearfield microwave. The sensor consists of 20×20 ELCs resonators. Each ELC acts as a pixel. High resolution images can be achieved with more number of pixels.

7.3 Design Methodology

Figure.7.1 shows the unit cell used in this work to collect the EM energy is the ELC resonator element, similar to the one reported earlier to resonate in terahertz [24]. The cell consists of two split ring resonators facing opposite each other, connected by a wire parallel to the split wire and hosted on a $t = 2.5mm$ thickness Rogers RT6006 substrate with a dielectric constant of $\epsilon_r = 6.15$ and a loss tangent of $tan\delta = 0.0027$. The cell is backed by a ground plane. The geometric dimensions of the cell were optimized to achieve high power conversion efficiency at $2.75GHz$. The strip length was $L = 7mm$, strip width was $W1 = 1.2mm$, width of the parallel wire was $W2 = 0.5mm$, split gap was $g = 0.5mm$, separation distance was $S = 0.25mm$, and copper thickness $t = 35mu$. a resistive load was connected to the ELC through a metallic via.

7.4 Numerical Models and Results

A 20×20 array of ELC resonators designed to image objects. Each ELC cell has a resistive load connected to it. The imaging idea here is to use the voltage across these resistive loads.

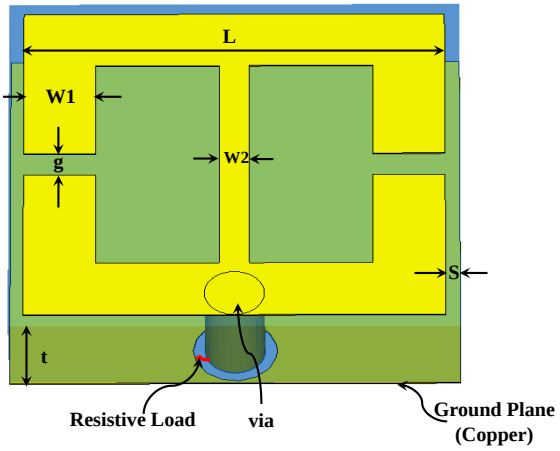

Figure 7.1: A schematic of EIC proposed unit cell.

The ELC array (metasurface sensor) is in the receiving mode that is if there is no object between the transmitter and the sensor, each ELC will receive specific power (voltage across the resistive load). While if there is any object between the transmitter and the sensor, the object will disturb the incident plane wave and the ELCs covered by the object will receive a power is different from the received power by uncovered ELCs (different voltage value across the resistive load). Presented below some examples to illustrate how the simplicity and the effectiveness of idea under study.

The ability of the metasurface sensors for imaging, both materials dielectric and metallic structures was studied and analyzed. The goal of the study is to is to reconstruct images of different objects. Fig.7.2 shows the metasurface sensor used to image various structures in this work.

7.4.1 Imaging Dielectric Structures

Different imaging examples have been study in this work. Fig.7.3 shows the metasurface sensor used for imaging three different dielectric bars (red, green, and blue). The size of the bars is 15 mm width and 30 mm length. The thickness of each bars kept the same 1 mm and the liftoff distance from the sensor was 1 mm. Three different dielectric properties of the materials were chosen (red bar=9.8, green bar=6.2 and blue bar=2.2). Fig.7.4 shows the imaging of the three different dielectric constant bars.

In the second example, the dielectric constant of the three bars kept the same 9.8 and

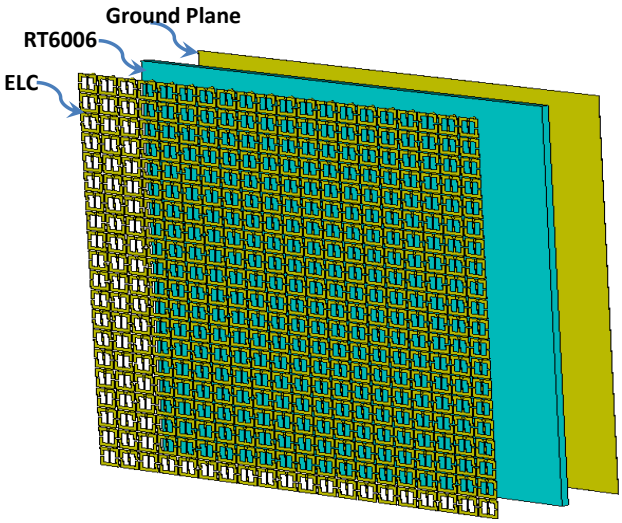

Figure 7.2: Diagram of the metasurface sensor is shown as exploded view, including the electrical inductive capacitive resonators, Rogers RT6006 substrate and ground plane (copper).

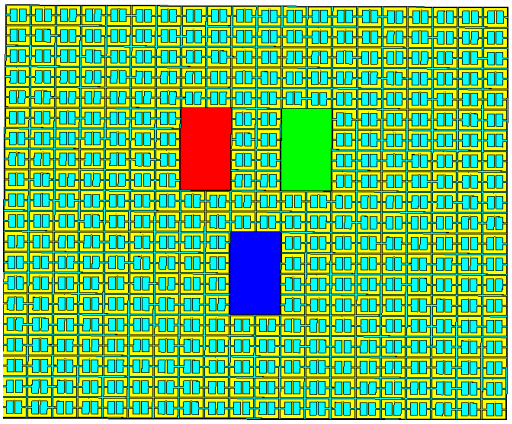

Figure 7.3: The designed metasurface sensor with three different bars.

the thickness of three of them kept 1 mm. The liftoff distance is different for the bars. Fig.7.5 shows the simulation results of the three bars with different liftoff distance.

In the last example, the thickness of the three bars examined. The dielectric constant and the liftoff distance kept the same 9.8 and 1 mm, respectively. Fig.7.6 shows the

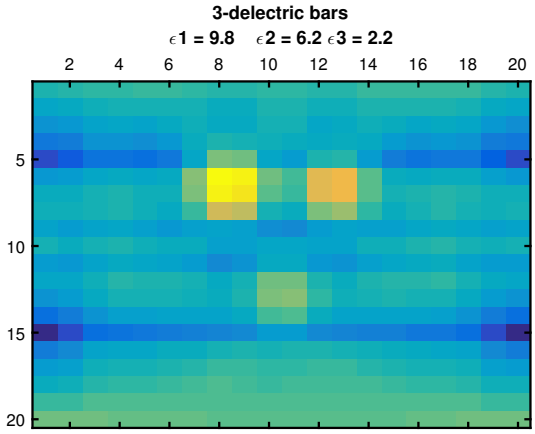

Figure 7.4: Three different dielectric materials.

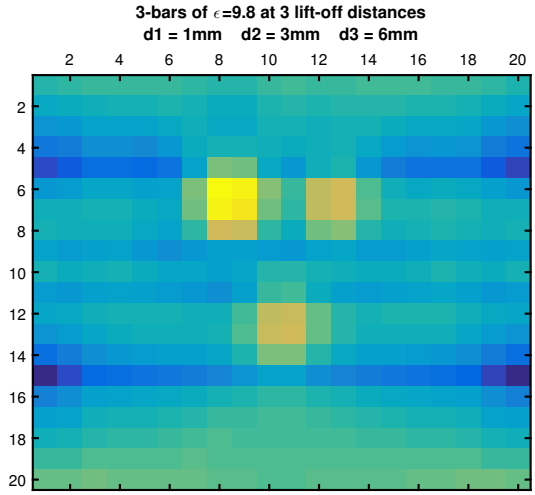

Figure 7.5: Three different liftoff distances.

simulation image of the bars with different thicknesses.

After Imaging different bars thickness, liftoff distances, and dielectric properties, a new dialectic shape is proposed to image. The symbol of University of Waterloo is known as UW. In this case of study, the UW shape is built with material dielectric constant of 9.8

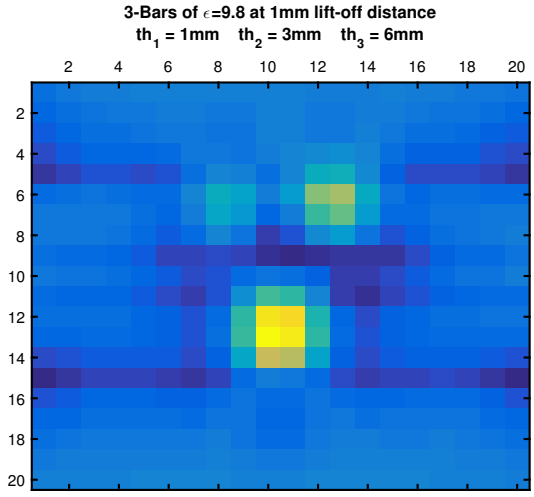

Figure 7.6: Three different thichnesses.

with and thickness of 1 mm and placed at a liftoff distance 1 mm, (see Fig.7.7). Fig.7.8 shows the simulation results of UW-shaped objects.

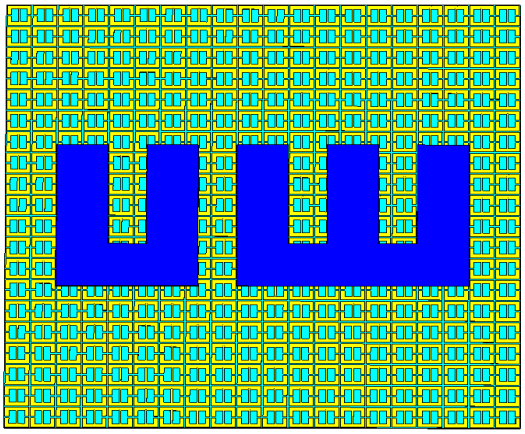

Figure 7.7: Metasurface sensor with UW shape.

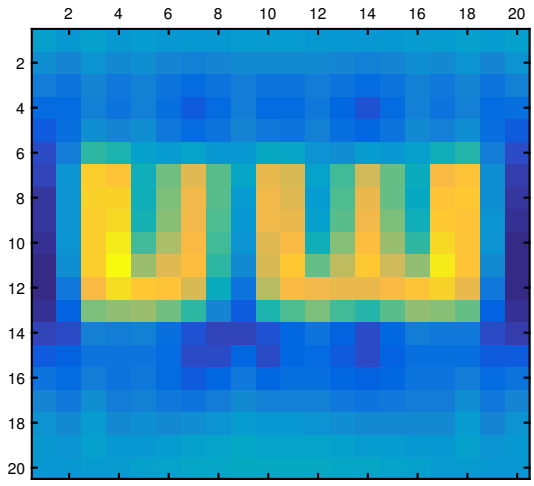

Figure 7.8: Image of UW shape.

7.4.2 Imaging Metallic Structures

The second simulated materials were a metallic structure consisting of UW shape. The UW shape has a 1mm thickness and 1mm liftoff distance

7.5 Conclusion

The metasurface sensor has strong ability to image different material structures with different shapes. As shown in the simulation results, the imaging resolution depends on many parameters. Images have the higher resolution for materials having higher dielectric constant, lower liftoff distance and thicker materials. The last part of the thesis shows the numerical simulation of using metasurfaces panels for imaging objects.

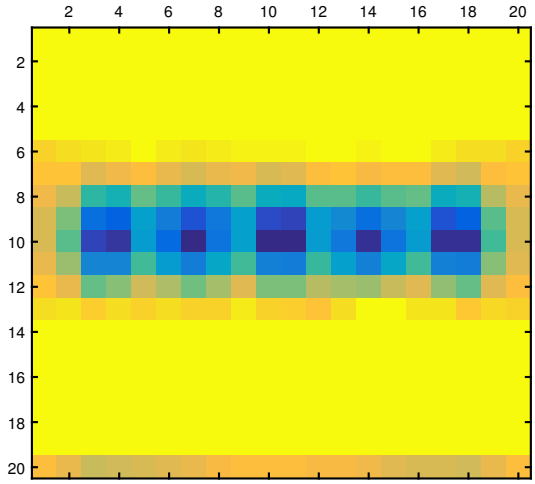

Figure 7.9: Image of metallic UW shape.

Chapter 8

Accomplished and Future Work

8.1 Accomplished Work

1. The first generation of metasurface antennas operating in the microwave regime is presented. The antenna was designed and simulated. A prototype was fabricated and tested showing a good agreement between numerical simulations and experimental results. (**Chapter 2**)

2. 2. A comprehensive study on new metasurface antenna features were investigated and compared with classical antennas. Some of these features are; gain enhancement, beam steering, and polarization. Also, testing the antenna in higher frequency regimes has been done in (**Chapter 3**)

3. 3. Huygens Principle studied and a new conformal antenna was introduced. The new antenna shows high advantages on conventional antennas in gain and beam steering by using very simple technique to control the beam directions. (**Chapter 4**)

4. A metasurface antenna as an electromagnetic energy collector based on electrically small resonators is presented. The metasurface antenna that harvests the microwave receiving energy and then channels it to one resistive load is introduced via a new mechanism by which all the received power is channeled to one load is proposed. A prototype was fabricated and tested showing good agreement between numerical simulations and experimental results. Both AC and DC results showing in this work. (**Chapter 5**)

5. Near Unity metasurface harvesting based on perfect absorbers was presented. An array of these cells, Electric Inductive Capacitive (ELC) resonators, operating in the microwave regime is proposed to collect the microwave energy. Then, we proposed different mechanisms, by which the received energy from each individual cell was channeled to a one same load rather than each cell channeling the energy to a load different from the others. A prototype was fabricated and tested showing good agreement between numerical simulations and experimental results. (**Chapter 6**)

6. 6. Metasurface imager introduced in this dissertation an extended application of metasurface proposed in (**Chapter 2**). The new metasurface imagers show a decent resolution images of the targeted imaging objects where different materials used in this work. (**Chapter 7**)

8.2 List of Publications

1. Mohamed El Badawe, Thamer S. Almoneef, and O.M. Ramahi. A True Metasurface Antenna. *Scientific Reports*, Vol. 6, pp. 19268, 2016 **(published)**.

2. Mohamed El Badawe, Thamer S. Almoneef, and O.M. Ramahi. A metasurface for conversion of electromagnetic radiation to DC. *AIP Advances*, Vol.7, No. 3, pp. 035112, 2017 **(published)**.

3. Mohamed El Badawe and O.M. Ramahi. Efficient Metasurface Rectenna for Electromagnetic Wireless Power Transfer and Energy Harvesting. *Progress In Electromagnetics Research 161 (2018): 35-40.* **(published)**.

4. Mohamed El Badawe and O.M. Ramahi. Design of Conformal Antennas using Electrically-Small Radiators. *IEEE Transactions on Antenna and Propagation*, 2018 **(Submitted)**.

5. Mohamed El Badawe, Thamer S. Almoneef, and O.M. Ramahi. A True Metasurface Antenna. *016 IEEE International Symposium on Antennas and Propagation (APSURSI)*,IEEE 2016. **(Conference)**.

6. Mohamed El Badawe and O.M. Ramahi. Generic Antenna Design using Metasurfaces. *2016 17th International Symposium on Antenna Technology and Applied Electromagnetics (ANTEM)*,IEEE 2016. pp. 609-610 **(Conference)**.

7. Mohamed El Badawe and O.M. Ramahi. Towards a Methodology for Antenna Design. *, 2017 The International Workshop on Antenna Technology (iWAT 2017)*,IEEE 2017. **(Conference)**.

8. Mohamed El Badawe and O.M. Ramahi. A cylindrical metasurface antenna. *017 IEEE International Symposium on Antennas and Propagation (APSURSI)*,IEEE 2017. pp. 1945–1946 **(Conference)**.

9. Mohamed El Badawe and O.M. Ramahi. A True Metasurface Antenna. *US Provisional Patent Application*. **(Patent)**.

8.3 Future Work

The following activates are planned and some of them are in progress:

1. **Analyze and compare** the concept to millimeter-waves and terahertz classic antennas.

2. **Apply** phase shifters to steer the beam electronically.

3. **Fabricate** the proposed conformal antenna and experimentally tested.

4. **Design and fabricate** the right rectification circuitry for the proposed harvesters to achieve higher radiation to DC conversion efficiency (**Chapter 5 and 6**).

5. **Fabricate** the metasurface imager and use it in the real world.

6. **Investigate** other potential applications of metasurfaces, practically the applications of metasurface antenna.

Bibliography

[1] N. Engheta and R. W. Ziolkowski, *Metamaterials: physics and engineering explorations*. John Wiley & Sons, 2006.

[2] A. Sihvola, "Metamaterials in electromagnetics," *Metamaterials*, vol. 1, no. 1, pp. 2–11, 2007.

[3] H. Lamb, "On group - velocity," *Proceedings of the London Mathematical Society*, vol. s2-1, no. 1, pp. 473–479, 1904. [Online]. Available: http://plms.oxfordjournals.org/content/s2-1/1/473.short

[4] L. I. L.I.Mandelshtam, "Group velocity in crystalline arrays," *Opt. Spektrsk*, vol. 3, no. 1, pp. 308–312, 1957.

[5] V. G. Veselago, "The electrodynamics of substances with simultaneously negative values of img align= absmiddle alt= eps/img and μ," *Physics-Uspekhi*, vol. 10, no. 4, pp. 509–514, 1968.

[6] D. R. Smith, W. J. Padilla, D. Vier, S. C. Nemat-Nasser, and S. Schultz, "Composite medium with simultaneously negative permeability and permittivity," *Physical review letters*, vol. 84, no. 18, p. 4184, 2000.

[7] R. A. Shelby, D. R. Smith, and S. Schultz, "Experimental verification of a negative index of refraction," *science*, vol. 292, no. 5514, pp. 77–79, 2001.

[8] C. L. Holloway, E. F. Kuester, J. Gordon, J. O. Hara, J. Booth, D. R. Smith *et al.*, "An overview of the theory and applications of metasurfaces: The two-dimensional equivalents of metamaterials," *Antennas and Propagation Magazine, IEEE*, vol. 54, no. 2, pp. 10–35, 2012.

[9] R. W. Ziolkowski and E. Heyman, "Wave propagation in media having negative permittivity and permeability," *Physical review E*, vol. 64, no. 5, p. 056625, 2001.

[10] C. Caloz, C.-C. Chang, and T. Itoh, "Full-wave verification of the fundamental properties of left-handed materials in waveguide configurations," *Journal of Applied Physics*, vol. 90, no. 11, pp. 5483–5486, 2001.

[11] I. V. Lindell, S. Tretyakov, K. Nikoskinen, and S. Ilvonen, "Bw mediamedia with negative parameters, capable of supporting backward waves," *Microwave and Optical Technology Letters*, vol. 31, no. 2, pp. 129–133, 2001.

[12] J. B. Pendry, "Negative refraction makes a perfect lens," *Physical review letters*, vol. 85, no. 18, p. 3966, 2000.

[13] A. K. Iyer and G. V. Eleftheriades, "Negative refractive index metamaterials supporting 2-d waves," in *Microwave Symposium Digest, 2002 IEEE MTT-S International*, vol. 2. IEEE, 2002, pp. 1067–1070.

[14] M. Silveirinha and N. Engheta, "Tunneling of electromagnetic energy through subwavelength channels and bends using ε-near-zero materials," *Physical review letters*, vol. 97, no. 15, p. 157403, 2006.

[15] W. Zhao, J. L. Bischof, J. Hutasoit, X. Liu, T. C. Fitzgibbons, J. R. Hayes, P. J. Sazio, C. Liu, J. K. Jain, J. V. Badding *et al.*, "Single-fluxon controlled resistance switching in centimeter-long superconducting gallium–indium eutectic nanowires," *Nano letters*, vol. 15, no. 1, pp. 153–158, 2014.

[16] M. Gokkavas, K. Guven, I. Bulu, K. Aydin, R. Penciu, M. Kafesaki, C. Soukoulis, and E. Ozbay, "Experimental demonstration of a left-handed metamaterial operating at 100 ghz," *Physical Review B*, vol. 73, no. 19, p. 193103, 2006.

[17] T.-J. Yen, W. Padilla, N. Fang, D. Vier, D. Smith, J. Pendry, D. Basov, and X. Zhang, "Terahertz magnetic response from artificial materials," *Science*, vol. 303, no. 5663, pp. 1494–1496, 2004.

[18] G. Dolling, M. Wegener, C. M. Soukoulis, and S. Linden, "Negative-index metamaterial at 780 nm wavelength," *Optics letters*, vol. 32, no. 1, pp. 53–55, 2007.

[19] M. Ruphuy, Z. Ren, and O. M. Ramahi, "Flat far field lenses and reflectors," *Progress In Electromagnetics Research M*, vol. 34, pp. 163–170, 2014.

[20] D. Schurig, J. Mock, B. Justice, S. A. Cummer, J. B. Pendry, A. Starr, and D. Smith, "Metamaterial electromagnetic cloak at microwave frequencies," *Science*, vol. 314, no. 5801, pp. 977–980, 2006.

[21] O. M. Ramahi, T. S. Almoneef, M. AlShareef, and M. S. Boybay, "Metamaterial particles for electromagnetic energy harvesting," *Applied Physics Letters*, vol. 101, no. 17, p. 173903, 2012.

[22] M. R. AlShareef and O. M. Ramahi, "Electrically small resonators for energy harvesting in the infrared regime," *Journal of Applied Physics*, vol. 114, no. 22, p. 223101, 2013.

[23] R. W. Ziolkowski and A. Erentok, "Metamaterial-based efficient electrically small antennas," *Antennas and Propagation, IEEE Transactions on*, vol. 54, no. 7, pp. 2113–2130, 2006.

[24] E. F. Kuester, M. Mohamed, M. Piket-May, C. L. Holloway *et al.*, "Averaged transition conditions for electromagnetic fields at a metafilm," *Antennas and Propagation, IEEE Transactions on*, vol. 51, no. 10, pp. 2641–2651, 2003.

[25] M. Lapine and S. Tretyakov, "Contemporary notes on metamaterials," *Microwaves, Antennas & Propagation, IET*, vol. 1, no. 1, pp. 3–11, 2007.

[26] K. Achouri, M. Salem, and C. Caloz, "General metasurface synthesis based on susceptibility tensors," 2014.

[27] M. Albooyeh *et al.*, "Electromagnetic characterization of metasurfaces," 2015.

[28] N. Landy, S. Sajuyigbe, J. Mock, D. Smith, and W. Padilla, "Perfect metamaterial absorber," *Physical review letters*, vol. 100, no. 20, p. 207402, 2008.

[29] X. Liu, T. Starr, A. F. Starr, and W. J. Padilla, "Infrared spatial and frequency selective metamaterial with near-unity absorbance," *Physical review letters*, vol. 104, no. 20, p. 207403, 2010.

[30] T. S. Almoneef and O. M. Ramahi, "Metamaterial electromagnetic energy harvester with near unity efficiency," *Applied Physics Letters*, vol. 106, no. 15, p. 153902, 2015.

[31] D. Shrekenhamer, W. Xu, S. Venkatesh, D. Schurig, S. Sonkusale, and W. J. Padilla, "Experimental realization of a metamaterial detector focal plane array," *Physical review letters*, vol. 109, no. 17, p. 177401, 2012.

[32] B. Wathey, J. Tierney, P. Lidström, and J. Westman, "The impact of microwave-assisted organic chemistry on drug discovery," *Drug Discovery Today*, vol. 7, no. 6, pp. 373–380, 2002.

[33] J. A. Gordon, C. L. Holloway, J. Booth, S. Kim, Y. Wang, J. Baker-Jarvis, and D. R. Novotny, "Fluid interactions with metafilms/metasurfaces for tuning, sensing, and microwave-assisted chemical processes," *Physical Review B*, vol. 83, no. 20, p. 205130, 2011.

[34] C. A. Balanis, *Antenna theory: analysis and design*. John Wiley & Sons, 2016.

[35] A. Erentok and R. W. Ziolkowski, "Metamaterial-inspired efficient electrically small antennas," *Antennas and Propagation, IEEE Transactions on*, vol. 56, no. 3, pp. 691–707, 2008.

[36] R. Garg, *Microstrip antenna design handbook*. Artech House, 2001.

[37] M. M. Alam, M. M. R. Sonchoy, and M. O. Goni, "Design and performance analysis of microstrip array antenna," in *Progress In Electromagnetic Research Symposium Proceedings, Moscow, Russia*, 2009, pp. 18–21.

[38] H. Wheeler *et al.*, "Fundamental limitations of small antennas," *Proceedings of the IRE*, vol. 35, no. 12, pp. 1479–1484, 1947.

[39] J. Liu and H. Zhao, "Cylindrical conformal omnidirectional antenna design," in *Wireless Networks and Information Systems, 2009. WNIS'09. International Conference on*. IEEE, 2009, pp. 19–22.

[40] B. Thors and L. Josefsson, "Radiation and scattering tradeoff design for conformal arrays," *Antennas and Propagation, IEEE Transactions on*, vol. 51, no. 5, pp. 1069–1076, 2003.

[41] P. Knott, "Design and experimental results of a spherical antenna array for a conformal array demonstrator," in *Antennas, 2007. INICA'07. 2nd International ITG Conference on*. IEEE, 2007, pp. 120–123.

[42] D. Sun, R. Shen, and X. Yan, "A broadband conformal phased array antenna on spherical surface," *International Journal of Antennas and Propagation*, vol. 2014, 2014.

[43] L. Josefsson and P. Persson, *Conformal array antenna theory and design*. John wiley & sons, 2006, vol. 29.

[44] H. J. Visser, "Second european workshop on conformal antennas," *Antennas and Propagation Magazine, IEEE*, vol. 44, no. 5, pp. 87–90, 2002.

[45] B. Piper and M. Bialkowski, "Electromagnetic modeling of conformal wideband and multi-band patch antennas by bridging a solid-object modeler with mom software," *Antennas and Propagation Magazine, IEEE*, vol. 46, no. 5, pp. 42–52, 2004.

[46] A. C. Patel, M. P. Vaghela, H. Bajwa, and H. Seddik, "Conformable patch antenna design for remote health monitoring," in *Applications and Technology Conference (LISAT), 2010 Long Island Systems.* IEEE, 2010, pp. 1–6.

[47] Z. Sipus, P. Persson, M. Lanne, M. Heckler, S. Maci, J. L. Masa-Campos, P. Knott, V. Erturk, and G. Vandenbosch, "Structuring research on conformal antennas a european collaboration," in *Antennas and Propagation, 2007. EuCAP 2007. The Second European Conference on.* IET, 2007, pp. 1–4.

[48] C. Loecker, P. Knott, R. Sekora, and S. Algermissen, "Antenna design for a conformal antenna array demonstrator," in *Antennas and Propagation (EUCAP), 2012 6th European Conference on.* IEEE, 2012, pp. 151–153.

[49] P. Pillai, E. Paster, L. Montemayor, C. Benson, and I. W. Hunter, "Development of soldier conformable antennae using conducting polymers," DTIC Document, Tech. Rep., 2010.

[50] R. J. Allard, D. H. Werner, and P. L. Werner, "Radiation pattern synthesis for arrays of conformal antennas mounted on arbitrarily-shaped three-dimensional platforms using genetic algorithms," *Antennas and Propagation, IEEE Transactions on*, vol. 51, no. 5, pp. 1054–1062, 2003.

[51] Y.-J. Zhang, S.-X. Gong, and Y.-X. Xu, "Radiation pattern synthesis for arrays of conformal antennas mounted on an irregular curved surface using modified genetic algorithms," *Journal of Electromagnetic Waves and Applications*, vol. 23, no. 10, pp. 1255–1264, 2009.

[52] L. Josefsson and P. Persson, "Conformal array synthesis including mutual coupling," *Electronics Letters*, vol. 35, no. 8, pp. 625–627, 1999.

[53] D. H. Werner, R. J. Allard, R. A. Martin, and R. Mittra, "A reciprocity approach for calculating radiation patterns of arbitrarily shaped microstrip antennas mounted on circularly cylindrical platforms," *Antennas and Propagation, IEEE Transactions on*, vol. 51, no. 4, pp. 730–738, 2003.

[54] Q. Wang and Q.-Q. He, "An arbitrary conformal array pattern synthesis method that include mutual coupling and platform effects," *Progress In Electromagnetics Research*, vol. 110, pp. 297–311, 2010.

[55] Y.-H. Di, X.-Y. Liu, and M. M. Tentzeris, "A conformable dual-band antenna equipped with amc for wban applications," in *Antennas and Propagation (APCAP), 2014 3rd Asia-Pacific Conference on*. IEEE, 2014, pp. 388–391.

[56] M. Bialkowski, S. Jellett, and R. Varnes, "Electronically steered antenna system for the australian mobilesat," in *Microwaves, Antennas and Propagation, IEE Proceedings*, vol. 143, no. 4. IET, 1996, pp. 347–352.

[57] J. S. Sun, D. S. Goshi, and T. Itoh, "Optimization and modeling of sparse conformal retrodirective array," *Antennas and Propagation, IEEE Transactions on*, vol. 58, no. 3, pp. 977–981, 2010.

[58] G. Li, S. Yang, Y. Chen, and Z.-P. Nie, "A novel electronic beam steering technique in time modulated antenna array," *Progress In Electromagnetics Research*, vol. 97, pp. 391–405, 2009.

[59] N. Tesla, "My inventions: the autobiography of nikola tesla/edited, with an introduction, by ben johnston. 1st hart bros. ed," *Williston, Vt.: Hart Bros*, 1982.

[60] W. C. Brown, "The history of power transmission by radio waves," *IEEE Transactions on Microwave Theory and Techniques*, pp. 1230–1242, 1984.

[61] P. E. Glaser, "Power from the sun: its future," *Science*, vol. 162, no. 3856, pp. 857–861, 1968.

[62] W. C. Brown, "The history of the development of the rectenna," in *Solar Power Satellite Microwave Power Transmission and Reception*, vol. 2141, 1980, p. 271.

[63] W. Brown, "Experiments in the transportation of energy by microwave beam," in *1958 IRE International Convention Record*, vol. 12. IEEE, 1966, pp. 8–17.

[64] Y.-H. Suh and K. Chang, "A high-efficiency dual-frequency rectenna for 2.45-and 5.8-ghz wireless power transmission," *Microwave Theory and Techniques, IEEE Transactions on*, vol. 50, no. 7, pp. 1784–1789, 2002.

[65] J. O. McSpadden, L. Fan, and K. Chang, "Design and experiments of a high-conversion-efficiency 5.8-ghz rectenna," *Microwave Theory and Techniques, IEEE Transactions on*, vol. 46, no. 12, pp. 2053–2060, 1998.

[66] J. Paradiso, T. Starner *et al.*, "Energy scavenging for mobile and wireless electronics," *Pervasive Computing, IEEE*, vol. 4, no. 1, pp. 18–27, 2005.

[67] U. Alvarado, A. Juanicorena, I. Adin, B. Sedano, I. Gutiérrez, and J. Nó, "Energy harvesting technologies for low-power electronics," *Transactions on Emerging Telecommunications Technologies*, vol. 23, no. 8, pp. 728–741, 2012.

[68] L. Guenda, E. Santana, A. Collado, K. Niotaki, N. B. Carvalho, and A. Georgiadis, "Electromagnetic energy harvestingglobal information database," *Transactions on Emerging Telecommunications Technologies*, vol. 25, no. 1, pp. 56–63, 2014.

[69] S. Roundy, P. K. Wright, and J. Rabaey, "A study of low level vibrations as a power source for wireless sensor nodes," *Computer communications*, vol. 26, no. 11, pp. 1131–1144, 2003.

[70] A. J. du Plessis, M. J. Huigsloot, and F. D. Discenzo, "Resonant packaged piezoelectric power harvester for machinery health monitoring," in *Smart Structures and Materials*. International Society for Optics and Photonics, 2005, pp. 224–235.

[71] I. Capel, H. Dorrell, E. Spencer, and M. Davis, "The amelioration of the suffering associated with spinal cord injury with subperception transcranial electrical stimulation," *Spinal Cord*, vol. 41, no. 2, pp. 109–117, 2003.

[72] W. Zhou, W.-H. Liao, and W. J. Li, "Analysis and design of a self-powered piezoelectric microaccelerometer," in *Smart Structures and Materials*. International Society for Optics and Photonics, 2005, pp. 233–240.

[73] H. J. Visser, A. C. Reniers, and J. A. Theeuwes, "Ambient rf energy scavenging: Gsm and wlan power density measurements," in *Microwave Conference, 2008. EuMC 2008. 38th European*. IEEE, 2008, pp. 721–724.

[74] B. Alavikia, T. S. Almoneef, and O. M. Ramahi, "Electromagnetic energy harvesting using complementary split-ring resonators," *Applied Physics Letters*, vol. 104, no. 16, p. 163903, 2014.

[75] S. Kharkovsky and R. Zoughi, "Microwave and millimeter wave nondestructive testing and evaluation - overview and recent advances," *Instrumentation Measurement Magazine, IEEE*, vol. 10, no. 2, pp. 26–38, April 2007.

[76] M. Ghasr, S. Kharkovsky, R. Zoughi, and R. Austin, "Comparison of near-field millimeter-wave probes for detecting corrosion precursor pitting under paint," *Instrumentation and Measurement, IEEE Transactions on*, vol. 54, no. 4, pp. 1497–1504, Aug 2005.

[77] E. C. Fear, X. Li, S. C. Hagness, and M. A. Stuchly, "Confocal microwave imaging for breast cancer detection: Localization of tumors in three dimensions," *IEEE Transactions on Biomedical Engineering*, vol. 49, no. 8, pp. 812–822, 2002.

[78] L. Garnero, A. Franchois, J.-P. Hugonin, C. Pichot, and N. Joachimowicz, "Microwave imaging-complex permittivity reconstruction-by simulated annealing," *IEEE Transactions on microwave theory and techniques*, vol. 39, no. 11, pp. 1801–1807, 1991.

[79] A. Ali, M. El Badawe, and O. M. Ramahi, "Microwave imaging of subsurface flaws in coated metallic structures using complementary split-ring resonators," *IEEE Sensors Journal*, vol. 16, no. 18, pp. 6890–6898, 2016.

[80] J. Hunt, J. Gollub, T. Driscoll, G. Lipworth, A. Mrozack, M. S. Reynolds, D. J. Brady, and D. R. Smith, "Metamaterial microwave holographic imaging system," *JOSA A*, vol. 31, no. 10, pp. 2109–2119, 2014.

[81] M. Kim and J. Rho, "Metamaterials and imaging," *Nano Convergence*, vol. 2, no. 1, p. 22, 2015.

[82] A. Ali, M. El Badawe, and O. M. Ramahi, "Microwave imaging of subsurface flaws in coated metallic structures using complementary split-ring resonators," *IEEE Sensors Journal*, vol. 16, no. 18, pp. 6890–6898, 2016.

[83] A. Albishi and O. M. Ramahi, "Detection of surface and subsurface cracks in metallic and non-metallic materials using a complementary split-ring resonator," *Sensors*, vol. 14, no. 10, pp. 19 354–19 370, 2014.

[84] M. S. Boybay and O. M. Ramahi, "Waveguide probes using single negative media," *IEEE Microwave and Wireless Components Letters*, vol. 19, no. 10, pp. 641–643, 2009.

[85] M. S. Sharawi, M. U. Khan, A. B. Numan, and D. N. Aloi, "A csrr loaded mimo antenna system for ism band operation," *Antennas and Propagation, IEEE Transactions on*, vol. 61, no. 8, pp. 4265–4274, 2013.

[86] M. M. Bait-Suwailam, O. F. Siddiqui, and O. M. Ramahi, "Mutual coupling reduction between microstrip patch antennas using slotted-complementary split-ring resonators," *Antennas and Wireless Propagation Letters, IEEE*, vol. 9, pp. 876–878, 2010.

[87] L. Yousefi and O. M. Ramahi, "Artificial magnetic materials using fractal hilbert curves," *Antennas and Propagation, IEEE Transactions on*, vol. 58, no. 8, pp. 2614–2622, 2010.

[88] H. Attia, L. Yousefi, M. M. Bait-Suwailam, M. S. Boybay, and O. M. Ramahi, "Enhanced-gain microstrip antenna using engineered magnetic superstrates," *Antennas and Wireless Propagation Letters, IEEE*, vol. 8, pp. 1198–1201, 2009.

[89] B.-I. Wu, W. Wang, J. Pacheco, X. Chen, J. Lu, T. M. Grzegorczyk, J. A. Kong, P. Kao, P. A. Theophelakes, and M. J. Hogan, "Anisotropic metamaterials as antenna substrate to enhance directivity," *Microwave and optical technology letters*, vol. 48, no. 4, pp. 680–683, 2006.

[90] D. Schurig, J. Mock, and D. Smith, "Electric-field-coupled resonators for negative permittivity metamaterials," *Applied Physics Letters*, vol. 88, no. 4, p. 041109, 2006.

[91] C. S. SUITE, "Computer simulation technology," *CST Computer Simulation Technology AG, www.cst.com*.

[92] D. M. Pozar, *Microwave engineering*. John Wiley & Sons, 2009.

[93] "Microstrip patch antenna calculator," http://www.emtalk.com/mpacalc.php.

[94] C. Pfeiffer and A. Grbic, "Metamaterial huygens surfaces: tailoring wave fronts with reflectionless sheets," *Physical review letters*, vol. 110, no. 19, p. 197401, 2013.

[95] N. Yu and F. Capasso, "Flat optics with designer metasurfaces," *Nature materials*, vol. 13, no. 2, pp. 139–150, 2014.

[96] G. Minatti, S. Maci, P. De Vita, A. Freni, and M. Sabbadini, "A metasurface antenna for space application," *Proceedings of ISAP2012*, vol. 3, p. 1, 2012.

[97] B. Thors and L. Josefsson, "Radiation and scattering tradeoff design for conformal arrays," *Antennas and Propagation, IEEE Transactions on*, vol. 51, no. 5, pp. 1069–1076, 2003.

[98] P. Knott, "Design and experimental results of a spherical antenna array for a conformal array demonstrator," in *Antennas, 2007. INICA'07. 2nd International ITG Conference on*. IEEE, 2007, pp. 120–123.

[99] L. Josefsson and P. Persson, "Conformal array synthesis including mutual coupling," *Electronics Letters*, vol. 35, no. 8, pp. 625–627, 1999.

[100] D. H. Werner, R. J. Allard, R. A. Martin, and R. Mittra, "A reciprocity approach for calculating radiation patterns of arbitrarily shaped microstrip antennas mounted on circularly cylindrical platforms," *Antennas and Propagation, IEEE Transactions on*, vol. 51, no. 4, pp. 730–738, 2003.

[101] G. Li, S. Yang, Y. Chen, and Z.-P. Nie, "A novel electronic beam steering technique in time modulated antenna array," *Progress In Electromagnetics Research*, vol. 97, pp. 391–405, 2009.

[102] Z.-B. Lu, A. Zhang, and X.-Y. Hou, "Pattern synthesis of cylindrical conformal array by the modified particle swarm optimization algorithm," *Progress In Electromagnetics Research*, vol. 79, pp. 415–426, 2008.

[103] G. Zeng, S. Li, and Z. Wei, "Research on conformal phased array antenna pattern synthesis," in *Proceedings of the 2012 International Conference on Information Technology and Software Engineering*. Springer, 2013, pp. 13–21.

[104] D. Parker and D. C. Zimmermann, "Phased arrays-part i: Theory and architectures," *IEEE transactions on microwave theory and techniques*, vol. 50, no. 3, pp. 678–687, 2002.

[105] J. L. Gmez-Tornero, "Analysis and design of conformal tapered leaky-wave antennas," *Antennas and Propagation, IEEE Transactions on*, vol. 10, pp. 1068–1071, 2011.

[106] T. S. Almoneef and O. M. Ramahi, "Metamaterial electromagnetic energy harvester with near unity efficiency," *Applied Physics Letters*, vol. 106, pp. 153 902–153 904, April 2015.

[107] G. Minatti, S. Maci, P. De Vita, A. Freni, and M. Sabbadini, "A metasurface antenna for space application," *Proceedings of ISAP2012*, vol. 3, p. 1, 2012.

[108] M. El Badawe, T. S. Almoneef, and O. M. Ramahi, "A true metasurface antenna," *Scientific reports*, vol. 6, 2016.

[109] M. Ruphuy, Z. Ren, and O. M. Ramahi, "Flat far field lenses and reflectors," *Progress In Electromagnetics Research M*, vol. 34, pp. 163–170, 2014.

[110] M. Ruphuy, O. Siddiqui, and O. M. Ramahi, "Electrically thin flat lenses and reflectors," *J. Opt. Soc. Am. A*, vol. 32, no. 9, pp. 1700–1706, Sep 2015. [Online]. Available: http://josaa.osa.org/abstract.cfm?URI=josaa-32-9-1700

[111] G. Monti, F. Congedo, D. De Donno, and L. Tarricone, "Monopole-based rectenna for microwave energy harvesting of uhf rfid systems," *Progress In Electromagnetics Research C*, vol. 31, pp. 109–121, 2012.

[112] H. Sun, Y.-x. Guo, M. He, and Z. Zhong, "Design of a high-efficiency 2.45-ghz rectenna for low-input-power energy harvesting," *IEEE Antennas and Wireless Propagation Letters*, vol. 11, pp. 929–932, 2012.

[113] P. E. Glaser, "An overview of the solar power satellite option," *Microwave Theory and Techniques, IEEE Transactions on*, vol. 40, no. 6, pp. 1230–1238, 1992.

[114] W. C. Brown, "Electronic and mechanical improvement of the receiving terminal of a free-space microwave power transmission system," *NASA STI/Recon Technical Report N*, vol. 77, p. 31613, 1977.

[115] W. Brown and J. Triner, "Experimental thin-film, etched-circuit rectenna," in *1982 IEEE MTT-S International Microwave Symposium Digest*, 1982, pp. 185–187.

[116] W.-H. Tu, S.-H. Hsu, and K. Chang, "Compact 5.8-ghz rectenna using stepped-impedance dipole antenna," *IEEE Antennas and Wireless Propagation Letters*, vol. 6, pp. 282–284, 2007.

[117] J. Kim, S. Cho, H.-J. Kim, J.-W. Choi, J. Jang, and J. Choi, "Exploiting the mutual coupling effect on dipole antennas for rf energy harvesting," *IEEE Antennas and Wireless Propagation Letters*, vol. 15, pp. 1301–1304, 2016.

[118] Y.-J. Ren, M. F. Farooqui, and K. Chang, "A compact dual-frequency rectifying antenna with high-orders harmonic-rejection," *IEEE Transactions on Antennas and Propagation*, vol. 55, no. 7, pp. 2110–2113, 2007.

[119] J. Heikkinen and M. Kivikoski, "A novel dual-frequency circularly polarized rectenna," *IEEE Antennas and Wireless Propagation Letters*, vol. 2, no. 1, pp. 330–333, 2003.

[120] Z. Harouni, L. Cirio, L. Osman, A. Gharsallah, and O. Picon, "A dual circularly polarized 2.45-ghz rectenna for wireless power transmission," *IEEE Antennas and Wireless Propagation Letters*, vol. 10, pp. 306–309, 2011.

[121] J. Zhang, Y. Huang, and P. Cao, "A wideband cross dipole rectenna for rf wireless harvesting," in *Antennas and Propagation (EuCAP), 2013 7th European Conference on*. IEEE, 2013, pp. 3063–3067.

[122] Y.-J. Ren and K. Chang, "5.8-ghz circularly polarized dual-diode rectenna and rectenna array for microwave power transmission," *IEEE Transactions on Microwave Theory and Techniques*, vol. 54, no. 4, pp. 1495–1502, 2006.

[123] J. A. Hagerty, F. B. Helmbrecht, W. H. McCalpin, R. Zane, and Z. B. Popovic, "Recycling ambient microwave energy with broad-band rectenna arrays," *IEEE Transactions on Microwave Theory and Techniques*, vol. 52, no. 3, pp. 1014–1024, 2004.

[124] M. Piñuela, P. D. Mitcheson, and S. Lucyszyn, "Ambient rf energy harvesting in urban and semi-urban environments," *IEEE Transactions on Microwave Theory and Techniques*, vol. 61, no. 7, pp. 2715–2726, 2013.

[125] B. Alavikia, T. S. Almoneef, and O. M. Ramahi, "Electromagnetic energy harvesting using complementary split-ring resonators," *Applied Physics Letters*, vol. 104, no. 16, p. 163903, 2014.

[126] ANSYS HFSS Version 15.0.0, Ansys Inc., http://www.ansys.com.

[127] N. Bascomb, *The New Cool: A Visionary Teacher, His FIRST Robotics Team, and the Ultimate Battle of Smarts*. Random House LLC, 2012.

[128] P. Richards, "Bolometers for infrared and millimeter waves," *Journal of Applied Physics*, vol. 76, no. 1, pp. 1–24, 1994.

[129] J. Hao, J. Wang, X. Liu, W. J. Padilla, L. Zhou, and M. Qiu, "High performance optical absorber based on a plasmonic metamaterial," *Applied Physics Letters*, vol. 96, no. 25, p. 251104, 2010.

[130] W. Padilla, M. Aronsson, C. Highstrete, M. Lee, A. Taylor, and R. Averitt, "Electrically resonant terahertz metamaterials: Theoretical and experimental investigations," *Physical Review B*, vol. 75, no. 4, p. 041102, 2007.

[131] E. C. Fear, X. Li, S. C. Hagness, and M. A. Stuchly, "Confocal microwave imaging for breast cancer detection: Localization of tumors in three dimensions," *IEEE Transactions on Biomedical Engineering*, vol. 49, no. 8, pp. 812–822, 2002.

[132] P. M. Meaney, M. W. Fanning, D. Li, S. P. Poplack, and K. D. Paulsen, "A clinical prototype for active microwave imaging of the breast," *IEEE Transactions on Microwave Theory and Techniques*, vol. 48, no. 11, pp. 1841–1853, 2000.

[133] R. Appleby and R. N. Anderton, "Millimeter-wave and submillimeter-wave imaging for security and surveillance," *Proceedings of the IEEE*, vol. 95, no. 8, pp. 1683–1690, 2007.

[134] F. Adib and D. Katabi, *See through walls with WiFi!* ACM, 2013, vol. 43, no. 4.